UNIVERSITY OF CALIFORNIA SAN DIEGO

Observations of seawater carbonate chemistry in the Southern California Current

A Dissertation submitted in partial satisfaction of the requirements
for the degree Doctor of Philosophy

in

Oceanography

by

Wiley H. Wolfe

Committee in charge:

Todd R. Martz, Chair
Katherine A. Barbeau
Andrew G. Dickson
Ralf Goericke
Armin Schwartzman
Uwe Send

2022

The Dissertation of Wiley H. Wolfe is approved, and it is acceptable in quality and form for publication on microfilm and electronically.

University of California San Diego

2022

DEDICATION

To those who made a child believe he could read.

TABLE OF CONTENTS

LIST OF FIGURES

LIST OF TABLES

ACKNOWLEDGEMENTS

Thank you to my family, friends and lab mates for helping hold me together over the past crazy five years. Thank you to Gilbert, Maureen and everyone in the SIO administration for answering endless questions and keeping the world turning.

Thank you to the SCOPE coordinators, Donna Shabkie, and everyone who volunteered with SCOPE. You and the program have helped shape my science communication and have had a significant positive impact on the local community.

Thank you to everyone who contributed to the inorganic carbon time series. I deeply appreciate the effort that went into every bottle that I did not have to analyze or quality control myself and each cruise I did not have to be on to collect them.

I greatly appreciate the funding that has made this journey possible. Thank you to the T. R. and Edith Folsom Graduate Fellowship. Thank you to the LOREX program for encouraging and funding international collaboration. Thank you to the CCE-LTER for funding both as an undergraduate and graduate student. Finally, with the greatest affection, thank you to the Ford Family Foundation, and the Schweiger Memorial Scholarship Fund who began this journey with me long before a Ph.D. was even a dream.

Thank you to the co-authors on my first publications. I appreciate your scientific input, guidance, and particularly finding my many typos. Thank you for enduring the rough start. I hope to continue to improve my scientific writing for future collaborations.

Thank you to my committee, Katherine Barbeau, Andrew Dickson, Ralf Goericke, Armin Schwartzman, and Uwe Send. I hope to continue to collaborate beyond my Ph.D.

Finally, this endeavor would not have been possible without the steadfast patience and support of Todd Martz. My deepest thanks for helping guide me here.

Chapter 1, in full, is a reprint of the material as it appears in European Geosciences Union, Ocean Science, 2021. Wolfe, W. H., Shipley, K. M., Bresnahan, P. J., Takeshita, Y., Wirth, T., & Martz, T. R. (2021). Technical note: Stability of tris pH buffer in artificial seawater stored in bags. *Ocean Science*, 17(3), 819-831. The dissertation author was the primary investigator and author of this paper.

Chapter 2, in full, is currently being prepared for submission for publication of the material in American Geophysical Union, Geophysical Research Letters, 2022, Wolfe, W. H., Martz, T. R., Dickson, A. G., Goericke, Ralf, Ohman, M. D. (2021). Ocean Acidification in the Southern California Current: A 37 Year Time Series. The dissertation author was the primary researcher and author of this paper.

Chapter 3, in part, is currently being prepared for submission for publication of the material in American Geophysical Union, Journal of Geophysical Research: Oceans. The dissertation author was the primary researcher and author of this material.

Chapter 4, in part, is currently being prepared for submission for publication of the material in Earth System Science Data. The dissertation author was the primary author of this chapter.

VITA

2015 Bachelor of Science in Chemical Engineering, Oregon State University

2018 Master of Science in Oceanography, University of California San Diego

2022 Doctor of Philosophy in Oceanography, University of California San Diego

PUBLICATIONS

Wolfe, W. H., Dickson, A. G., Goericke, R., Ohman, M. D., Martz, T. R. (in prep.). Ocean Acidification in the Southern California Current: A 37 Year Time Series. *Geophysical Research Letters.*

Miller, B., Wolfe, W. H., Gentry, J., Grewal, G., Highley, C. B., De Vita, R., Vaughan, M. H., Caliari, S. R. (in prep.). Supramolecular Fibrous Hydrogel Augmentation of Uterosacral Ligament Suspension for Treatment of Pelvic Organ Prolapse. *Advanced Healthcare Materials.*

Wolfe, W. H., Shipley, K. M., Bresnahan, P. J., Takeshita, Y., Wirth, T., & Martz, T. R. (2021). Technical note: Stability of tris pH buffer in artificial seawater stored in bags. *Ocean Science, 17*(3), 819-831.

Nesbit, K. T., Wolfe, W., Mullane, K. K., Chamberlain, E. J., Rasina, B. A., Saberski, E., & Jones, S. A. (2021). SCOPE: A volunteer-led STEM outreach program connecting communities to research. *Connected Science Learning*, *3*(6).

ABSTRACT OF THE DISSERTATION

Observations and calibration techniques of seawater carbonate chemistry in the Southern California Current

by

Wiley H. Wolfe

Doctor of Philosophy in Oceanography

University of California San Diego, 2022

Professor Todd R. Martz, Chair

The ocean has taken up roughly a quarter of the total anthropogenic carbon emissions (Gruber et al., 2019). This addition causes changes in carbonate system equilibrium, decreasing ocean pH, which impacts marine organisms, ecosystems, and humans reliant on marine resources (Doney et al., 2020). The study of the changing carbonate chemistry and its impact on the ocean requires the refinement of measurement techniques, observational programs, models and the sharing of data. Chapter 1 focuses on measurement techniques by assessing the stability of tris pH buffer in artificial seawater stored in bags. These bagged

reference materials can be used by both benchtop and autonomous instruments to aid in quality control of measurements of carbonate chemistry. Chapter 2 focuses on continued observation, with the oldest inorganic carbon time series in the Pacific. This time series in the Southern California Current helps confirm the rate of anthropogenic ocean acidification observed in other regions of the ocean. Chapter 3 focuses on models by using seasonal cycles determined in Chapter 2 to build a mixed layer carbon budget at the location of the time series. Chapter 4 focuses on the sharing of data by summarizing and publishing previously unavailable observations of carbonate chemistry in the Southern California Current going back as far as 1983.

CHAPTER 1

Technical note: Stability of tris pH buffer in artificial seawater stored in bags

Chapter 1, in full, is a reprint of the material as it appears in European Geosciences Union, Ocean Science, 2021. Wolfe, W. H., Shipley, K. M., Bresnahan, P. J., Takeshita, Y., Wirth, T., & Martz, T. R. (2021). Technical note: Stability of tris pH buffer in artificial seawater stored in bags. *Ocean Science*, 17(3), 819-831. The dissertation author was the primary investigator and author of this paper.

Ocean Sci., 17, 819–831, 2021
https://doi.org/10.5194/os-17-819-2021

Ocean Science Open Access EGU

Technical note: Stability of tris pH buffer in artificial seawater stored in bags

Wiley H. Wolfe[1], Kenisha M. Shipley[1], Philip J. Bresnahan[2], Yuichiro Takeshita[3], Taylor Wirth[1], and Todd R. Martz[1]

[1]Scripps Institution of Oceanography, University of California San Diego, La Jolla, 92093, USA
[2]Department of Earth and Ocean Sciences, University of North Carolina Wilmington, Wilmington, 28403, USA
[3]Monterey Bay Aquarium Research Institute, Moss Landing, 95093, USA

Correspondence: Philip J. Bresnahan (bresnahanp@uncw.edu)

Received: 15 December 2020 – Discussion started: 16 February 2021
Revised: 14 May 2021 – Accepted: 17 May 2021 – Published: 30 June 2021

Abstract. Equimolal tris (2-amino-2-hydroxymethyl-propane-1,3-diol) buffer in artificial seawater is a well characterized and commonly used standard for oceanographic pH measurements. We evaluated the stability of tris pH when stored in purportedly gas-impermeable bags across a variety of experimental conditions, including bag type and storage in air vs. seawater over 300 d. Bench-top spectrophotometric pH analysis revealed that the pH of tris stored in bags decreased at a rate of $0.0058 \pm 0.0011\ \mathrm{yr}^{-1}$ (mean slope $\pm 95\,\%$ confidence interval of slope). The upper and lower bounds of expected pH change at $t = 365$ d, calculated using the averages and confidence intervals of slope and intercept of measured pH change vs. time data, were -0.0042 and -0.0076 from initial pH. Analyses of total dissolved inorganic carbon confirmed that a combination of CO_2 infiltration and/or microbial respiration led to the observed decrease in pH. Eliminating the change in pH of bagged tris remains a goal, yet the rate of pH change is lower than many processes of interest and demonstrates the potential of bagged tris for sensor calibration and validation of autonomous in situ pH measurements.

1 Introduction

Ocean pH is a key measurement used for tracking biogeochemical processes such as photosynthesis, respiration, and calcification (Takeshita et al., 2016) and represents perhaps the most recognized variable associated with ocean acidification (OA), the decrease in ocean pH due to the uptake of anthropogenic carbon dioxide (Doney et al., 2009). OA progresses with a global average pH decline of 0.002 per year in the surface open ocean (Bates et al., 2014), and the accumulated and projected near-term effects of OA have been shown to have deleterious effects on many calcifying organisms (Cooley and Doney, 2009). Beyond the narrow scope of calcifiers, organismal response is complex, exhibiting varied responses across processes such as reproduction, growth rate, and sensory perception. Organismal responses are further complicated by their impact on ecosystem level dynamics, such as altering competition and predator–prey relationships (Doney et al., 2020). Furthermore, pH effects are often exacerbated by concomitant stressors, such as decreased dissolved oxygen or increased temperature. Ultimately, OA will affect humans through impacts on fisheries, aquaculture, and shoreline protection (Branch et al., 2013; Doney et al., 2020).

The quality of pH measurement required to observe various phenomena is often broken into "climate" and "weather" levels of uncertainty (Newton et al., 2015), or 0.003 and 0.02, respectively. Discrete sampling has been shown to be capable of meeting the climate level of uncertainty when best practices are followed, yet many labs do not consistently meet this standard (Bockmon and Dickson, 2015). Furthermore, while discrete, bench-top methodologies can be the most accurate, the ocean's vast size limits the oceanographic community's ability to make ship-based discrete pH measurements to decadal reoccupations of a few major sections per ocean basin (Sloyan et al., 2019). The sparsity of ship-board measurements hinders our ability to assess sub-decadal processes, such as seasonal cycles or bloom events, over much of the ocean (Karl, 2010) and highlights the need for autonomous, high-frequency pH measurements. Technological

Published by Copernicus Publications on behalf of the European Geosciences Union.

advancements have led to more routine autonomous pH measurements over the past decade, providing opportunities to fill some gaps in time and space in discrete sampling programs (e.g., Byrne, 2014; Martz et al., 2015; Lai et al., 2018; Wang et al., 2019; Tilbrook et al., 2019). Globally, pH sensors now operate on hundreds of autonomous platforms including moorings and profiling floats, delivering unique data sets in the form of Eulerian and depth-resolved Lagrangian time series (Johnson et al., 2017; Bushinsky et al., 2019; Sutton et al., 2019). While sensors increase data coverage, many sensor-based pH measurements, particularly on moored systems, continue to fall short of both climate and weather levels of uncertainty, as highlighted in the intercomparison tests carried out by the Alliance for Coastal Technologies (ACT, 2012) and by the Wendy Schmidt Ocean Health XPRIZE (Okazaki et al., 2017).

Independent validation is typically required for autonomous sensors to meet both weather and climate levels of uncertainty. For example, autonomous underway pCO_2 systems (Pierrot et al., 2009), moorings (Bushinsky et al., 2019), and autonomous surface vehicles (Chavez et al., 2017; Sabine et al., 2020) are able to provide climate quality observations with an uncertainty of $\pm 2\,\mu$atm because traceable standard gases are frequently measured in situ. For pH measurements on profiling floats (Johnson et al., 2016), sensor performance is validated by comparing to a deep reference pH field that is calculated using empirical algorithms (Williams et al., 2016; Bittig et al., 2018; Carter et al., 2018). This approach has demonstrated the ability to obtain high-quality pH measurements from a network of profiling floats (Johnson et al., 2017) but requires measurements in the deep ocean where pH is comparatively stable. It is atypical for other pH sensors, including coastal moored sensors, to have an automated or remote validation. Therefore, on such deployments, validation has largely relied on discrete samples taken alongside the sensor (Bresnahan et al., 2014; McLaughlin et al., 2017; Takeshita et al., 2018), which presents unique challenges, primarily that spatiotemporal discrepancy can lead to errors of > 0.1, especially in highly dynamic systems (Bresnahan et al., 2014).

Similar to the method in use by pCO_2 systems, one approach to validate in situ pH sensors is by measuring a reference material or pH standard, repeatedly during a sensor deployment. The most commonly used standard for oceanographic pH measurement is an equimolal tris (2-amino-2-hydroxymethyl-propane-1,3-diol) buffer in artificial seawater (ASW), hereafter referred to as tris or tris-ASW (DelValls and Dickson, 1998; Papadimitriou et al., 2016). The pH of tris has been characterized over a range of temperature, salinity, and pressure (DelValls and Dickson, 1998; Rodriguez et al., 2015; Takeshita et al., 2017; Müller et al., 2018), allowing for accurate calculation of tris pH across a wide range of marine conditions. Furthermore, when stored in borosilicate bottles and under ideal conditions, these buffers have been shown to be stable to better than 0.0005 over a year (Dickson, 1993; Nemzer and Dickson, 2005), making tris a good candidate for in situ validation of long-term deployments of autonomous pH sensors. To be utilized for in situ applications, the reference solution must be stored in bags (as in Hales et al., 2005; Seidel et al., 2008; Sayles and Eck, 2009; Spaulding et al., 2014; Wang et al., 2015; Lai et al., 2018). Recently, in situ sensor validation using bagged tris was demonstrated by Lai et al. (2018) during a 150 d deployment of an autonomous pH sensor, where the tris standard was measured in situ every 5 d. However, the stability of tris when stored in bags has not been quantified systematically using spectrophotometric bench-top pH measurement techniques recommended as best practice (Dickson et al., 2007).

In this work we quantified the stability of tris stored in bags for 300 d. Tris from four separately prepared batches was stored in two bag types either in a lab or submerged in seawater. In addition, one batch was stored in borosilicate bottles in the lab as a control. Spectrophotometric pH measurements were made approximately every 2 months on each bag of tris. Throughout the experiment, certified reference materials (CRMs) for oceanic CO_2 measurements (Dickson, 2001) were used to assess the stability of the spectrophotometric pH system.

2 Methods

Two bag types were tested for storing tris (Fig. 1). Bag type 1 was custom made based on a design used in the "Burke-o-Lator" system (Hales et al., 2005; Bandstra et al., 2006), made from PAKDRY 7500 barrier film (IMPAK P75C0919). The barrier film is made of layers of polyester and nylon with a sealant layer of metallocene polyethylene. Two 23 cm $\times$ 48 cm ($9'' \times 19''$) sheets were heat sealed on three sides, forming a pocket, and a 1.9 cm ($3/4''$) diameter hole was cut into one of the pocket walls for the bulkhead fitting and bulkhead nut (McMaster-Carr 8674T55). The bulkhead was sealed into the wall with a silicone gasket (McMaster-Carr 9010K13) and washer (McMaster-Carr 95649A256) and coated with silicone sealant (McMaster-Carr 74955A53). A "push-to-connect" ball valve fitting (McMaster-Carr 4379K41) was attached to the bulkhead. The modified pocket was rinsed, dried, and heat sealed along the final edge to create a ~ 4 L bag. Bags were left to dry for at least 24 h before filling. Bag type 2 was a commercially available 3 L Cali-5-Bond bag purchased from Calibrated Instruments and used without modification. It is a multi-layer bag made of plastic, aluminum foil (to prevent liquid and gas permeation), a layer of inert high-density polyethylene (to form a non-reactive inner wall), and a polycarbonate Stopcock Luer valve.

In this experiment, four batches of tris were prepared following the procedure in DelValls and Dickson (1998), using off-the-shelf reagents with no additional standardization or purification (e.g., recrystallization of salts). The focus of this paper is stability of bagged tris over time and does not pri-

Figure 1. A picture of bag type 1 and 2 used to store tris in this study.

oritize obtaining highly accurate equimolal tris (as would be necessary for characterization of thermodynamic constants, for example). The calculated pH of tris in this study was 8.2652 at 20 °C, based on quantity of reagents used. This is 0.0135 higher than the pH of equimolal tris, 8.2517 at 20 °C (DelValls and Dickson, 1998). The pH discrepancy was due to a unit error in the measurement of HCl (our preparation used mol L^{-1} rather than the prescribed mol kg-sol^{-1}). This unit error resulted in a tris : trisH^+ of 1 : 0.97 that slightly differs from the 1 : 1 of truly equimolal tris. As this ratio is nearly equimolal, the term "equimolal" will continue to be used throughout this study. The details of the specific reagents used to prepare the tris solution can be found in Table A1.

Three stability tests were initiated at different times over the course of 18 months. The initiation of a given test is defined as the date of preparation of the tris used in that test. A summary of the differences between these tests is shown in Table 1 and described here. Each bag has a unique identifier in the format of "batch number, bag number, lab or tank." If this identifier is duplicative, the bags are differentiated with letters A to D. Each bag was rinsed before filling: 3 times with deionized water (DI), 5 times with ultrapure water (> 18 MΩ resistivity), and at least 3 times with 200 mL of tris. Tris bags were stored on a lab bench or in a 5000 L test tank filled with ozone-sterilized, filtered seawater. Bag type 2 experienced delamination of exterior layers when stored in seawater during test 2 and was not used in further testing. Tris from batch 4 was also stored in borosilicate bottles following the procedure in Nemzer and Dickson (2005). In addition to pH measurements, dissolved inorganic carbon (C_T) was measured on both bagged and bottled tris during test 3 to see if changes in pH were due to increased CO_2. C_T samples were measured using a custom-built system based on an infrared (IR) analyzer (LI-COR 7000) similar to systems used by O'Sullivan and Millero (1998) and Friederich et al. (2002). This IR measurement system is capable of measuring relatively low C_T without requiring method adjustment and has been used to make near-zero C_T measurements (Paulsen and Dickson, unpublished data). C_T measurements were made on CRMs (Batch 179 and 183). The precision of the C_T measurements was ±1.4 µmol kg^{-1} (pooled SD, $n_{\text{samples}} = 15$, $n_{\text{measurements}} = 44$).

Tris pH was measured every 55 ± 20 d (mean ± SD of measurement interval) throughout the experiment. The pH of tris was measured in triplicate at each time point with spectrophotometry using m-cresol purple as the indicator dye using the system described in Carter et al. (2013). Absorbance measurements were made in a 10 cm jacketed cell, and the temperature was measured directly adjacent to the cell outflow using a NIST-traceable thermometer (±0.1 °C, QTI DTU6028P-001-SC). Blank and sample were held for 3 min in the jacketed flow cell prior to absorbance measurements.

On average, temperature was stable to within a 0.02 °C range over the course of the day; the mean temperature throughout the experiment was 20.09 ± 0.23 °C (1σ), although temperature was 0.6 °C higher than the average

Table 1. Tris preparation and storage.

	Bag type	Tris batch	Date made	Storage location	Rinse procedure	C_T measured
Test 1	1 and 2	1 and 2	13 December 2017	Lab and tank	3× DI, 5× ultrapure, 3× tris	No
Test 2	1 and 2	3	13 April 2018	Lab and tank	3× DI, 5× ultrapure, 3× tris	No
Test 3	1 and bottle	4	26 February 2019	Lab	3× DI, 5× ultrapure, ≥ 6× tris	Yes

on one measurement day. Spectrophotometric pH measurements are reported at 20 °C by adjusting the measured pH value at the measured cell temperature T_C (pH_{spec,T_C}) to 20 °C ($pH_{spec,20\,°C}$) using the known temperature dependence of tris (pH_{tris}) as follows:

$$pH_{spec,20\,°C} = pH_{spec,T_C} - (pH_{tris,T_C} - pH_{tris,20\,°C}). \quad (1)$$

pH_{tris,T_C} and $pH_{tris,20\,°C}$ are the theoretical pH of tris (at the measured temperature and 20 °C respectively) and were calculated using Eq. (18) in DelValls and Dickson (1998). This adjustment assumes that any potential difference in $\partial pH/\partial T$ between that corresponding to equimolal tris and that corresponding to our 1 : 0.97 tris : $trisH^+$ ratio has a negligible effect over the small temperature range observed.

To account for pH-dependent errors from impurities in unpurified mCP, a pH-dependent correction factor was determined based on the protocol outlined in Takeshita et al. (2021). Briefly, pH of natural seawater with different ratios of added tris : $trisH^+$ was measured subsequently using impure dye (pH_{impure}; from Aldrich, lot MKBH6858V) and purified dye (pH_{pure}; from Robert Byrne's laboratory, University of South Florida; Liu et al., 2011) over a range of pH between 7.4 to 8.2 at approximately 0.2 intervals. Varying ratios of tris : $trisH^+$ were used to obtain different solution pH, and to buffer any changes in pH during the experiment, which negates the need for dye perturbation corrections in this characterization. Triplicate measurements were made at each pH. A second-order pH-dependent error was observed as previously described, following the equation ($R^2 = 0.975$, RMSE = 0.000434)

$$pH_{pure} = -0.0047777 \times pH_{impure}{}^2 + 1.0668875 \times pH_{impure} - 0.2359740. \quad (2)$$

All subsequent pH_{spec} measurements in this study were conducted with impure dye and are reported with this dye impurity correction (Eq. 2) applied. The correction adjusted the reported pH by 0.0093±0.0002 (mean ± SD, $n = 126$). No dye perturbation correction was used (a correction for a change in pH caused by the addition of the dye), as the high buffering capacity of tris, in combination with a dye adjusted to a pH similar to that of tris, results in a negligible change in measured pH.

Measurements of tris batches 1 and 2 made in the first 150 d have been removed from the data set due to procedural changes made to the spectrophotometric pH system to correct for problems with temperature equilibration. Outliers were removed from the spectrophotometric pH measurements if the absorbance at 760 nm was above 0.005 or below −0.002 (indicative of a measurement problem, such as a bubble or lamp drift), resulting in the removal of 2 out of 163 measurements. Additionally, outliers were removed from the data set if they were greater than 3 SD from the mean of a measurement triplicate, where SD is calculated as using all sets of triplicates (1 SD = 0.0004, $n = 55$), resulting in the removal of 2 of 161 remaining measurements. The remaining 159 measurements were used for the analysis presented here. An analysis of variation, or ANOVA, was used to detect the dependence of the results on tris batch, bag/bottle, type and storage location. Analysis was performed using MATLAB R2020a and the standard function "anovan" Throughout the experiment, CRMs (procured from Andrew Dickson, Scripps Institution of Oceanography) for seawater C_T and total alkalinity were measured regularly to verify instrument performance (Dickson, 2001). A time series of CRM measurements over the duration of the work described here showed no systematic drift. (Fig. A1 in Appendix A). To assess if the change in pH was driven by the addition of CO_2, the final pH and available C_T measurements were compared with a model described here. The theoretical change in tris-artificial seawater (ASW) pH due to an increase in C_T is straightforward to calculate, since both tris and CO_2 acid–base equilibria are well-characterized in seawater and ASW media. The pH is calculated for tris-ASW + C_T using an equilibrium model following the approach described in Sect. 2 of Dickson et al. (2007) for the case of known alkalinity and C_T. In the case of ASW, the seawater equilibrium constants for CO_2 are appropriate because minor ions present in seawater and not ASW do not appreciably affect the CO_2 equilibrium constants (particularly when the goal is to compute relative changes in pH) as the ionic background of ASW is closely matched to that of seawater at salinity = 35. In our model, minor acid–base species important to seawater alkalinity but not present in ASW (borate, phosphate, silicate, fluoride) are set to zero. The definition of total alkalinity is modified to include the tris acid–base system following the definition of acid-base donor/acceptor criteria given by Dickson (1981): tris is assigned as a level-1 proton acceptor and tris-H^+ is at the zero level. Thus, in our model, $tris_{tot} = 0.08$ molal, alkalinity = 0.04 molal, and C_T is a variable. An algorithm (see Annexe 1 in Dickson et al., 2007) is then used to find the root

of the alkalinity equation in its residual form by solving for pH.

3 Results and discussion

Figure 2 depicts $pH_{spec,20\,^\circ C}$, stored in either a bag or bottle, as a function of time and is subdivided for tests 1, 2, and 3. A linear decrease was observed for all bags or bottles. A linear regression was calculated for each experimental condition and, in the cases where measurements at $t = 0$ were removed due to protocol changes described above, the line was extrapolated back to $t = 0$, shown by the dotted line. The measured or extrapolated y intercept is reported as the initial pH in Table 2. In all tests, trend lines are extrapolated to $t = 365$ d to illustrate observed and predicted change over the course of a year as shown by the solid line. For ease of visual comparison, the y axis of each subplot has an identical pH range of 0.017.

Only bags from test 3, using tris batch 4 and bag type 1, have direct initial pH measurements and replicate bags. Initial pH measurements of these 4 bags were 8.2630 ± 0.0007 (mean $\pm$ SD, $n = 12$). Importantly, the very low SD suggests that a single initial pH measurement is representative of all replicate bags filled with a single tris batch, if the preparation procedure used in test 3 is followed. This inter-bag consistency is beneficial because it reduces the number of initial pH measurements required when filling multiple bags. There is also strong agreement in initial pH measurements between bagged and bottled tris in test 3, with the initial pH of bottled tris 0.0007 higher than bagged tris (8.26327 ± 0.0004, $n = 6$). The differences in filling procedure or impurities between bags and bottles in test 3 appear to have little effect on the initial pH. The mean initial pH of tris batch 4 is 0.002 ($n = 5$) lower than calculated $pH_{tris,20\,^\circ C}$ (Fig. A2). This difference between the mean initial pH of tris batch 4 and calculated $pH_{tris,20\,^\circ C}$ is similar in direction and magnitude to those reported in other studies: DeGrandpre et al. (2014) reported -0.0012 ± 0.0025, and Müller and Rehder (2018) reported -0.002 to -0.008 (measured pH minus pH_{tris,T_C}). With standard laboratory equipment and off-the-shelf reagents, an uncertainty of 0.006 is expected in prepared tris (Paulsen and Dickson, 2020). Measurements were also made on Dickson standard tris (batch T35) using the same instrument, and the pH was 0.0019 higher than the calculated $pH_{tris,20\,^\circ C}$ ($n = 2$). In tests 1 and 2, the initial pH was extrapolated from a linear regression. The extrapolated initial pH values are more variable and lower (on average) than those directly measured (Fig. A2). These differences may be a result of the extrapolation or different experimental variables such as the increased rinsing of bags, or the single bag type and storage location used in test 3.

Figure 3 depicts a composite of all test results as the change from the initial pH of tris ($\Delta pH = pH^{t=day}_{spec,20\,^\circ C} - pH^{t=0}_{spec,20\,^\circ C}$) as a function of time elapsed since bagging. A linear regression on all pH measurements, excluding the outlier of "batch 2, bag 1, lab", of tris stored in bag types 1 or 2, has a slope of $-0.0058 \pm 0.0011\ yr^{-1}$ (mean $\pm$ 95 % confidence interval (CI)). The upper and lower bounds of ΔpH at $t = 365$ d, -0.0042, and -0.0076 are important to consider when utilizing this bagged storage method of tris. These bounds provide the broadest expected range in pH change over a year of storage and include both the intercept and slope confidence intervals ($slope_{CI}$ and $intercept_{CI}$, respectively). For example, the upper bound of ΔpH at $t = 365$ d is calculated as upper bound = (slope + $slope_{CI}$) $\times$ 365 + intercept + $intercept_{CI}$. The outlier (batch 2, bag 1, lab) was excluded due to noticeable damage to the bag (see Fig. A3 in Appendix A), which is believed to have caused its pH to decrease at more than 2 times the average rate of the other bags. The damage appears to be a break in the metallic bag layer, potentially caused by creasing or pinching of the bag during handling. This observation highlights the importance of maintaining bag integrity, particularly during use in the field. A successful 2-week field deployment has been conducted using the tris bags described here and a modified SeapHOx in a shallow, coral reef flat (Bresnahan et al., 2021). This 2-week deployment was significantly shorter than the year of storage described here, and further field testing in longer deployments in varied environments is required before widespread use of this technology. For the longer time frame depicted in Fig. 3, the only comparable example found in the literature is the work of Lai et al. (2018). In this work, Lai et al. (2018) used bagged tris for sensor calibration, with in situ tris measurements made over 150 d. Lai et al. (2018) did not report a change in the pH of bagged tris over the deployment; however, the reported precision of the SAMI-pH in situ instrument (± 0.003) would not resolve the expected change shown in our Fig. 3. Therefore, the results of Lai et al. (2018) are not inconsistent with our study.

A significant increase in C_T was observed for all types of bags and bottles in Experiment 3 (Fig. 4). A high correlation between solution pH and C_T was observed, with a slope of -0.0029 ± 0.0006 pH per $100\,\mu mol\,kg^{-1}$ ($n = 14$, $r^2 = 0.70$), suggesting that the change in tris pH and C_T was primarily driven by an increase in CO_2. The observed slope agrees closely with a theoretical model prediction of a linear decrease in pH of -0.0024 per $100\,\mu mol\,kg^{-1}$ of C_T added (over the range of C_T observed). There are two possible sources of the increasing C_T: gas exchange of CO_2 with the environment and microbial respiration within the storage vessel. Gas exchange should not be a significant source of CO_2 for tris stored in a borosilicate bottle, as this is the standard equipment used to store seawater CO_2 and tris buffers and is known to minimize gas exchange (Dickson et al., 2007). Therefore, it is likely that respiration was the primary driver for the increase in C_T for tris stored in bottles. On average, the pH decrease in tris stored in bags was larger than that in the standard bottle (Fig. 2), indicating either an additional source of CO_2 from gas exchange, or larger amounts of res-

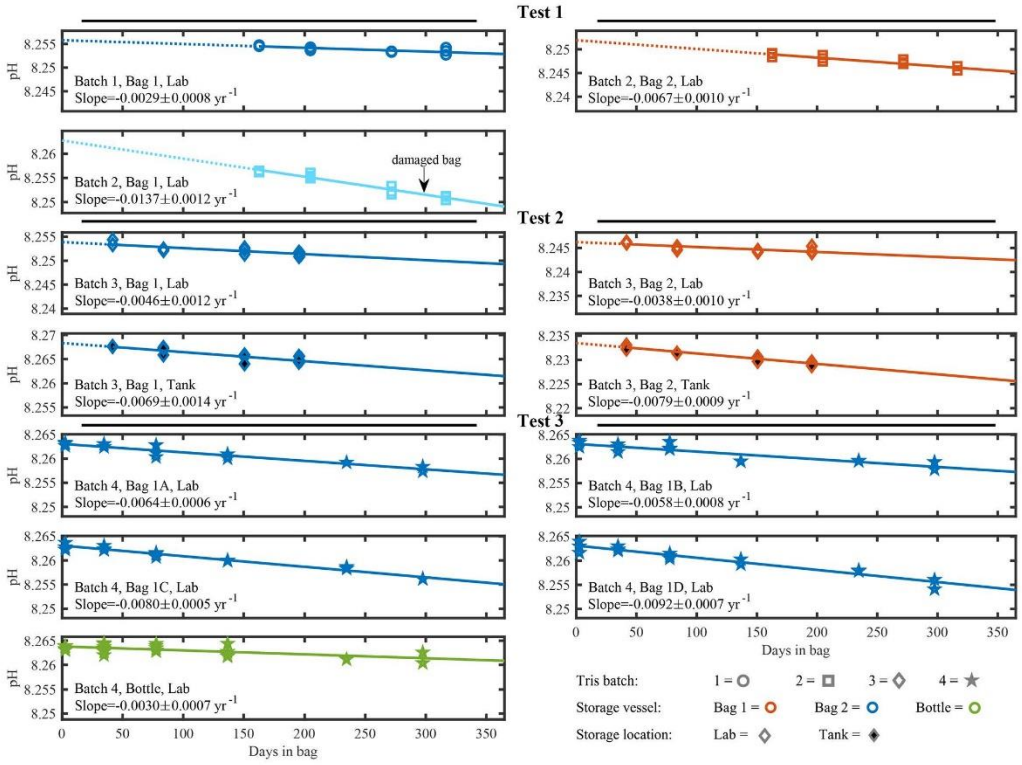

Figure 2. Individual time series of measured pH in tris buffer solutions. Tris batch is indicated by shape, storage vessel by color, and storage location by fill. This marker system is also followed in Fig. A2. The solid line is a linear regression starting at the first included pH measurement and ending 365 d after the tris was bagged. The dotted line illustrates the extrapolation back to 0 d stored in bag when measurements at $t = 0$ do not exist. The range of the y axis scale is fixed at 0.017 pH for all subplots.

piration. Distinguishing between these two theorized sources would require measurements of additional parameters such as dissolved organic carbon.

The pH stability of tris could be improved by reducing either likely source of C_T: gas exchange or microbial respiration. For bags, CO_2 may diffuse through the fittings, gasket, or bag walls, particularly if damaged. The relatively small breaks in the aluminum foil layer caused "batch 2, bag 1, lab" to decrease more than twice as fast as the average bag. Storage bag, fitting, and gasket material, as well as careful handling, are therefore important factors in minimizing gas exchange. For example, silicone is permeable to CO_2 and thus could have been a path of gas exchange into the tris for this experiment. As noted above, Nemzer and Dickson (2005) found an almost negligible change of 0.5 mpH yr^{-1} in bottled tris. Our bottled tris changed at -3.0 mpH yr^{-1} ($n = 10$ bottles measured over 161 d), approximately half the rate of the tris stored in bags. While -3.0 mpH yr^{-1} is near the detection limit of our measurements, it suggests that the bottling protocol used in this study was not as well controlled as that of Nemzer and Dickson (2005). For example, the Dickson lab at Scripps Institution of Oceanography regularly uses an annealing oven to combust all trace organic films that may persist on glass bottles, but in our study, bottles were not annealed. Although bags cannot be annealed, future steps that may be worth consideration to reduce microbial respiration in bags include addition of a biocide to the tris solution, acid cleaning the bags, and using ultraviolet light to remove organics from the ultrapure water used to prepare tris. There are some disadvantages to these proposed steps. Addition of a biocide may not be ideal for use in sensitive environments if the tris is discharged after use and would alter the composition of the solution slightly. While rinsing or prolonged soaking of the bags with an acid may help to remove organics, it is unclear if it would have negative effects on the integrity of the bags. Beyond removing organics on the bag

Table 2. Linear regression statistics from trend lines shown in Figs. 1 and 2. The last row shows the regression statistics for tris from all batches, in either bag type, stored in the lab or test tank. Slope and intercept are shown as mean ±95 % CI. The reported intercept is the regression intercept; when initial pH measurements are available, they differ by less than 0.0003 from regression intercept.

Batch and storage method	Slope (mpH yr^{-1})	Intercept (initial pH)	RMSE (mpH)	r^2	n
Batch 1, bag 1, lab	-2.9 ± 1.7	8.2558 ± 0.0012	0.43	0.59	12
Batch 2, bag 1, lab[a]	-13.7 ± 2.7	8.2627 ± 0.0018	0.61	0.94	11
Batch 2, bag 2, lab	-6.7 ± 2.2	8.2519 ± 0.0015	0.55	0.82	12
Batch 3, bag 1, lab	-4.6 ± 2.7	8.2539 ± 0.0010	0.62	0.62	11
Batch 3, bag 1, tank	-6.9 ± 3.2	8.2683 ± 0.0012	0.73	0.73	11
Batch 3, bag 2, lab	-3.8 ± 2.1	8.2462 ± 0.0008	0.54	0.61	12
Batch 3, bag 2, tank	-7.9 ± 2.1	8.2335 ± 0.0008	0.44	0.92	9
Batch 4, bag 1A, lab	-6.4 ± 1.3	8.2630 ± 0.0005	0.64	0.90	14
Batch 4, bag 1B, lab	-5.8 ± 1.8	8.2631 ± 0.0008	0.91	0.79	15
Batch 4, bag 1C, lab	-8.0 ± 1.0	8.2631 ± 0.0004	0.49	0.96	15
Batch 4, bag 1D, lab	-9.2 ± 1.6	8.2631 ± 0.0007	0.80	0.92	15
Batch 4, bottle, lab	-3.0 ± 1.4	8.2638 ± 0.0005	0.81	0.44	25
All batches, all bags, lab or tank[b]	-5.8 ± 1.1	–	0.72	0.66	126
Calculated tris pH[c]	–	8.2652	–	–	–

[a] Indicates the outlier (batch 2, bag 1, lab) caused by a damaged bag. The outlier, "batch 2, bag 1, lab", was not used in the "All batches, all bags, lab or tank" composite.
[b] In all batches, all bags, lab or tank, the slope was calculated with a linear fit of all (non-outlier) tris measurements. The RMSE is the mean RMSE of all (non-outlier) bag fits.
[c] The calculated tris pH was calculated at 20 °C; however, this calculated pH is 0.0135 higher than equimolal tris as noted above (DelValls and Dickson, 1998).

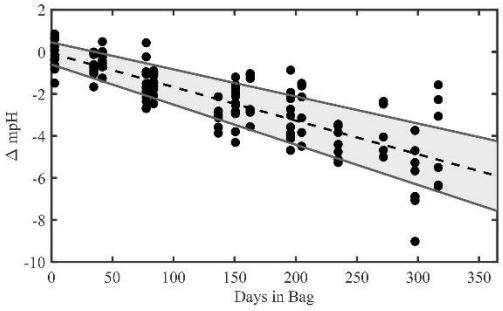

Figure 3. Combined time series of measured pH in tris buffer solutions. The dots represent every measurement made on a (non-damaged) bag of tris. The dotted line is the "all bags, all batches, lab or tank" regression. The grey shaded region is the observational 95 % CI. The CI is intended to estimate the future pH of a tris bag (with known initial pH and an unmeasured bag specific rate of change). The upper and lower bounds are −0.0042 and −0.0076 pH per year, respectively.

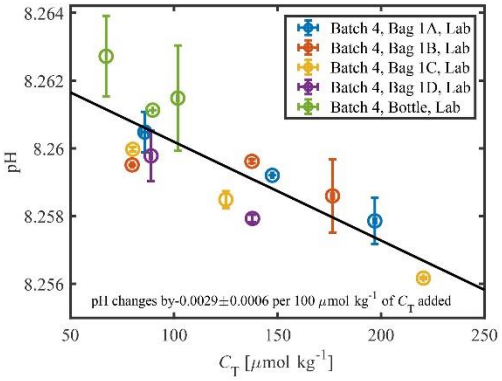

Figure 4. pH plotted against C_T shows a linear relationship between the two parameters in a tris buffer with a slope of −0.0029 pH for every 100 µmol kg^{-1} of C_T added. The measurements shown are from three sampling occurrences between 130–300 d stored on bags and bottles used in Test 3. Only two measurements are shown for "batch 4, bag 1d, lab" because it ran empty before C_T were made.

surfaces, care should be taken to avoid introducing organic contaminates into the tris during the solution preparation and bag-filling procedures to minimize future respiration.

Both bag type 1 and 2 experienced problems with structural integrity during this experiment. A single type 2 bag experienced delamination of exterior bag layers when stored submerged in seawater, causing the eventual tearing and failure of the bag when handling. Bag type 2 was not used in test 3 due to this failure. It should be noted that in other studies which successfully used bag type 2, the bag was submerged in seawater for less time than in this experiment (Sayles and Eck, 2009; Aßmann et al., 2011; Wang et al., 2015). A single bag type 1 had the subtler problem

of small breaks in the aluminum foil bag layer, likely causing an increased pH rate of change. In non-damaged bags, factors such as bag type/bottle, lab/tank storage, or tris batch did not have statistically significant (p value < 0.05) correlations with the pH change of tris (p values 0.12, 0.11 and 0.09, respectively). The results of the ANOVA support that tris can be held in bag type 1 or 2 and stored in a lab or tank, and the pH will change similarly regardless of storage method for up to 300 d. Additional bag types could be tested, such as bags made by Pollution Measurement Corp. used by Lai et al. (2018) or Scholle DuraShield used by Takeshita et al. (2015).

These results suggest that when bags are carefully handled prior to and after filling, tris pH changes are small over time. Specific recommendations for further work include the following: bags must be handled with care and enclosed in protective containers to prevent damage, bags must be rinsed with tris prior to filling, and additional testing is merited to determine sources of and methods to reduce contamination, such as acid washing.

4 Conclusions

This article describes our characterization of the stability of tris buffer in artificial seawater when stored in purportedly gas-impermeable bags. Several different tests, initiated over the course of a year and a half and lasting up to 300 d, exhibited an average decrease of 5.8 mpH yr^{-1}. In comparison, tris stored in standard borosilicate bottles was shown to have a decrease of 3.0 mpH yr^{-1}. For yearlong deployments, an expected pH change of -0.0058 is well below the weather quality threshold of 0.02 pH units. This low rate of change demonstrates the value of bagged tris for in situ validation of autonomous pH sensors (regardless of sensor operating principles), particularly in highly dynamic areas where repeatability of calibration based on discrete samples is challenging. Given the thorough characterization of tris over wide ranges of environmental variables, this contribution can aid in the traceability and intercomparability of pH sensor measurements. While valuable at the current stage of development (as demonstrated by, for example, Lai et al., 2018 and Bresnahan et al., 2021), further development would ideally result in a commercially available bag and filling procedure that can yield a rate of pH change less than the climate threshold of 0.003 per year. This will require further tests to identify the source of CO_2, gas exchange, or microbial respiration, as well as steps to reduce or eliminate these sources.

Periodic measurement of bagged tris in situ would allow for detection of sensor drift. Most in situ pH sensors are deployed in the euphotic zone in coastal areas, typically resulting in expedited biofouling and sedimentation and leading to sensor drift (Bresnahan et al., 2014) that could be identified and potentially corrected. Such periodic calibration/validation would aid in identifying sensor issues and allow for greater consistency and continuity between a time series and planned or vicarious crossovers where an automated calibration can be used to augment or replace pre- and post-deployment calibrations/validations.

Appendix A

Table A1. Detailed information about the specific reagents used to make the tris solution.

Chemical	Manufacture	Part number	Lot number	Batch	Assay	Grade
tris	Fisher Scientific	T395-1	170360	all	99.8 %	Certified ACS
NaCl	Fisher Scientific	S641-212	127252	all	99.0 % to 100.5 %	BP/EP/FCC/USP*
Na_2SO_4	Fisher Scientific	S421-1	134837	all	99.8 %	Certified ACS
KCl	Fisher Scientific	P217-500	174416	all	99.7 %	Certified ACS
$MgCl_2$	Teknova	M0304	M030427E1401	all	1 M	Biotechnology
$CaCl_2$	Amresco	E506–500 mL	0982C098	all	0.95–1.05 M	Biotechnology
HCl	Fisher Scientific	SA48-1	175004	1, 2, 3	0.999 N	Certified
HCl	Fisher Scientific	SA48-1	188768	4	1.003 N	Certified

* Reagent chemicals that meet or surpass specifications of the British Pharmacopeia (BP), European Pharmacopeia (EP), Food Chemicals Codex (FCC), United States Pharmacopeia (USP).

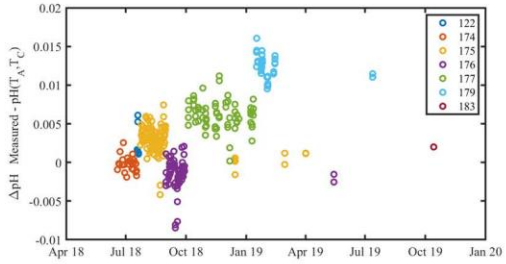

Figure A1. A time series of the residual between measured and calculated CRM pH throughout the experiment. Marker color denotes CRM batch number. There is a clear variability between measured and calculated pH, which is typical of CRM batches (Andrew Dickson, personal communication, 2019). There was no observable systematic drift in the pH system during the experiment. The mean standard deviation of pH measurements within a CRM batch is 0.0016, which is comparable to the 0.0019 reported in Bockmon and Dickson (2015). The same 760 nm absorbance wavelength outlier removal procedure used for tris measurements was applied to CRM measurements.

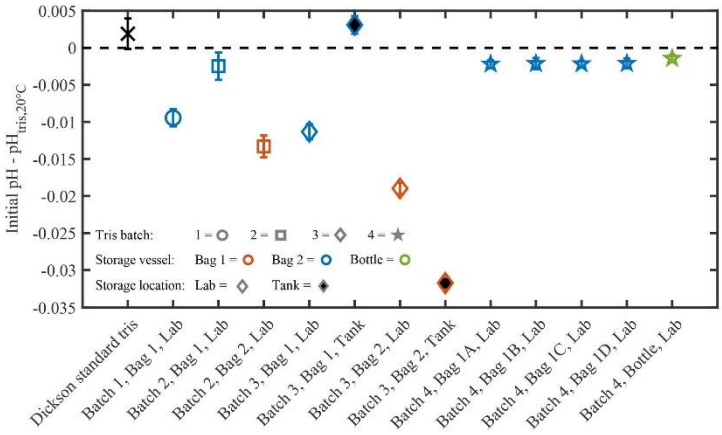

Figure A2. The initial pH residual of each tris bag or bottle measured in this experiment. The initial pH is reported as a residual from the calculated pH at 20 °C. The initial pH was measured directly for tris batch 4 and extrapolated for tris batches 1–3. Additionally, two bottles of Dickson standard tris (show by the black "X") were measured on 12 October 2018. The zero black dashed line is the calculated pH of tris at 20 °C, based upon the measured reagent concentrations (DelValls and Dickson, 1998).

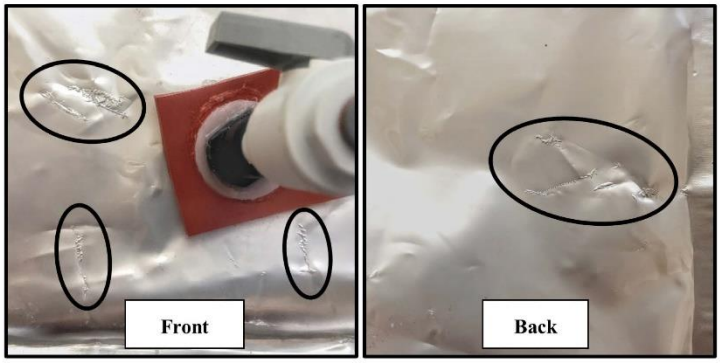

Figure A3. The ovals indicate marks on the exterior of "batch 2, bag 1, lab". These marks appear to be damage to the interior metallic layer, possibly due to creasing of the bag. These marks were not present on any other bag used in this study.

Data availability. pH and C_T data are available via the UC San Diego Library Digital Collections at https://doi.org/10.6075/J0QC022G (Wolfe et al., 2021).

Author contributions. WW performed formal analysis, visualization, and writing (original draft preparation). KS and TW contributed to investigation and writing (review and editing). PB, YT, and TM contributed to funding acquisition, conceptualization, formal analysis, and writing (review and editing).

Competing interests. The authors declare that they have no conflict of interest.

Acknowledgements. We thank May-Linn Paulsen and Andrew Dickson's laboratory for sharing their tris expertise throughout this project. We thank the National Science Foundation Ocean Technology and Interdisciplinary Coordination (NSF-OTIC 1736905 and NSF-OTIC 1736864) and the David and Lucile Packard Foundation for supporting this work.

Financial support. This research has been supported by the National Science Foundation (grant no. 1736905).

Review statement. This paper was edited by Mario Hoppema and reviewed by Jens Daniel Müller and one anonymous referee.

References

ACT: Protocols for the Performance Verification of In Situ pH Sensors, Alliance for Coastal Technologies, Solomons, Maryland, USA, https://doi.org/10.25607/OBP-331, 2012.

Aßmann, S., Frank, C., and Körtzinger, A.: Spectrophotometric high-precision seawater pH determination for use in underway measuring systems, Ocean Sci., 7, 597–607, https://doi.org/10.5194/os-7-597-2011, 2011.

Bandstra, L., Hales, B., and Takahashi, T.: High-frequency measurements of total CO_2: Method development and first oceanographic observations, Mar. Chem., 100, 24–38, https://doi.org/10.1016/j.marchem.2005.10.009, 2006.

Bates, N., Astor, Y., Church, M., Currie, K., Dore, J., Gonzalez-Davila, M., Lorenzoni, L., Muller-Karger, F., Olafsson, J., and Santana-Casiano, J.: A Time-Series View of Changing Surface Ocean Chemistry Due to Ocean Uptake of Anthropogenic CO_2 and Ocean Acidification, J. Oceanogr., 27, 126–141, https://doi.org/10.5670/oceanog.2014.16, 2014.

Bittig, H. C., Steinhoff, T., Claustre, H., Fiedler, B., Williams, N. L., Sauzède, R., Körtzinger, A., and Gattuso, J.-P.: An Alternative to Static Climatologies: Robust Estimation of Open Ocean CO_2 Variables and Nutrient Concentrations From T, S, and O_2 Data Using Bayesian Neural Networks, Front. Mar. Sci., 5, 328, https://doi.org/10.3389/fmars.2018.00328, 2018.

Bockmon, E. E. and Dickson, A. G.: An inter-laboratory comparison assessing the quality of seawater carbon dioxide measurements, Mar. Chem., 171, 36–43, https://doi.org/10.1016/j.marchem.2015.02.002, 2015.

Branch, T. A., DeJoseph, B. M., Ray, L. J., and Wagner, C. A.: Impacts of ocean acidification on marine seafood, Trends Ecol. Evol., 28, 178–186, https://doi.org/10.1016/j.tree.2012.10.001, 2013.

Bresnahan, P. J., Martz, T. R., Takeshita, Y., Johnson, K. S., and LaShomb, M.: Best practices for autonomous measurement of seawater pH with the Honeywell Durafet, Methods in Oceanography, 9, 44–60, https://doi.org/10.1016/j.mio.2014.08.003, 2014.

Bresnahan, P. J., Takeshita, Y., Wirth, T., Martz, T. R., Cyronak, T., Albright, R., Wolfe, K., Warren, J. K., and Mertz, K.: Autonomous in situ calibration of ion-sensitive field effect transistor pH sensors, Limnol. Oceanogr.-Meth., 19, 132–144, https://doi.org/10.1002/lom3.10410, 2021.

Bushinsky, S. M., Takeshita, Y., and Williams, N. L.: Observing changes in ocean carbonate chemistry: our autonomous future, Current Climate Change Reports, 5, 207–220, https://doi.org/10.1007/s40641-019-00129-8, 2019.

Byrne, R. H.: Measuring Ocean Acidification: New Technology for a New Era of Ocean Chemistry, Environ. Sci. Technol., 48, 5352–5360, https://doi.org/10.1021/es405819p, 2014.

Carter, B., Radich, J., Doyle, H., and Dickson, A.: An automated system for spectrophotometric seawater pH measurements, Limnol. Oceanogr.-Meth., 11, 16–27, https://doi.org/10.4319/lom.2013.11.16, 2013.

Carter, B. R., Feely, R. A., Williams, N. L., Dickson, A. G., Fong, M. B., and Takeshita, Y.: Updated methods for global locally interpolated estimation of alkalinity, pH, and nitrate, Limnol. Oceanogr.-Meth., 16, 119–131, https://doi.org/10.1002/lom3.10232, 2018.

Chavez, F., Pennington, J. T., Michisaki, R., Blum, M., Chavez, G., Friederich, J., Jones, B., Herlien, R., Kieft, B., Hobson, B., Ren, A., Ryan, J., Sevadjian, J., Wahl, C., Walz, K., Yamahara, K., Friederich, G., and Messié, M.: Climate Variability and Change: Response of a Coastal Ocean Ecosystem, J. Oceanogr., 30, 128–145, https://doi.org/10.5670/oceanog.2017.429, 2017.

Cooley, S. R. and Doney, S. C.: Anticipating ocean acidification's economic consequences for commercial fisheries, Environ. Res. Lett., 4, 8, https://doi.org/10.1088/1748-9326/4/2/024007, 2009.

DeGrandpre, M. D., Spaulding, R. S., Newton, J. O., Jaqueth, E. J., Hamblock, S. E., Umansky, A. A., and Harris, K. E.: Considerations for the measurement of spectrophotometric pH for ocean acidification and other studies, Limnol. Oceanogr.-Meth., 12, 830–839, https://doi.org/10.4319/lom.2014.12.830, 2014.

DelValls, T. and Dickson, A.: The pH of buffers based on 2-amino-2-hydroxymethyl-1,3-propanediol ('tris') in synthetic sea water, Deep-Sea Res. Pt. I, 45, 1541–1554, https://doi.org/10.1016/S0967-0637(98)00019-3, 1998.

Dickson, A. G.: An exact definition of total alkalinity and a procedure for the estimation of alkalinity and total inorganic carbon from titration data, Deep-Sea Res. Pt. I, 28, 609–623, 1981.

Dickson, A. G.: pH buffers for sea-water media based on the total hydrogen-ion concentration scale, Deep-Sea Res. Pt. I, 40, 107–118, https://doi.org/10.1016/0967-0637(93)90055-8, 1993.

Dickson, A. G.: Reference materials for oceanic CO_2 measurements, J. Oceanogr., 14, 21–22, 2001.

Dickson, A. G., Sabine, C. L., and Christian, J. R.: Guide to Best Practices for Ocean CO_2 Measurements, PICES Special Publication 3, North Pacific Marine Science Organization, Sidney, British Columbia, 191 pp., 2007.

Doney, S. C., Fabry, V. J., Feely, R. A., and Kleypas, J. A.: Ocean acidification: the other CO_2 problem, Annu. Rev. Mar. Sci., 1, 169–192, https://doi.org/10.1146/annurev.marine.010908.163834, 2009.

Doney, S. C., Busch, D. S., Cooley, S. R., and Kroeker, K. J.: The impacts of ocean acidification on marine ecosystems and reliant human communities, Annu. Rev. Env. Resour., 45, 83–112, https://doi.org/10.1146/annurev-environ-012320-083019, 2020.

Friederich, G., Walz, P., Burczynski, M., and Chavez, F.: Inorganic carbon in the central California upwelling system during the 1997–1999 El Niño–La Niña event, Prog. Oceanogr., 54, 185–203, https://doi.org/10.1016/S0079-6611(02)00049-6, 2002.

Hales, B., Takahashi, T., and Bandstra, L.: Atmospheric CO_2 uptake by a coastal upwelling system, Global Biogeochem. Cy., 19, GB1009, https://doi.org/10.1029/2004gb002295, 2005.

Johnson, K. S., Jannasch, H. W., Coletti, L. J., Elrod, V. A., Martz, T. R., Takeshita, Y., Carlson, R. J., and Connery, J. G.: Deep-Sea DuraFET: A Pressure Tolerant pH Sensor Designed for Global Sensor Networks, Anal. Chem., 88, 3249–3256, https://doi.org/10.1021/acs.analchem.5b04653, 2016.

Johnson, K. S., Plant, J. N., Coletti, L. J., Jannasch, H. W., Sakamoto, C. M., Riser, S. C., Swift, D. D., Williams, N. L., Boss, E., Haëntjens, N., Talley, L. D., and Sarmiento, J. L.: Biogeochemical sensor performance in the SOCCOM profiling float array, J. Geophys. Res.-Oceans, 122, 6416–6436, https://doi.org/10.1002/2017jc012838, 2017.

Karl, D. M.: Oceanic ecosystem time-series programs: Ten lessons learned, J. Oceanogr., 23, 104–125, https://doi.org/10.5670/oceanog.2010.27, 2010.

Lai, C.-Z., DeGrandpre, M. D., and Darlington, R. C.: Autonomous Optofluidic Chemical Analyzers for Marine Applications: Insights from the Submersible Autonomous Moored Instruments (SAMI) for pH and pCO_2, Front. Mar. Sci., 4, 438, https://doi.org/10.3389/fmars.2017.00438, 2018.

Liu, X. W., Patsavas, M. C., and Byrne, R. H.: Purification and Characterization of meta-Cresol Purple for Spectrophotometric Seawater pH Measurements, Environ. Sci. Technol., 45, 4862–4868, https://doi.org/10.1021/es200665d, 2011.

Martz, T. R., Daly, K. L., Byrne, R. H., Stillman, J. H., and Turk, D.: Technology for ocean acidification research needs and availability, J. Oceanogr., 28, 40–47, https://doi.org/10.5670/oceanog.2015.30, 2015.

McLaughlin, K., Dickson, A., Weisberg, S. B., Coale, K., Elrod, V., Hunter, C., Johnson, K. S., Kram, S., Kudela, R., Martz, T., Negrey, K., Passow, U., Shaughnessy, F., Smith, J. E., Tadesse, D., Washburn, L., and Weis, K. R.: An evaluation of ISFET sensors for coastal pH monitoring applications, Regional Studies in Marine Science, 12, 11–18, https://doi.org/10.1016/j.rsma.2017.02.008, 2017.

Müller, J., Bastkowski, F., Sander, B., Seitz, S., Turner, D., Dickson, A., and Rehder, G.: Metrology for pH Measurements in Brackish Waters-Part 1: Extending Electrochemical pH(T) Measurements of TRIS Buffers to Salinities 5–20, Fron. Mar. Sci., 5, 176, https://doi.org/10.3389/fmars.2018.00176, 2018.

Müller, J. D. and Rehder, G.: Metrology of pH Measurements in Brackish Waters – Part 2: Experimental Characterization of Purified meta-Cresol Purple for Spectrophotometric pHT Measurements, Frontiers in Marine Science, 5, 177, https://doi.org/10.3389/fmars.2018.00177, 2018.

Nemzer, B. and Dickson, A.: The stability and reproducibility of Tris buffers in synthetic seawater, Mar. Chem., 96, 237–242, https://doi.org/10.1016/j.marchem.2005.01.004, 2005.

Newton, J., Feely, R., Jewett, E., Williamson, P., and Mathis, J.: Global Ocean Acidification Observing Network: Requirements and Governance Plan, 2nd Edn., Global ocean acidification observing network, Seattle, Washington, USA, 2015.

O'Sullivan, D. W. and Millero, F. J.: Continual measurement of the total inorganic carbon in surface seawater, Mar. Chem., 60, 75–83, https://doi.org/10.1016/s0304-4203(97)00079-0, 1998.

Okazaki, R. R., Sutton, A. J., Feely, R. A., Dickson, A. G., Alin, S. R., Sabine, C. L., Bunje, P. M. E., and Virmani, J. I.: Evaluation of marine pH sensors under controlled and natural conditions for the Wendy Schmidt Ocean Health XPRIZE, Limnol. Oceanogr.-Meth., 15, 586–600, https://doi.org/10.1002/lom3.10189, 2017.

Paulsen, M. L. and Dickson, A. G.: Preparation of 2-amino-2-hydroxymethyl-1, 3-propanediol (TRIS) pHT buffers in synthetic seawater, Limnol. Oceanogr.-Meth., 18, 504–515, https://doi.org/10.1002/lom3.10383, 2020.

Papadimitriou, S., Loucaides, S., Rérolle, V., Achterberg, E. P., Dickson, A. G., Mowlem, M., and Kennedy, H.: The measurement of pH in saline and hypersaline media at sub-zero temperatures: Characterization of Tris buffers, Mar. Chem., 184, 11–20, https://doi.org/10.1016/j.marchem.2016.06.002, 2016.

Pierrot, D., Neill, C., Sullivan, K., Castle, R., Wanninkhof, R., Lüger, H., Johannessen, T., Olsen, A., Feely, R. A., and Cosca, C. E.: Recommendations for autonomous underway pCO_2 measuring systems and data-reduction routines, Deep-Sea Res. Pt. II, 56, 512–522, https://doi.org/10.1016/j.dsr2.2008.12.005, 2009.

Rodriguez, C., Huang, F., and Millero, F. J.: The partial molal volume and compressibility of Tris and Tris–HCl in water and 0.725 m NaCl as a function of temperature, Deep-Sea Res. Pt. I, 104, 41–51, https://doi.org/10.1016/j.dsr.2015.06.008, 2015.

Sabine, C., Sutton, A., McCabe, K., Lawrence-Slavas, N., Alin, S., Feely, R., Jenkins, R., Maenner, S., Meinig, C., and Thomas, J.: Evaluation of a new carbon dioxide system for autonomous surface vehicles, J. Atmos. Ocean. Tech., 37, 1305–1317, https://doi.org/10.1175/JTECH-D-20-0010.1, 2020.

Sayles, F. L. and Eck, C.: An autonomous instrument for time series analysis of TCO_2 from oceanographic moorings, Deep-Sea Res. Pt. I, 56, 1590–1603, https://doi.org/10.1016/j.dsr.2009.04.006, 2009.

Seidel, M. P., DeGrandpre, M. D., and Dickson, A. G.: A sensor for in situ indicator-based measurements of seawater pH, Mar. Chem., 109, 18–28, https://doi.org/10.1016/j.marchem.2007.11.013, 2008.

Sloyan, B. M., Wanninkhof, R., Kramp, M., Johnson, G. C., Talley, L. D., Tanhua, T., McDonagh, E., Cusack, C., O'Rourke, E., McGovern, E., Katsumata, K., Diggs, S., Hummon, J., Ishii, M., Azetsu-Scott, K., Boss, E., Ansorge, I.,

Perez, F. F., Mercier, H., Williams, M. J. M., Anderson, L., Lee, J. H., Murata, A., Kouketsu, S., Jeansson, E., Hoppema, M., and Campos, E.: The Global Ocean Ship-Based Hydrographic Investigations Program (GO-SHIP): A Platform for Integrated Multidisciplinary Ocean Sci., Front. Mar. Sci., 6, 445, https://doi.org/10.3389/fmars.2019.00445, 2019.

Spaulding, R. S., DeGrandpre, M. D., Beck, J. C., Hart, R. D., Peterson, B., De Carlo, E. H., Drupp, P. S., and Hammar, T. R.: Autonomous in Situ Measurements of Seawater Alkalinity, Environ. Sci. Technol., 48, 9573–9581, https://doi.org/10.1021/es501615x, 2014.

Sutton, A. J., Feely, R. A., Maenner-Jones, S., Musielwicz, S., Osborne, J., Dietrich, C., Monacci, N., Cross, J., Bott, R., Kozyr, A., Andersson, A. J., Bates, N. R., Cai, W.-J., Cronin, M. F., De Carlo, E. H., Hales, B., Howden, S. D., Lee, C. M., Manzello, D. P., McPhaden, M. J., Meléndez, M., Mickett, J. B., Newton, J. A., Noakes, S. E., Noh, J. H., Olafsdottir, S. R., Salisbury, J. E., Send, U., Trull, T. W., Vandemark, D. C., and Weller, R. A.: Autonomous seawater pCO_2 and pH time series from 40 surface buoys and the emergence of anthropogenic trends, Earth Syst. Sci. Data, 11, 421–439, https://doi.org/10.5194/essd-11-421-2019, 2019.

Takeshita, Y., Frieder, C. A., Martz, T. R., Ballard, J. R., Feely, R. A., Kram, S., Nam, S., Navarro, M. O., Price, N. N., and Smith, J. E.: Including high-frequency variability in coastal ocean acidification projections, Biogeosciences, 12, 5853–5870, https://doi.org/10.5194/bg-12-5853-2015, 2015.

Takeshita, Y., McGillis, W., Briggs, E. M., Carter, A. L., Donham, E. M., Martz, T. R., Price, N. N., and Smith, J. E.: Assessment of net community production and calcification of a coral reef using a boundary layer approach, J. Geophys. Res.-Oceans, 121, 5655–5671, https://doi.org/10.1002/2016JC011886, 2016.

Takeshita, Y., Martz, T. R., Coletti, L. J., Dickson, A. G., Jannasch, H. W., and Johnson, K. S.: The effects of pressure on pH of Tris buffer in synthetic seawater, Mar. Chem., 188, 1–5, https://doi.org/10.1016/j.marchem.2016.11.002, 2017.

Takeshita, Y., Johnson, K. S., Martz, T. R., Plant, J. N., and Sarmiento, J. L.: Assessment of Autonomous pH Measurements for Determining Surface Seawater Partial Pressure of CO_2, J. Geophys. Res.-Oceans, 123, 4003–4013, https://doi.org/10.1029/2017jc013387, 2018.

Takeshita, Y., Warren, J. K., Liu, X., Spaulding, R. S., Byrne, R. H., Carter, B. R., DeGrandpre, M. D., Murata, A., and Watanabe, S.: Consistency and stability of purified meta-cresol purple for spectrophotometric pH measurements in seawater, Mar. Chem., in review, 2021.

Tilbrook, B., Jewett, E. B., DeGrandpre, M. D., Hernandez-Ayon, J. M., Feely, R. A., Gledhill, D. K., Hansson, L., Isensee, K., Kurz, M. L., Newton, J. A., Siedlecki, S. A., Chai, F., Dupont, S., Graco, M., Calvo, E., Greeley, D., Kapsenberg, L., Lebrec, M., Pelejero, C., Schoo, K. L., and Telszewski, M.: An Enhanced Ocean Acidification Observing Network: From People to Technology to Data Synthesis and Information Exchange, Frontiers in Marine Science, 6, 21, https://doi.org/10.3389/fmars.2019.00337, 2019.

Wang, Z. A., Sonnichsen, F. N., Bradley, A. M., Hoering, K. A., Lanagan, T. M., Chu, S. N., Hammar, T. R., and Camilli, R.: In Situ Sensor Technology for Simultaneous Spectrophotometric Measurements of Seawater Total Dissolved Inorganic Carbon and pH, Environ. Sci. Technol., 49, 4441–4449, https://doi.org/10.1021/es504893n, 2015.

Wang, Z. A., Moustahfid, H., Mueller, A. V., Michel, A. P. M., Mowlem, M., Glazer, B. T., Mooney, T. A., Michaels, W., McQuillan, J. S., Robidart, J. C., Churchill, J., Sourisseau, M., Daniel, A., Schaap, A., Monk, S., Friedman, K., and Brehmer, P.: Advancing Observation of Ocean Biogeochemistry, Biology, and Ecosystems With Cost-Effective in situ Sensing Technologies, Frontiers in Marine Science, 6, 22, https://doi.org/10.3389/fmars.2019.00519, 2019.

Williams, N. L., Juranek, L. W., Johnson, K. S., Feely, R. A., Riser, S. C., Talley, L. D., Russell, J. L., Sarmiento, J. L., and Wanninkhof, R.: Empirical algorithms to estimate water column pH in the Southern Ocean, Geophys. Res. Lett., 43, 3415–3422, https://doi.org/10.1002/2016gl068539, 2016.

Wolfe, W. H., Shipley, K. M., Bresnahan, P. J., Takeshita, Y., Wirth, T., and Martz, T. R.: Data from: Technical note: stability of tris pH buffer in artificial seawater stored in bags, UC San Diego Library Digital Collections, https://doi.org/10.6075/J0QC022G, 2021.

CHAPTER 2

Ocean Acidification in the Southern California Current: A 37 Year Time Series

Abstract

Long-term ocean time series have proven to be the most robust approach for direct observation of climate change processes such as Ocean Acidification. The California Cooperative Oceanic Fisheries Investigations (CalCOFI) program has collected quarterly samples for seawater inorganic carbon since the 1980's. The longest, most consistent, sampling of surface waters is at CalCOFI line 90 station 90 from 1984–present, with a gap from 2002–2008. Here we present the first analysis of this 37- year time series. Station 90.90 exhibits an unambiguous acidification signal in agreement with the global surface ocean (decrease in pH of -0.0015 ± 0.0001 yr^{-1}), as well as a distinct seasonal cycle. The long-term trend in total dissolved inorganic carbon (0.71 ± 0.04 µmol kg^{-1} yr^{-1}) drives a corresponding rise in pCO_2 (1.57 ± 0.09 µatm yr^{-1}). On the seasonal scale, temperature and total dissolved inorganic carbon influence variability in the carbonate system with similar magnitudes.

Plain Language Summary

Samples of seawater inorganic carbon have been collected offshore of Southern California since the 1980's. The surface water there shows a clear trend of ocean acidification. Ocean acidification is a decrease in the pH of seawater, which affects seawater chemistry and marine organisms, especially marine calcifiers. The rate of acidification matches other locations in the open ocean where this rate has been measured. This result helps confirm that the rate of

ocean acidification is caused by increasing atmospheric carbon dioxide, as scientists have previously predicted.

2.1 Introduction

Atmospheric carbon dioxide (CO_2) levels today are nearly 50% higher than during pre-industrial times and are predicted to increase at similar or accelerating rates over the next hundred years (Friedlingstein et al., 2022). The ocean has taken up roughly a quarter of the total anthropogenic emissions (Gruber et al., 2019), resulting in decreased ocean pH and associated changes in carbonate system equilibrium due to ocean acidification (OA) (Doney et al., 2020). Globally, the ocean pH has decreased by ~0.1 since the beginning of the Industrial Revolution and is projected to drop by as much over the next 60 years (Fassbender et al., 2021). These trends have been modeled (Turi et al., 2016) and detected (Chavez et al., 2017) in the California Current System.

The California Oceanic Fisheries Investigation (CalCOFI) program was formed in 1949 to study the pelagic ecosystem of the Southern California Current (SCC) in response to the collapse of an economically important sardine fishery (Hewitt, 1988). The original sampling design included quarterly cruises making a grid pattern of profiles to 500 meters of physically and biologically important parameters such as temperature, salinity, oxygen, nutrients, and zooplankton biomass. Observations of carbonate chemistry were incorporated in 1983 when Charles David Keeling initiated time series measurements at Hawaii, Bermuda (N. Bates et al., 2014) and the SCC. The most continuous time series in the SCC is surface waters (0–20 m) at CalCOFI Line 90 Station 90 (station 90.90). Observations were made between 1984–present, with a gap from 2002–2008. The long-term trends established by this work add a direct

observation of ocean acidification and climate change to the few existing time series of ocean carbonate chemistry (Bates et al., 2014).

2.2 Methods

2.2.1 Sampling at station 90.90

CalCOFI station 90.90 is located at 31.4°N, 122°W, approximately 450 km from shore, with a water depth of approximately 4000 m. Due to its location in the western California Current, station 90.90 lies near the eastern edge of the North Pacific Subtropical Gyre exhibiting an oligotrophic open-ocean regime (Checkley & Barth, 2009) (the mean phosphate and nitrate concentrations were 0.3 μM and 0.1 μM respectively in sea surface samples with inorganic carbon measurements). All observations discussed here were collected near the sea surface (0–20 m), with an average depth of 5.2 m. Although a small subset of these measurements (2009–2015) have been publicly available for several years (see open research), the remaining 22 years of observations have not been published until this work.

Observations used in this work cover the period 1984–2021 with a gap from 2002–2008. Bottle samples were collected on quarterly CalCOFI cruises at station 90.90. Mercuric chloride was added (as a biocide and preservative) and the samples were sealed and stored in borosilicate glass bottles following best practices (Dickson et al., 2007). Storage times ranged from one month to multiple years before analysis.

2.2.2 Analytical methods

Bottle samples were analyzed for total alkalinity (A_T) and dissolved inorganic carbon (C_T). A_T was measured using a closed cell titration (Bradshaw et al., 1981) until 1992 and an

open cell titration (Dickson et al., 2003) after 1992. C_T was measured using vacuum extraction and manometry (Lueker, 1998; Lueker et al., 2000) until 1992, coulometry (Johnson et al., 1987) from 1992–2015 and an infrared (IR) analyzer (Goyet & Snover, 1993; O'Sullivan & Millero, 1998) after 2015. Accuracy of A_T and C_T is estimated to range from 2-5 μmol kg^{-1} and 1-3 μmol kg^{-1}, respectively, over the dataset.

2.2.3 Calculating additional carbonate chemistry parameters

The partial pressure of CO_2 in seawater (pCO_2), pH, carbonate ion concentration ($[CO_3^{2-}]$), saturation states of aragonite and calcite ($\Omega_{aragonite}$, $\Omega_{calcite}$), and Revelle Factor ($\partial \ln[CO_2]/\partial \ln C_T$), were calculated in MATLAB using CO2SYS (van Heuven et al., 2011) from A_T, C_T, temperature and salinity with coefficients recommended by Lueker et al. (2000). A_T and C_T were salinity normalized (indicated by nA_T and nC_T,) to the average salinity of the time series (33.3, n = 107).

2.2.4 Seasonal cycle

Monthly binning is a common approach used to extract the seasonal cycle (Bates et al., 2012; Takahashi et al., 2009). In this work the 12-month climatology was computed from quarterly observations using a 3-month sliding bin. Where, for example, April is represented as the average of all observations from March, April, and May. Due to variability in the scheduling of CalCOFI cruises, there are some observations in each month before binning (Figure 2.S1). The resulting 12-month climatology was used to seasonally detrend the observations. The climatology was used to calculate the relative contributions of salinity, temperature, A_T, and C_T to the seasonal cycle of pCO_2. The climatology of a single parameter and the average of the

remaining three were used with CO2SYS to calculate individual contributions, at time t, as follows,

$$\Delta pCO_{2,t}^{\text{temperature}} = pCO_2\left(\overline{A_T}, \overline{C_T}, \overline{S}, T_t\right) - \overline{pCO_2} \quad (2.1)$$

$$\Delta pCO_{2,t}^{\text{salinity}} = pCO_2\left(\overline{A_T}, \overline{C_T}, S_t, \overline{T}\right) - \overline{pCO_2} \quad (2.2)$$

$$\Delta pCO_{2,t}^{C_T} = pCO_2\left(\overline{A_T}, C_{T_t}, \overline{S}, \overline{T}\right) - \overline{pCO_2} \quad (2.3)$$

$$\Delta pCO_{2,t}^{A_T} = pCO_2\left(A_{T_t}, \overline{C_T}, \overline{S}, \overline{T}\right) - \overline{pCO_2} \quad (2.4)$$

The same procedure was used to calculate the contribution to the long-term trends in pCO_2 (Figure 2.S2).

2.2.5 Data processing

Model I linear regression (function fitlm in MATLAB) was performed on observations (Figure 2.S3, Table 2.S1) and seasonally detrended data (Table 2.1). The slope, error, r^2, *p*-value and *n* values are reported. Power spectral density (PSD) analysis was performed using Lomb-Scargle periodograms with the 'plomb' function in MATLAB (Figure 2.S3) (VanderPlas, 2018). Observations were also compared to empirically derived proxy estimates "ESPER_MIXED" (Carter et al., 2021; Morgan, 1994; van Heuven et al., 2011) and to a climatology (Landschützer et al., 2020) derived from data sources (Global Ocean Data Analysis Project; GLODAP, The Surface Ocean CO_2 Atlas; SOCAT) independent from the CalCOFI CO_2 record.

2.3 Results and discussion

The time series exhibits an unambiguous ocean acidification signal in agreement with the global surface ocean (decrease in pH of ~0.0015 yr, Figure 2.1, Table 2.1), as well as a distinct seasonal cycle (Figure 1, right column). The sea surface pCO_2 at station 90.90 is driven by

increasing total inorganic carbon (C_T) at a decadal scale and a combination of C_T and temperature at a seasonal scale. There was no significant trend in ocean temperature, salinity, A_T or nA_T at station 90.90. However, longer term near shore studies in the CCE have shown increasing temperatures shoreward of the California Current (Rasmussen et al., 2020).

Natural variability at station 90.90 along with the six-year gap in data (resulting from, e.g., year-to-year differences in the proportion of North Pacific Gyre vs California Current water masses) confound the identification of long period patterns such as El Nino, or the Pacific Decadal Oscillation. Perhaps the most obvious anomaly is a perturbation in temperature and salinity during 2014–2016 (Figure 2.1). This anomaly may be a result of the 2014/15 North Pacific marine heatwave, the strong 2015/16 El Nino, or a combination of the two (Di Lorenzo & Mantua, 2016; Jacox et al., 2016; Lilly et al., 2019).

Power spectral density (PSD) analysis of the detrended time series showed the presence of a strong annual signal in temperature and C_T, as well as in all calculated carbonate system variables (Figure 2.S4). While temporal anomalies in this time series may be worthy of further investigation, the goal of this work is to present the 1st order OA trend, mean seasonal cycle, and to finally make the quality-controlled time series publicly available. Follow-on work with this time series may consider implementing gap-filling techniques for the 2002-2008 period (Vance et al., 2022) and alternative modes of trend detection such as simultaneous fitting of harmonics and underlying trends as well as development of a mixed layer carbon budget at station 90.90.

For comparison to observations presented here, we estimate C_T and A_T with two sets of predictor variables using the MATLAB function ESPER_Mixed. First, we used temperature and salinity, second, we included all available predictor variables, temperature, salinity, phosphate, nitrate, silicic acid, and oxygen (in addition to latitude, longitude, depth, and year in both cases).

Using temperature and salinity, the comparison for C_T showed measurements were 6 ± 15 μmol kg^{-1} (mean ± std) higher than ESPER with less variability (Figure 2.S5). The comparison of A_T showed measurements were 4 ± 4 μmol kg^{-1} (mean ± std) lower than ESPER with similar variability (Figure 2.S6). Both C_T and A_T are significantly different than the ESPER predictions ($p<<0.05$).

When using all available predictor variables, the comparison for C_T showed measurements were 0.1 ± 6 μmol kg^{-1} (mean ± std) higher than ESPER with similar variability (Figure S7). The comparison of A_T showed measurements were 3 ± 4 μmol kg^{-1} (mean ± std) different than ESPER with similar variability (Figure S8). Only A_T was significantly different than the ESPER predictions ($p<<0.05$). It is unsurprising that the ESPER more accurately predicted C_T and A_T when using all available predictor variables.

There was no significant trend in the A_T residuals when using either set of predictor variables. However, there was a significant trend in the C_T residuals in both sets of predictor variables. Indicating the ESPER predicted C_T trend was 0.3 μmol kg^{-1} yr^{-1} higher than the observed trend. Both sets of predictor variables resulted in the same trend, albeit with a higher standard deviation when using fewer predictors. There appears to be a discrepancy between the OA trend observed and the trend built into ESPER. There appears to be a decrease in phosphate over the time series, which could have impacted the trend one of the ESPER predictions, but not both. The decrease in phosphate may signal a change in biogeochemistry of the region and is possibly worth further investigation.

The main drivers of pCO_2 seasonality are temperature and C_T, with little contribution from A_T or salinity (Figure 2.2). Each contributes 57%, 34%, 8%, and 1% of the pCO_2 seasonality, respectively. The effects of temperature and C_T on pCO_2 are out of phase, which

cancels out much of their impact on pCO_2. In turn, C_T is driven by gas exchange, net ecosystem metabolism (NEM) and mixing (Chapter 3). On a decadal timescale, increasing C_T is the only significant driver of pCO_2, contributing 93% (Figure 2.S2). Although it is beyond the scope of this work, a mixed layer carbon budget at station 90.90 is the subject of a separate manuscript in progress.

The sea surface pCO_2 trend matches the atmospheric CO_2 trend at Mauna Loa over the same timeframe, although the sea surface pCO_2 has significantly greater variability, a feature common to all ocean time series (Figure 2.S9) (C. Keeling et al., 2005; R. Keeling & C. Keeling, 2017). The measured seasonal cycle of sea surface pCO_2 matches reasonably well with the grid point corresponding to station 90.90 extracted from the climatology of Landschützer et al. (2020) (Figure 2.S10). The monthly pCO_2 minimum is similar (less than 2 μatm different) but the measured seasonal cycle has a larger peak-trough amplitude (42 compared to 29 μatm) and a phase shifted maximum pCO_2 that appears to lead the climatology by 2 months (July vs. September). When corrected to a common reference year of 2006 (using the observed trend to adjust station 90.90 mean year of 2002 to Landschützer et al. mean year of 2006) the mean difference is +6 μatm (observed – Landschützer et al. climatology). This difference may be explained by the greater amplitude in the station 90.90 monthly data. However, neither of the seasonal cycles are corrected to a reference year and the mean measurement year is 4 years apart (observed, 2002; Landschützer et al., 2006). Subsequent analysis of the carbon budget including air-sea flux will be used to determine the significance of both the phase, amplitude, and mean difference between the observations and climatology at this location. An important next step should be assimilating the data presented in this work into empirical algorithms and climatology products of the CO_2 system at the station 90.90 study site.

While we point out discrepancies between previously published estimates or climatologies and the observations presented in this work, the commonly used tools are not focused specifically on station 90.90 and remain valuable for comparisons to this time series and the global ocean.

2.4 Conclusions

This work establishes station 90.90 as one of very few long-standing marine inorganic carbon time series, one of five started in the 1980's, and the earliest in the Pacific (Bates et al., 2014). Over 37 years, the sea surface at station 90.90 has decreased in pH by 0.0015 yr^{-1} and increased in pCO_2 and C_T by 1.6 μatm yr^{-1} and 0.7 μmol kg^{-1} yr^{-1}. respectively. These trends are in close agreement with other open ocean trends documented in the Central North Pacific, and Sargasso Sea (N. Bates et al., 2014). Use of empirical proxy relationships introduces a bias in carbonate system estimates, underscoring the need for sustained measurements. We also report a strong annual cycle in carbonate system variables, with dominant control of the seasonal cycle by temperature and total inorganic carbon. In contrast, the long-term secular trend in carbonate system variables is directly related to an increase in total inorganic carbon.

2.5 Open research

All of the inorganic carbon samples collected on CalCOFI cruises will become publicly available through the CalCOFI data portal, https://calcofi.org/data/oceanographic-data/dic/, after a subsequent publication in progress and the defense of WHW's Ph.D. The atmospheric CO_2 data from Mauna Loa are from Dr. Ralph Keeling, Scripps Institution of Oceanography (scrippsco2.ucsd.edu/data/atmospheric_co2/primary_mlo_co2_record/, DOI:

http://doi.org/10.6075/J08W3BHW) or Dr. Pieter Tans, National Oceanic and Atmospheric Administration, Global Monitoring Laboratory (gml.noaa.gov/ccgg/trends/).

2.6 Acknowledgments

Measurements have been supported by a variety of funding sources including NSF (California Current Ecosystem Long Term Ecological Research, award OCE-16-37632), and NOAA Climate Program Office. The crew and scientists on CalCOFI cruises, and the people who made these measurements over the last 37 years are too numerous to list here but this work would not have been possible without their efforts. Guy Emanuele aided in locating historical data.

Chapter 2, in full, is currently being prepared for submission for publication of the material in American Geophysical Union, Geophysical Research Letters, 2022, Wolfe, W. H., Martz, T. R., Dickson, A. G., Goericke, Ralf, Ohman, M. D. (2021). Ocean Acidification in the Southern California Current: A 37 Year Time Series. The dissertation author was the primary researcher and author of this paper.

2.7 Figures and tables

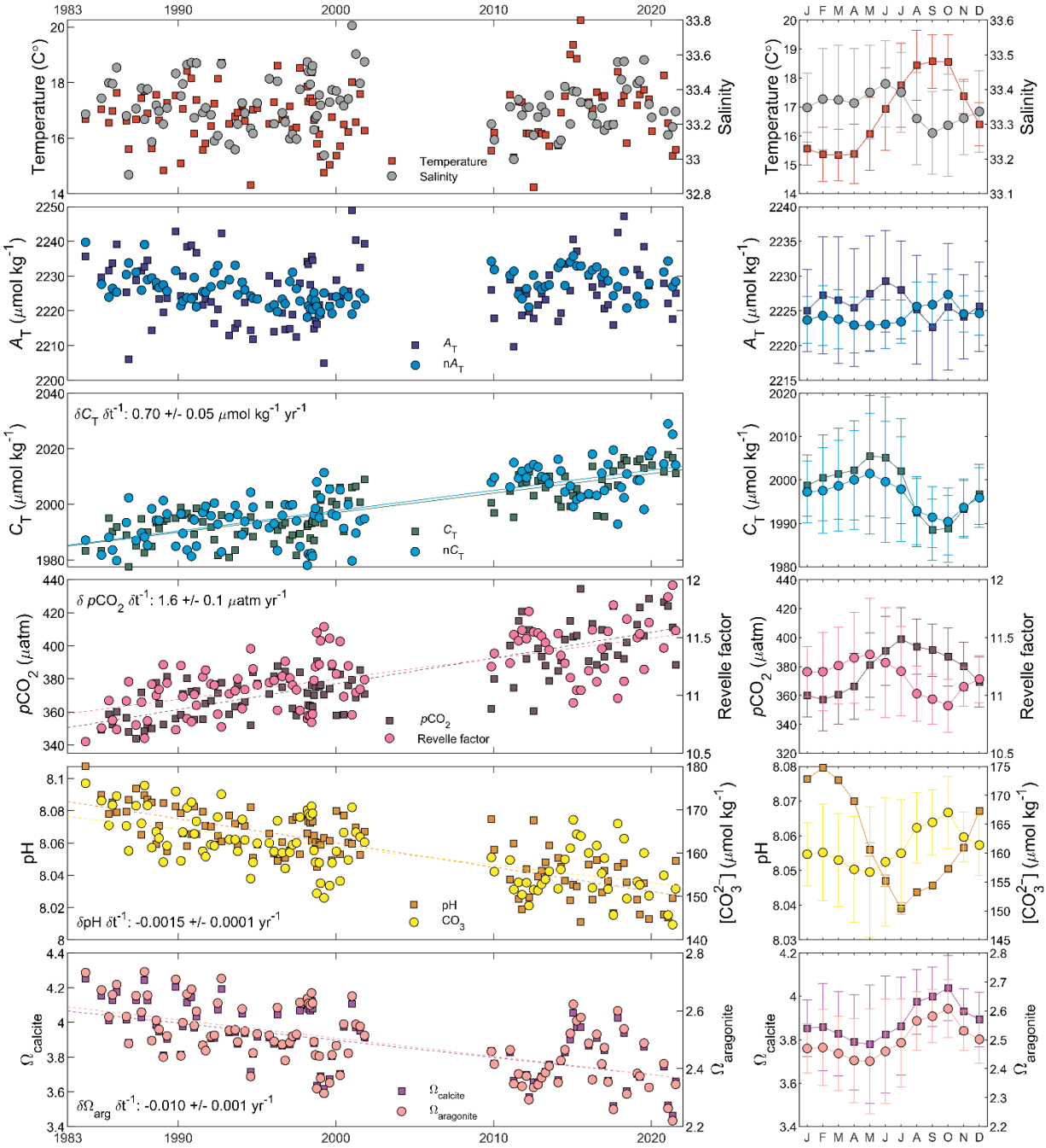

Figure 2.1. Quarterly observations (Left) and average seasonal cycles (Right). "n" indicates salinity normalization to the mean salinity (33.3). a) Temperature and salinity, b) Total alkalinity (A_T) and nA_T, c) Total inorganic carbon (C_T) and nC_T, d) pCO_2 (µatm) and Revelle factor, e) pH and CO_3, and f) $\Omega_{calcite}$ and $\Omega_{aragonite}$. There is no significant trend in temperature, salinity or A_T ($p > 0.35$). The ocean acidification trend (shown in panels c-f) is within the range of observations made at other time series sites (N. Bates et al., 2014). Regression statistics for time series are shown in Table 1. Descriptive statistics for seasonal cycles are shown in Table 2.S2.

Table 2.1. Regression statistics of sea surface hydrography and seawater carbon chemistry (from Figure 2.1).

Parameter	Slope	standard error	units	*n*	r^2	*p*-value
Hydrography						
Temperature	0.0078	0.009	°C yr^{-1}	107	0.0070	0.3928
Salinity	-0.0005	0.0013	yr^{-1}	107	0.0012	0.7272
Ocean acidification indicators						
pH	-0.0015	0.0001	yr^{-1}	105	0.6769	0.0000
CO_3^{2-}	-0.41	0.05	μmol kg^{-1} yr^{-1}	105	0.4113	0.0000
$\Omega_{calcite}$	-0.0099	0.0012	yr^{-1}	105	0.4071	0.0000
$\Omega_{aragonite}$	-0.0063	0.0008	yr^{-1}	105	0.3750	0.0000
seawater carbonate chemistry						
C_T	0.70	0.05	μmol kg^{-1} yr^{-1}	107	0.6624	0.0000
nC_T	0.73	0.06	μmol kg^{-1} yr^{-1}	107	0.5577	0.0000
A_T	0.03	0.08	μmol kg^{-1} yr^{-1}	105	0.0012	0.7289
nA_T	0.06	0.04	μmol kg^{-1} yr^{-1}	105	0.0231	0.1215
pCO_2	1.56	0.11	μatm yr^{-1}	105	0.6731	0.0000
Revelle factor	0.018	0.002	yr^{-1}	105	0.4656	0.0000

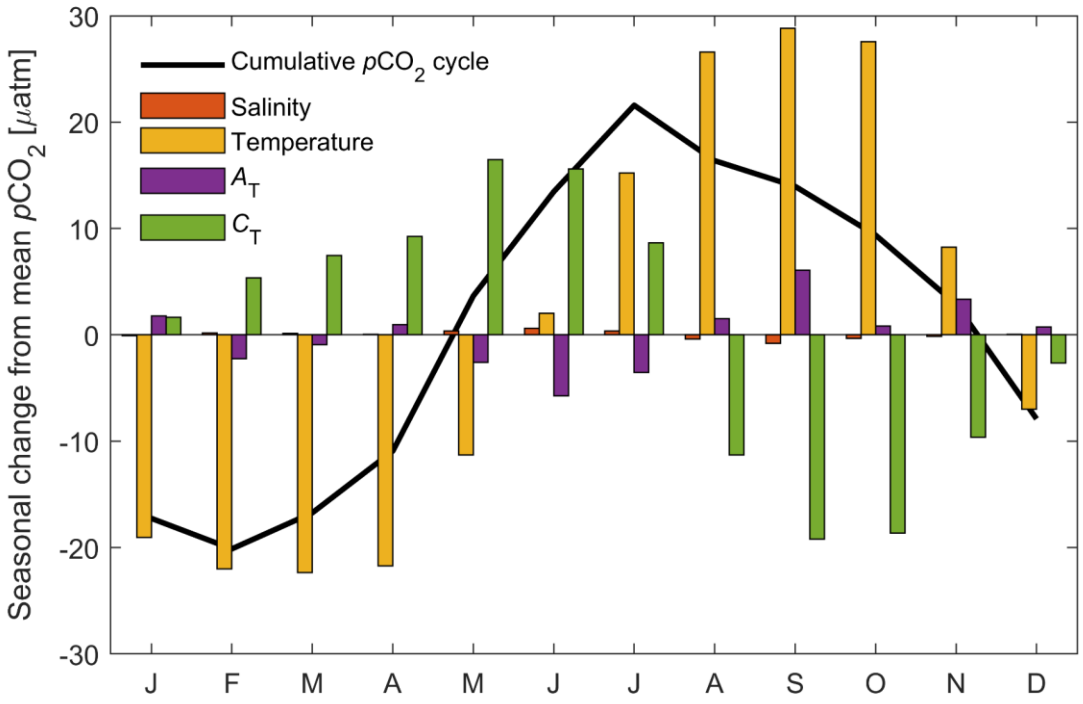

Figure 2.2. Contributions to the seasonal cycle of sea surface pCO_2. The relative contributions of salinity, temperature, A_T and C_T were computed using CO2SYS (van Heuven et al., 2011).

2.8 Supplementary figures and tables

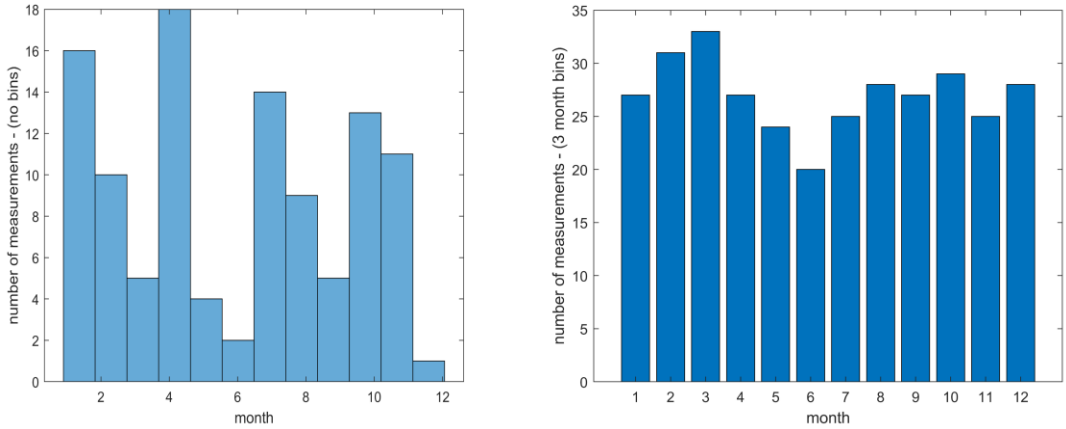

Figure 2.S1. The number of observations from each month over the time series, before (left) and after binning (right).

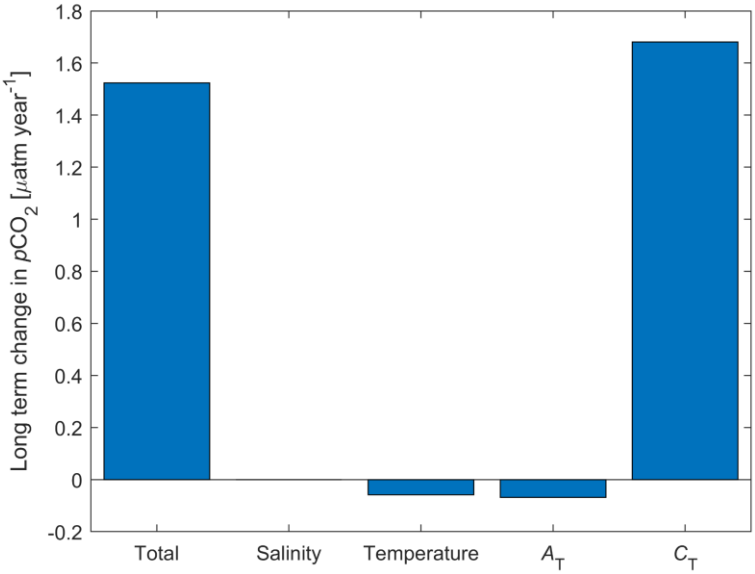

Figure 2.S2. Contributions of salinity, temperature, A_T, and C_T to the long-term trend in sea surface pCO_2.

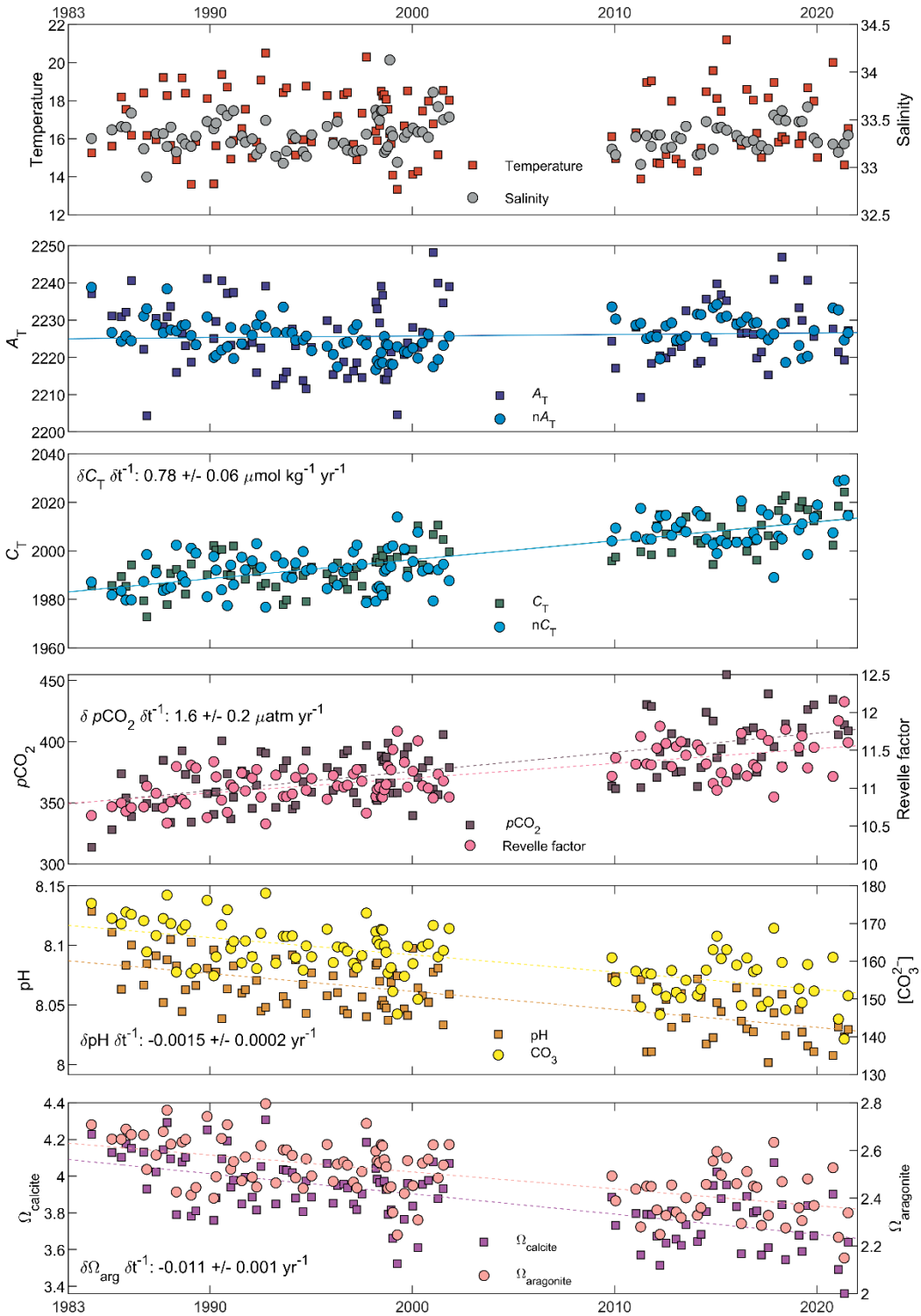

Figure 2.S3. The time series observations at station 90.90 without seasonal detrending. Regression statistics shown in Table 2.S1.

Table 2.S1. Trend statistics from station 90.90 presented without seasonal detrending (from Figure 2.S1).

Parameter	Slope	standard error	units	*n*	r^2	*p*-value
Hydrography						
Temperature	-0.0041	0.0148	°C yr^{-1}	107	0.0007	0.7824
Salinity	0.0001	0.0013	yr^{-1}	107	0.0001	0.9310
Ocean acidification indicators						
pH	-0.0015	0.0002	yr^{-1}	105	0.4435	0.0000
CO_3^{2-}	-0.4563	0.0519	µmol kg^{-1} yr^{-1}	105	0.4286	0.0000
$\Omega_{calcite}$	-0.011	0.0013	yr^{-1}	105	0.4202	0.0000
$\Omega_{aragonite}$	-0.0071	0.0009	yr^{-1}	105	0.3804	0.0000
seawater carbonate chemistry						
C_T	0.7846	0.0604	µmol kg^{-1} yr^{-1}	107	0.6167	0.0000
nC_T	0.7781	0.0658	µmol kg^{-1} yr^{-1}	107	0.5710	0.0000
A_T	0.0431	0.0775	µmol kg^{-1} yr^{-1}	105	0.0030	0.5796
nA_T	0.0403	0.0396	µmol kg^{-1} yr^{-1}	105	0.0100	0.3109
pCO_2	1.5654	0.1724	µatm yr^{-1}	105	0.4445	0.0000
Revelle factor	0.0195	0.002	yr^{-1}	105	0.4687	0.0000

Table 2.S2. Descriptive statistics of the seasonal cycles shown in Figure 1, right. The peak of seasonal cycle and peak-trough amplitude of surface hydrography and seawater carbon chemistry (from Figure 2.1, right).

Parameter	peak	standard error	amplitude	standard error	units
Hydrography					
Temperature	18.6	1.0	3.2	2.0	°C yr^{-1}
Salinity	33.4	0.1	0.1	0.3	yr^{-1}
Ocean acidification indicators					
pH	8.08	0.02	0.04	0.04	yr^{-1}
CO_3^{2-}	167	4	10	15	μmol kg^{-1} yr^{-1}
$\Omega_{calcite}$	4.04	0.10	0.26	0.37	yr^{-1}
$\Omega_{aragonite}$	2.61	0.07	0.18	0.25	yr^{-1}
seawater carbonate chemistry					
C_T	2006	14	17	22	μmol kg^{-1} yr^{-1}
nC_T	2002	17	11	24	μmol kg^{-1} yr^{-1}
A_T	2229	7	7	16	μmol kg^{-1} yr^{-1}
nA_T	2228	3	4	6	μmol kg^{-1} yr^{-1}
pCO_2	399	19	42	40	μatm yr^{-1}
Revelle factor	11.4	0.5	0.4	0.6	yr^{-1}

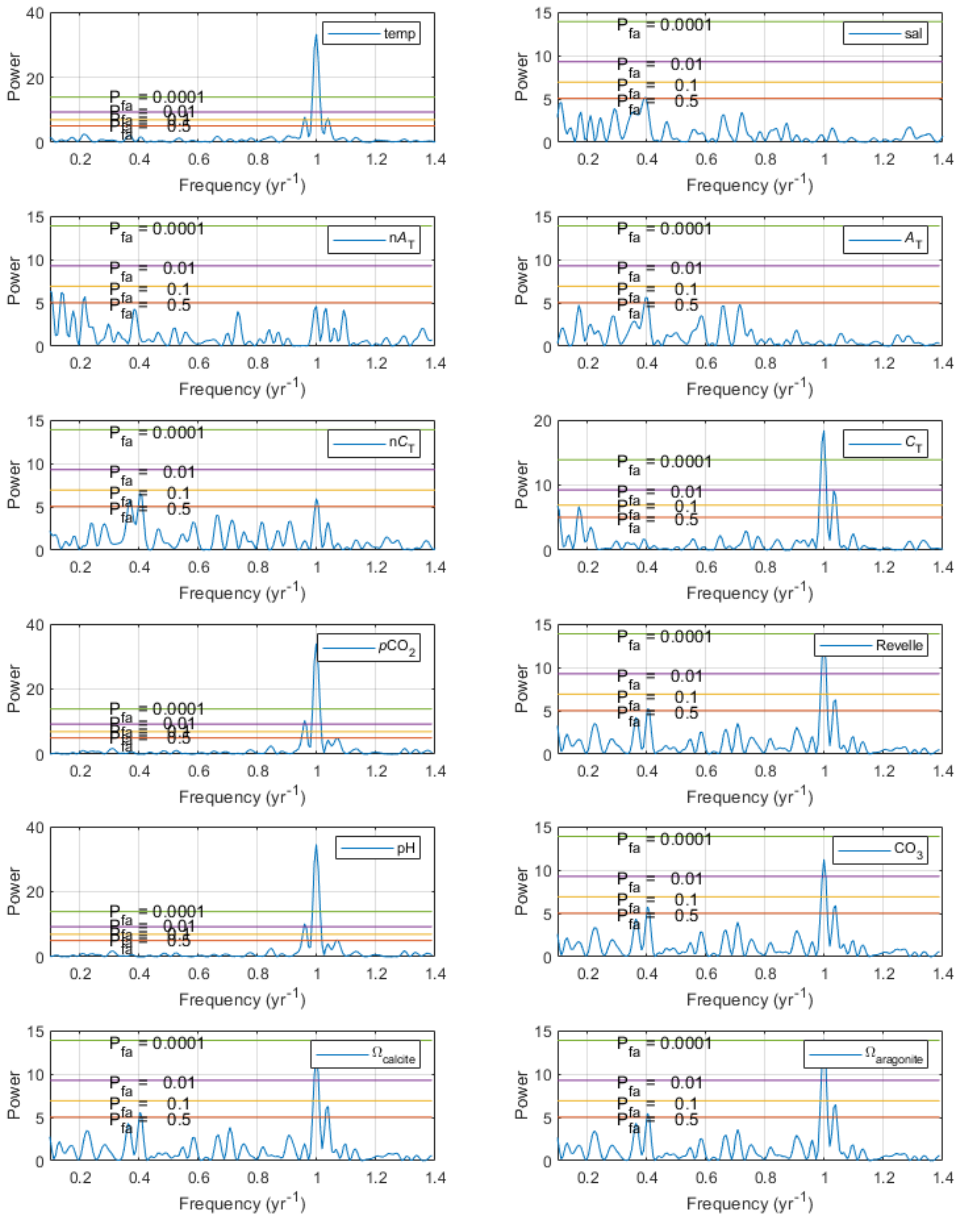

Figure 2.S4. Power spectral density of each time series variable calculated using the MATLAB function 'plomb'**.** Frequencies between 0.1 and 1.4 yr^{-1}. Most parameters exhibit a strong annual signal.

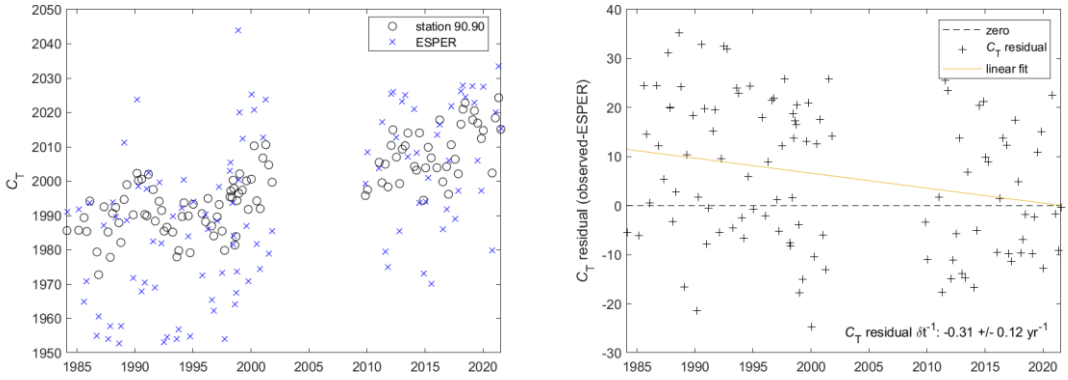

Figure 2.S5. ESPER predictions using only temperature, salinity, latitude, longitude, depth, and year. (Left) Observed and ESPER predicted C_T over time. (Right) The residual C_T, Observed – ESPER, over time.

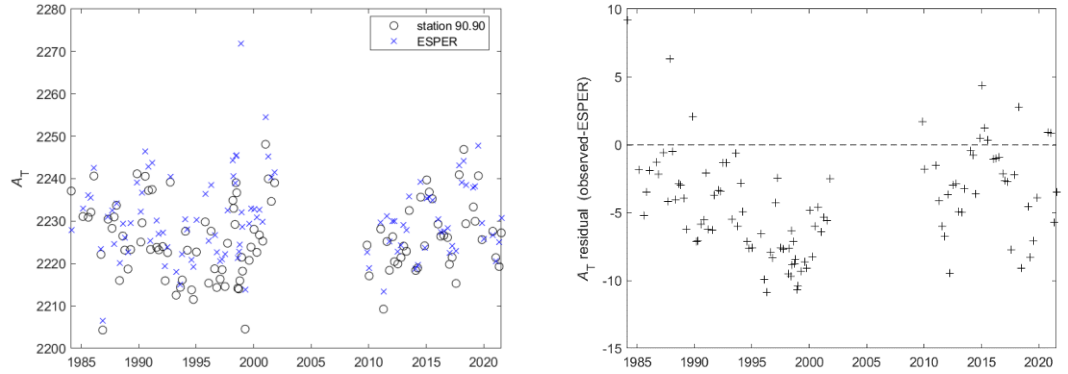

Figure 2.S6. ESPER predictions using only temperature, salinity, latitude, longitude, depth, and year. (Left) Observed and ESPER predicted A_T over time. (Right) The residual A_T, Observed – ESPER, over time.

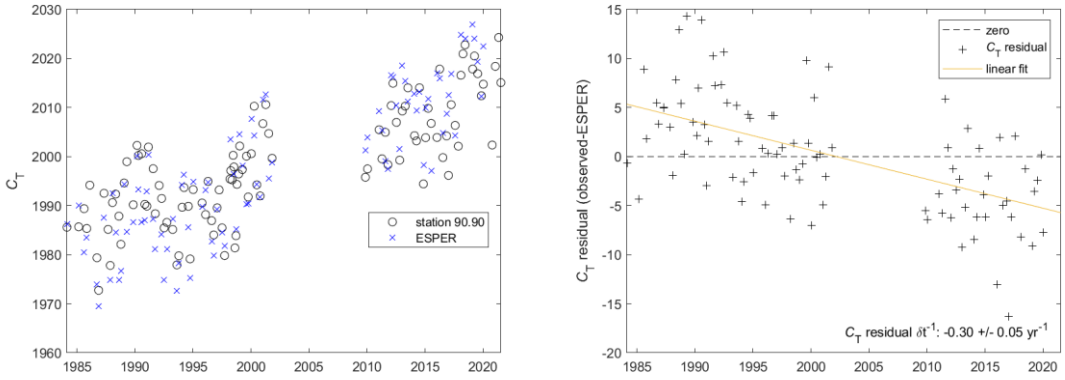

Figure 2.S7. ESPER predictions using all available predictor variables, temperature, salinity, phosphate, nitrate, silicic acid, oxygen, latitude, longitude, depth, and year. (Left) Observed and ESPER predicted C_T over time. (Right) The residual C_T, Observed – ESPER, over time.

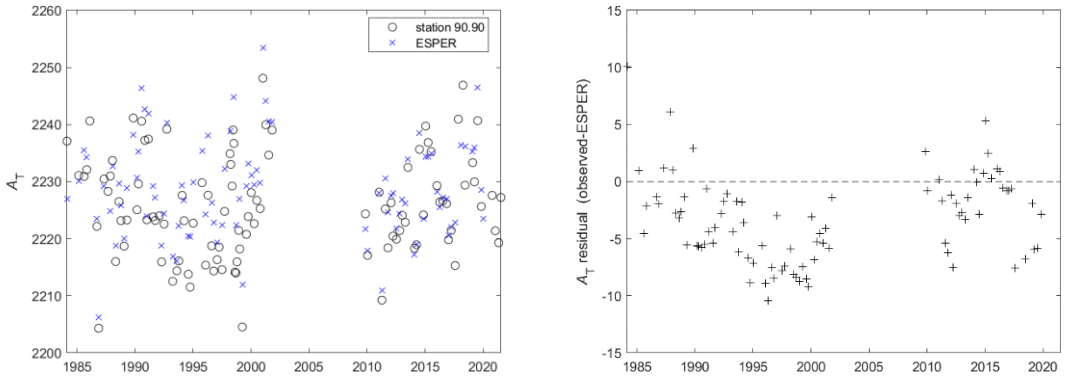

Figure 2.S8. ESPER predictions here used all available predictor variables, temperature, salinity, phosphate, nitrate, silicic acid, oxygen, latitude, longitude, depth, and year. (Left) Observed and ESPER predicted A_T over time. (Right) The residual A_T, Observed – ESPER, over time.

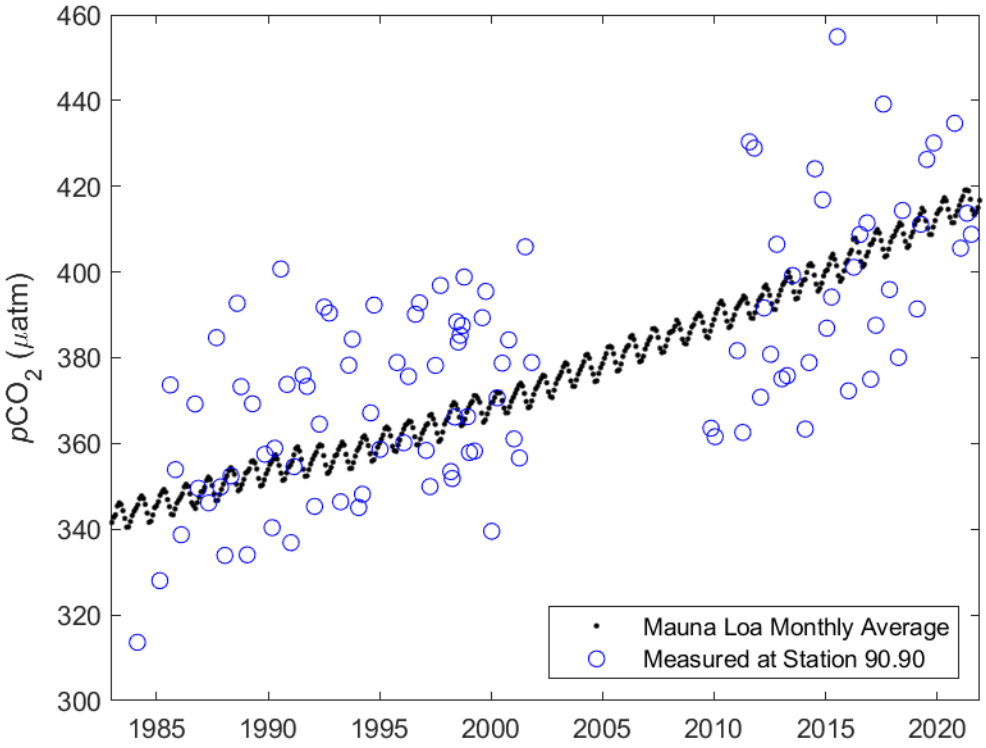

Figure 2.S9. The sea surface pCO_2 at station 90.90 compared to the atmospheric CO_2 record at Mauna Loa.

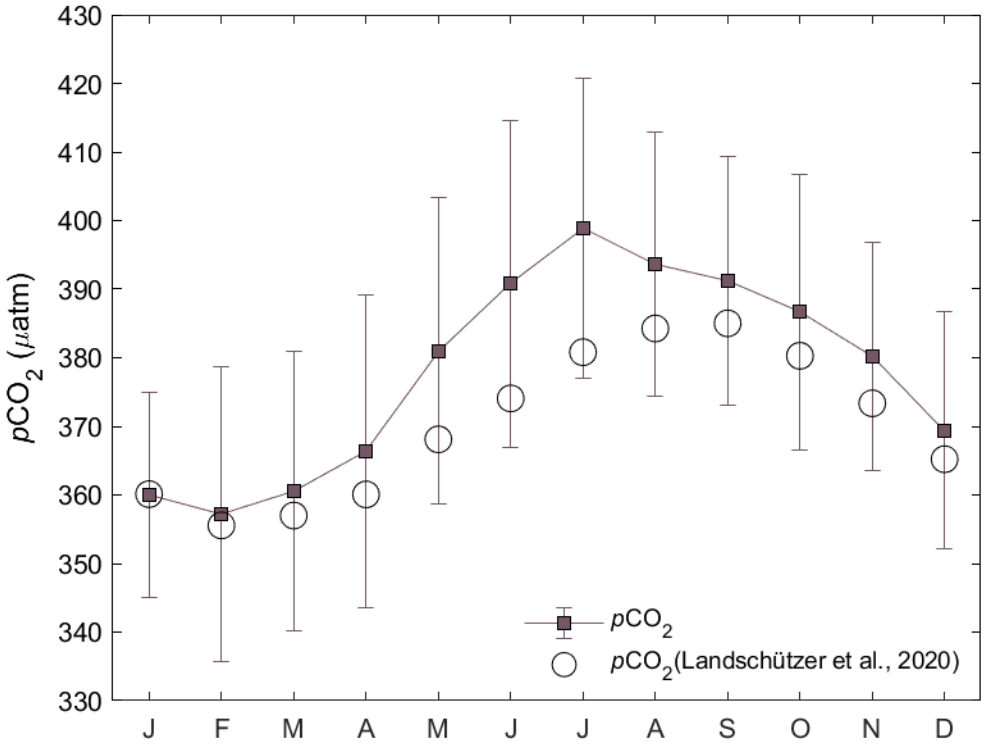

Figure 2.S10. The measured pCO_2 cycle at station 90.90 (computed from A_T and C_T) compared to Landschützer et al. (2020). The Landschützer et al. climatology is from the grid point containing station 90.90. It should be noted that neither seasonal cycle is corrected to a reference year. The measured seasonal cycle has a mean measurement year of 2002 where the Landschützer et al. climatology has a mean measurement year of 2006. If corrected, the difference between the seasonal cycles would be slightly greater than shown here.

CHAPTER 3

Annual mixed layer carbon budget in the Southern California Current system

Abstract

In this work we utilized the seasonal cycles from California Cooperative Oceanic Fisheries Investigations (CalCOFI) line 90 station 90 to estimate the mixed layer net community production (NCP). This uses a monthly mixed layer carbon budget based upon climatological data described in. The model indicated a mix seasonal CO_2 uptake and off gassing with a slight annual net source to the atmosphere of -0.24 ± 0.39 mol m^{-2} yr^{-1}. As well as an autotrophic NCP of 0.38 ± 0.40 mol m^{-2} yr^{-1}. The air-sea gas exchange matched previous studies in the region. However, the NCP is lower than some measurements made in the California Current and at the locations of other time series.

3.1 Introduction

The California Current System is a highly productive eastern boundary upwelling region. Upwelled deep water provides significant nutrients to the nearshore, the California Current System has shown to have significant lateral transport of organic matter and nutrients up to 800 km offshore (Nagai et al., 2015). The study site discussed here, CalCOFI line 90, station 90, (denoted as station 90.90 for this chapter) is located at 31.4°N, 122°W, approximately 450 km from shore, with a water depth of approximately 4000 m. While offshore from upwelling locations, station 90.90 is within the region of lateral transport which may contribute to its net community production (NCP).

There are various methods used to measure productivity in the surface ocean. There is discussion in the literature as to the best method to measure productivity and if some parameters

can even be measured (net primary productivity vs net community production) (Regaudie-de-Gioux et al., 2014). The use of mixed layer carbon budget to estimate parameters productivity has been well established for ship based time series(Gruber et al., 1998; C. Keeling et al., 2004), moorings (Fassbender et al., 2016; Yang et al., 2021) and floats (Riser & Johnson, 2008; Yang et al., 2017).

3.2 Methods

3.2.1 Model and data used

The mixed layer mass balance used in this chapter follows work by Yang et al. (2021), Fassbender et al. (Fassbender et al., 2016) and Emerson (2014). Where $\frac{dMLD \cdot C_T}{dt}$ is the monthly change in the inventory of mixed layer inorganic carbon, and $F_{gas}, F_{ent}, F_{dif}, F_{bio},$ and F_{adv} are the fluxes impacting the inventory due to air-sea gas exchange, entrainment, diffusion, negative net community production (NCP) and horizontal advection, respectively (mol m^{-2} $month^{-1}$). A positive flux is representative of an addition of C_T to the mixed layer. The F_{adv} term is not evaluated in this chapter but will be included in the final manuscript presenting this work.

$$\frac{dMLD \cdot C_T}{dt} = F_{gas} + F_{ent} + F_{dif} + F_{bio} + F_{adv} \quad (3.1)$$

The C_T is based on the seasonal cycle described in Chapter 2, and the mixed layer depth (MLD) is from a climatology by Holte et al. (2017). The time step for this model is one month, reflective of the monthly climatology it is based upon. Figure 3.1 is a monthly climatology of the input variables.

Where F_{gas} is the CO_2 flux due to air-sea gas exchange (mol m^{-2} $month^{-1}$).

$$F_{gas} = k \cdot K_0 \cdot \left(pCO_{2,air} - pCO_{2,sea}\right) \quad (3.2)$$

Where k, the gas transfer velocity, and K_0 , the CO_2 solubility, are from Wanninkhof (2014) and Weiss (1974) respectively.The atmospheric CO_2 concentration ($pCO_{2,air}$), used was the mean value from the Mauna Loa Observatory between 1984 and 2020 of 376 μatm, with the average seasonal cycle included (max May = 379.2 μatm, min Sept = 372.6 μatm) (C. Keeling et al., 2005; R. Keeling & C. Keeling, 2017). The sea surface pCO_2, ($pCO_{2,water}$) is again from the seasonal cycle described in Chapter 2.

$$k = 0.251 \cdot wind^2 \cdot \left(\frac{Sc}{660}\right)^{-0.5} \tag{3.3}$$

The k used here is intended for a 6-hour wind product, however, monthly averaged winds are used here. This difference will cause an underestimation in the air-sea gas exchange and is reflected by using a greater uncertainty in k later in this chapter. An alternative approach is to use a Rayleigh distribution of wind speeds to determine the coefficient (here, 0.251(cm h^{-1})(m s^{-1})$^{-2}$), but this too includes bias (Wanninkhof et al., 2002). The monthly 10 m height wind speed product used was from the National Oceanic and Atmospheric Administration, National Centers for Environmental Information (https://www.ncei.noaa.gov/thredds/catalog/uv/monthly_agg/catalog.html?dataset=uv/monthly_agg/Aggregation_of_Monthly_Ocean_Wind_best.ncd).

Where F_{ent} is the flux due to the mixing of waters as the MLD changes depth, entrainment or detainment (mol m^{-2} $month^{-1}$).

When the MLD is shoaling,

$$F_{ent} = \frac{dMLD}{dt} \cdot C_{T,surface} \tag{3.4}$$

When the MLD is deepening,

$$F_{ent} = \frac{dMLD}{dt} \cdot C_{T,deep} \tag{3.5}$$

Where $C_{T,surface}$ is the C_T reported in the seasonal cycle in Chapter 2,

$$C_{T,deep} = C_{T,surface} + 0.5\left(\frac{dMLD}{dt} \cdot \frac{dC_T}{dz}\right) \quad (3.6)$$

$C_{T,deep}$ was calculated using the change in MLD $\left(\frac{dMLD}{dt}\right)$ and a gradient in C_T at the base of the mixed layer $\left(\frac{dC_T}{dz}\right)$. The gradient used was 0.16 μmol kg^{-1} m^{-1}, which was determined from the slope of C_T measurements between 20 −60 m depth from data set described in Chapter 4.

Where F_{dif} is the diffusive flux across the mixed layer (mol m^{-2} month^{-1}),

$$F_{dif} = k_z \cdot \frac{dC_T}{dz} \quad (3.7)$$

The value of 5 ×10^{-5} m s^{-1} was chosen for k_z , in line with values used by Todd et al. (2011) in the California Current.

Where F_{bio} is the negative NCP and is calculated as the difference between $\frac{dMLD \cdot C_T}{dt}$ and sum of the remaining terms $F_{gas} + F_{ent} + F_{dif}$. Vertical or horizontal advection, and evaporation or precipitation were not considered in this model.

3.2.2 Uncertainty estimation

A sensitivity analysis was employed to estimate uncertainty following the approximate method of numerical differentiation (Ellison & Williams, 2012; Kragten, 1994). In this analysis, errors for seven input terms (Table 3.1) are estimated and propagated through Equations 3.2–3.7 using the approximation

$$u(y,x_i) \approx y(x_1,x_2,..(x_i+u(x_i))..x_n) - y(x_1,x_2,..x_i..x_n) \quad (3.8)$$

Propagated errors are then used to compute combined standard uncertainty for F_{gas}, F_{ent}, F_{dif}, $MLD \cdot C_T$ and F_{bio}, respectively, using

$$u(F_{gas}) = \sqrt{\left(u(F_{gas}, \Delta pCO_2)\right)^2 + \left(u(F_{gas}, k)\right)^2 + \left(u(F_{gas}, wind)\right)^2} \quad (3.9)$$

$$u(F_{ent}) = \sqrt{\left(u(F_{ent}, \Delta MLD)\right)^2 + \left(u(F_{ent}, dC_T\ ddepth)\right)^2 + \left(u(F_{ent}, C_T)\right)^2} \quad (3.10)$$

$$u(F_{dif}) = \sqrt{\left(u(F_{dif}, k_z)\right)^2 + \left(u(F_{dif}, dC_T\ ddepth)\right)^2} \quad (3.11)$$

$$u(dMLD \cdot C_T) = \sqrt{\left(u(dMLD \cdot C_T, \Delta MLD)\right)^2 + \left(u(dMLD \cdot C_T, C_T)\right)^2} \quad (3.12)$$

$$u(F_{bio}) = \sqrt{\begin{matrix}\left(u(F_{bio}, \Delta p\mathrm{CO}_2)\right)^2 + \left(u(F_{bio}, k)\right)^2 + \left(u(F_{bio}, wind)\right)^2 \\ +\left(u(F_{bio}, \Delta MLD)\right)^2 + \left(u(F_{bio}, dC_T\ ddepth)\right)^2 \\ +\left(u(F_{bio}, C_T)\right)^2 + \left(u(F_{bio}, k_z)\right)^2\end{matrix}} \quad (3.13)$$

and reported in Table 3.2. This method does not take into account correlated errors.

The $\Delta p\mathrm{CO}_2$(air-sea) and C_T uncertainties were based on the climatology from Chapter 2. Similarly, the $\frac{dC_T}{dz}$ uncertainty was chosen to be 30% based upon C_T measurements from station 90.90. The k uncertainty was chosen to be 30%, which is greater than the 20% reported in Wanninkhof (2014) and was used due to the monthly averaged winds. The uncertainty in the monthly change in mixed layer depth, ΔMLD, was chosen to be 10%. The uncertainty in the wind speed was chosen to be 1 m s^{-1}. The uncertainty in k_z was chosen to be 50% (Yang et al., 2017).

3.3 Results and discussion

3.3.1 Model results

Figure 3.2 shows the monthly contribution of F_{gas}, F_{ent}, F_{dif}, $dMLD \cdot C_T$ and F_{bio} to the mixed layer inorganic carbon inventory in mol m^{-2} $month^{-1}$. F_{gas} closely followed $\Delta p\mathrm{CO}_2$ with CO_2 absorption in January–April and CO_2 off gassing the remainder of the year. The net effect was -0.24 ± 0.39 mol m^{-2} yr^{-1}, being a source to the atmosphere. F_{dif} was a constant 0.02 mol m^{-}

^{2} month^{-1}, with a net effect of 0.26 ± 0.15 mol m^{-2} yr^{-1}. This was the only flux with an uncertainty that did not encompass zero, which is realistic as a diffusive flux of inorganic carbon from the mixed layer to the deeper ocean is unlikely.

The contributions of F_{ent} and $dMLD \cdot C_T$ are orders of magnitude greater than the other terms in the budget on a monthly basis but are similar in net annual effect. F_{ent} and $dMLD \cdot C_T$ contributed 0.23 ± 0.15 and -0.13 ± 0.01 mol m^{-2} yr^{-1}, respectively. On a monthly basis, F_{ent} and $dMLD \cdot C_T$ are very similar in magnitude and opposite in sign. This is used in Figure 3.3 to plot $dMLD \cdot C_T - F_{ent}$ along with the cumulative contribution of the other fluxes.

The calculated F_{bio}, has a net effect of -0.38 ± 0.4 mol m^{-2} yr^{-1}, net autotrophic over the year. The F_{bio} term shows net autotrophy (i.e., the removal of inorganic carbon to the mixed layer) December–May and net heterotrophy the remainder of the year. The months of net heterotrophy roughly coincide with the months of CO_2 off gassing.

3.3.2 Comparison of results

Other NCP measurements using O_2/Ar made in the California Current vary largely (between – 5 and 28 mol m^{-2} yr^{-1}) with a strong decrease in primary productivity rates moving further offshore (Kranz et al., 2020). Focusing on other offshore measurements from two separate years (P1604 Cycle 2, P1706 Cycle 2 and 3), NCP values were reported were between -4 and 2, mol m^{-2} yr^{-1} (Kranz et al., 2020). The NCP estimated here of 0.38 ± 0.4 mol m^{-2} yr^{-1} is reasonable when compared to those measurements. A separate study reports the NCP within the California Current to be 4.4 ± 1.5 and offshore of the current to be 3.3 ± 1.0 mol m^{-2} yr^{-1} (Munro et al., 2013) in which even the offshore NCP is greater than the NCP estimated here. Previous work has found discrepancies between monthly climatologies and more continuous observations used to estimate mixed layer NCP (Riser & Johnson, 2008). The annual NCP of other well

studied locations such as, Ocean Station Papa (2.3 mol m^{-2} yr^{-1}), Hawaii Ocean Time-series (2.5 mol m^{-2} yr^{-1}) and Bermuda Atlantic Time-series (3.8 mol m^{-2} yr^{-1}), all have a higher annual NCP than the estimate generated in this work (Emerson, 2014).

3.3.3 Future work

Future work should be focused on on understanding the discrepancy between NCP estimated here and measurements made in the Southern California Current. The inclusion of horizontal advection, F_{adv}, will likely improve the NCP estimate. Horizontal advection could potentially be estimated using the mean surface flow at station 90.90 and a C_T gradient calculated using ESPER (Carter et al., 2021). The gradient of C_T over depth, $\frac{dC_T}{dz}$, is an area that could also use further validation. The value calculated from C_T samples does not account for seasonal variability and effects both F_{ent} and F_{dif}. Inclusion of seasonal variability in k_z may improve the model. Refinement of the MLD climatology used in this work is another avenue for improvement. The chosen climatology currently causes considerable variability in ΔMLD, specifically in March–June, which has a large impact on $dMLD \cdot C_T$ and F_{ent}. The MLD could be estimated from temperature and salinity observations co-current with the inorganic carbon sample collection, using either bottle or sensor measurements. One approach to refine the carbon budget could be to create a similar budget at line 80 station 80 as well as a budget that includes the higher frequency data available from the CCE-1 mooring and compare results of the two types of budgets (Ohman et al., 2013).

Further development on this model could include refinement of the air-sea gas exchange. This could be achieved by incorporating higher frequency wind data or using a coefficient chosen to calculate the gas transfer velocity specifically for monthly wind products. However,

the value of F_{gas} (-0.24 ± 0.39 mol m^{-2} yr^{-1}) is similar to the near zero net CO_2 flux estimation in this location of the California Current System based on SOCAT data (Sharp et al., 2022).

3.4 Conclusions

Mixed layer carbon budgets have frequently been used to estimate NCP. While the Southern California Current region as a whole is both highly productive and highly variable, the mixed layer carbon budget calculated shows only a slightly autotrophic NCP of 0.38 ± 0.40 mol m^{-2} yr^{-1}. This is within the variability of the region but generally less than previous studies indicate. Additionally, the air-sea gas exchange agrees with previous studies in the region showing a small net source to the atmosphere, with months of both off gassing and CO_2 absorption.

3.5 Acknowledgments

Chapter 3, in part, is currently being prepared for submission for publication of the material in American Geophysical Union, Journal of Geophysical Research: Oceans. The dissertation author was the primary researcher and author of this material.

3.6 Figures and tables

Table 3.1. The input variables and assigned uncertainties to the mixed layer carbon budget. "*" denotes the annual mean of the monthly input variable. "**" denotes the mean of the absolute value of the ΔMLD as the annual mean must be zero.

input	value	uncertainty	units
$\Delta\ pCO_2$ (air-sea)	8.4*	10	μatm
k	10.3*	30%	cm hr^{-1}
wind	6.5*	1	m s^{-1}
ΔMLD	7.8**	10%	m
$dC_T\ dz^{-1}$	0.16	30%	μmol kg^{-1} m^{-1}
C_T	2000.8*	8	μmol kg^{-1}
Kz	0.00005	50%	m^{-2} s^{-1}

Table 3.2. The output variables and estimated uncertainties to the mixed layer carbon budget. A positive value represents an addition of carbon to the mixed layer.

output	value	uncertainty	units
F_{gas}	-0.24	0.39	mol m^{-2} yr^{-1}
F_{ent}	0.23	0.15	mol m^{-2} yr^{-1}
F_{dif}	0.26	0.15	mol m^{-2} yr^{-1}
dMLD C_T	-0.13	0.01	mol m^{-2} yr^{-1}
F_{bio}	-0.38	0.40	mol m^{-2} yr^{-1}

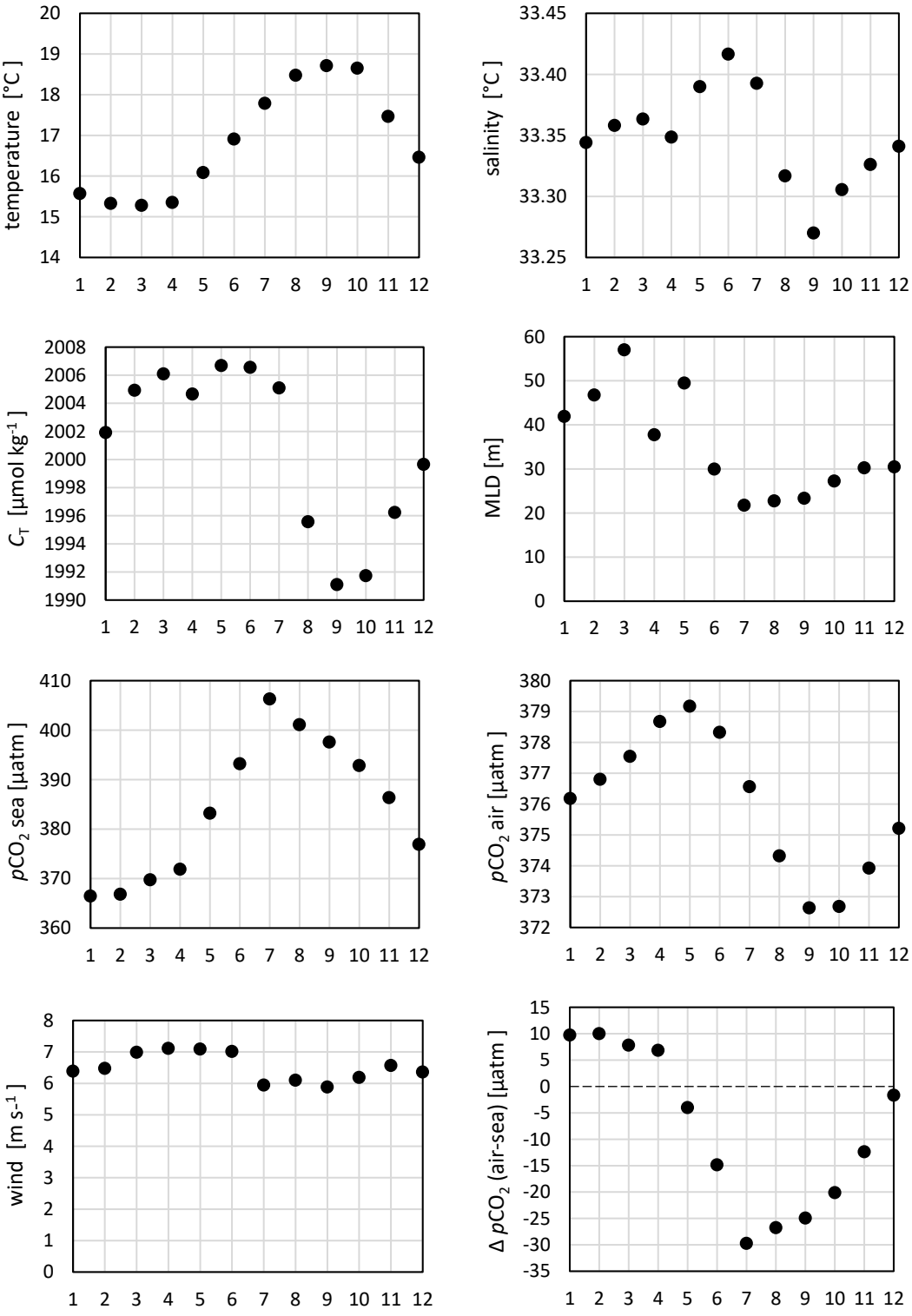

Figure 3.1 The seasonal cycle of input variables. Not all variables here appear in Table 3.1.

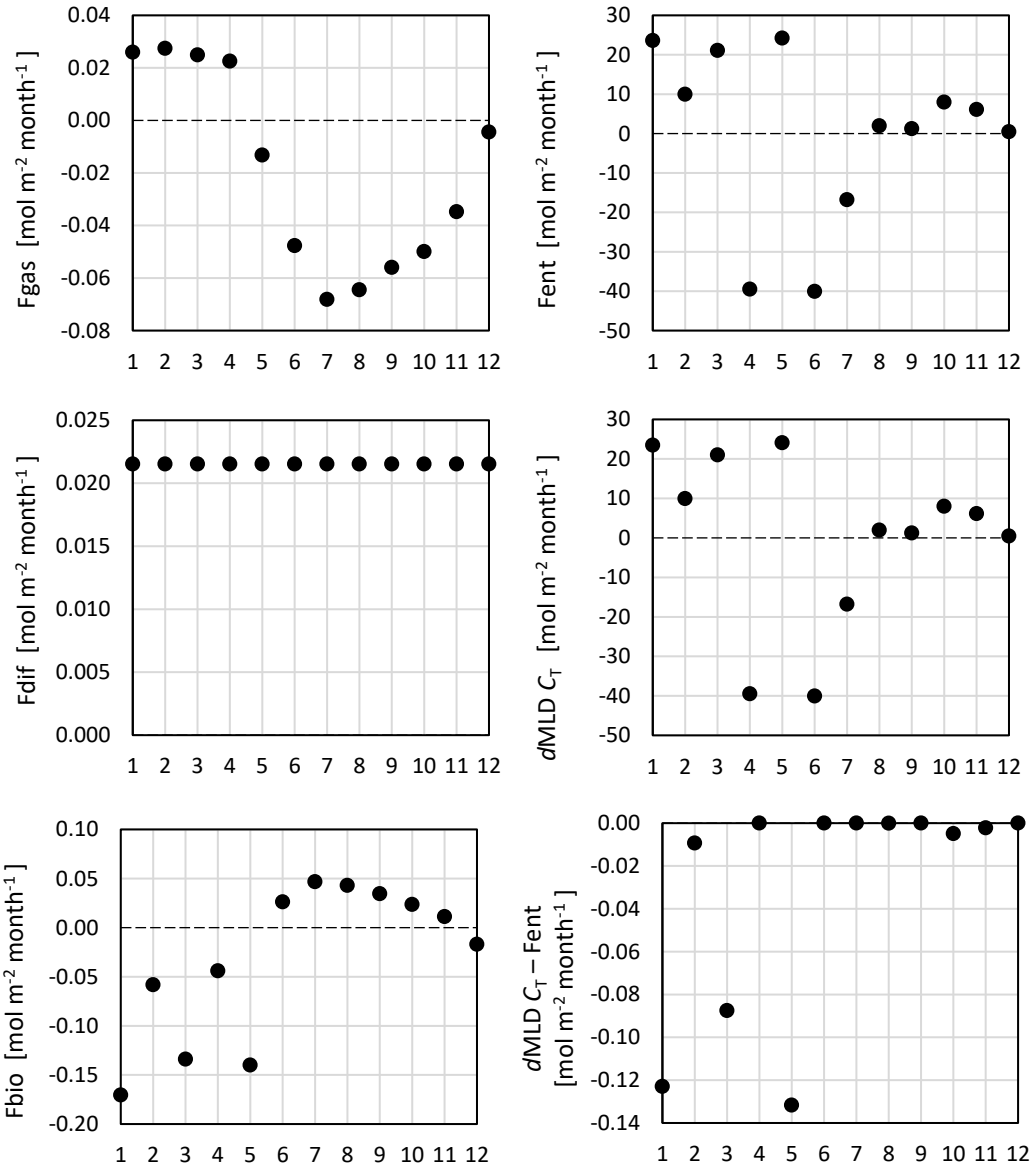

Figure 3.2 The monthly flux for variables included in the mixed layer carbon budget. A positive value represents an addition of carbon to the mixed layer.

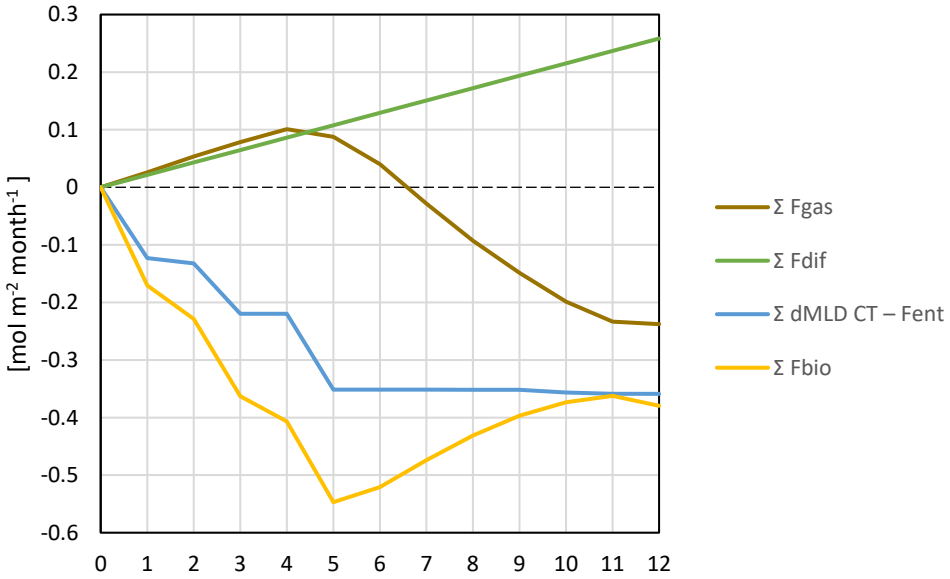

Figure 3.3. The cumulative contribution to the mixed layer carbon budget over a year. A positive value represents an addition of carbon to the mixed layer.

CHAPTER 4

An overview of inorganic carbon observations in the Southern California Current made on CalCOFI cruises

Abstract

In this work we provide an overview of inorganic carbon observations made on hydrographic bottle samples collected on California Cooperative Oceanic Fisheries Investigations (CalCOFI) Cruises. The majority of the observations described in this chapter (4238 C_T, 4065 A_T, and 1858 pH observations), have not been previously publicly available. This chapter includes a summary of the spatial and temporal distribution of the observations. We discuss how these observations compare to existing methods used to estimate inorganic carbon parameters as well as a first order analysis of some of the trends present at the most sampled locations. The goal of this chapter is to disseminate quality controlled data, provide a summary overview of the observations, and bring awareness of this data set to the broader scientific community and relevant stakeholders.

4.1 Introduction

CalCOFI has collected hydrographic and biological data since the 1950's (Hewitt, 1988) and began collecting seawater samples for CO_2 analysis in 1983. Ocean acidification monitoring has continued through the present, with a six-year gap (2002–2007). In 1983, analysis of total dissolved inorganic carbon (C_T) and total alkalinity (A_T) on bottle samples was carried out by Dave Keeling's laboratory at the same time that his lab began measuring samples from Hydrostation S in the Atlantic near the present-day Bermuda Atlantic Time-series Study (BATS). Five years later (1988) the official BATS and Hawaii Ocean Time-series (HOT) began

(Bates et al., 2014). Thus, CalCOFI station 90.90 and Hydrostation S are the earliest locations of CO_2 time series in the Pacific and Atlantic Oceans, respectively.

The early vision of the inorganic carbon time series was to have a sea surface record shoreward of the California Current, within the California Current, and offshore of the California Current, line and station 90 70; 90 90; and 90 120 respectively (personal communication, Guy Emanuele). These observations began in 1983 and continued until the 1990's. Of those three early time series locations, line 90 station 90 has endured as the most consistent record and is the subject of Chapter 2. As time progressed, the focus shifted to more nearshore stations with greater depth coverage, while continuing the surface sampling at some offshore locations.

As Chapter 4 will include measurements distributed over the Southern California Current (SCC), a brief explanation of the CalCOFI grid numbering pattern is prudent. The CalCOFI grid, Figure 4.1, is made of lines and stations, where lines run approximately normal to the coastline. Both line and station numbering start at non-zero values as the CalCOFI grid once included a much larger area. A difference of 10 in line number is equivalent to 120 nautical miles (nmi). A difference of 10 in station number is equivalent to 40 nmi (Weber & Moore, 2013).

4.2 Methods

4.2.1 Analytical methods and sample collection

Bottle samples were analyzed for total alkalinity (A_T) and dissolved inorganic carbon (C_T). A_T was measured using a closed cell titration (Bradshaw et al., 1981) until 1992 and an open cell titration (Dickson et al., 2003) after 1992. C_T was measured using vacuum extraction and manometry (Lueker, 1998; Lueker et al., 2000) until 1992, coulometry (Johnson et al., 1987) from 1992–2015 and an infrared (IR) analyzer (Goyet & Snover, 1993; O'Sullivan & Millero,

1998) after 2015. Accuracy of A_T and C_T is estimated to range from 2–5 μmol kg^{-1} and 1–3 μmol kg^{-1}, respectively, over the dataset. In more recent years, after 2014, spectrophotometric pH (Dickson et al., 2007) was measured, allowing an evaluation of internal consistency among the measured CO_2 system parameters. An unpurified m-cresol purple as the indicator dye was used in these pH measurements. Due to this, a pH-dependent correction factor was applied. This general procedure has been documented previously (Liu et al., 2011; Takeshita et al., 2021) and is specific to the system used for pH measurements between 2014–2021 (Wolfe et al., 2021).

Bottle samples were collected during quarterly CalCOFI cruises. Mercuric chloride was added (as a biocide and preservative) and the samples were sealed and stored in borosilicate glass bottles following best practices (Dickson et al., 2007). Storage times ranged from one month to multiple years before analysis. Some of the early samples may have been collected using different bottle types, but this does not appear to have a notable impact on the data quality.

4.2.2 Calculating additional carbonate chemistry parameters

The same methods described in Chapter 2 are also used in Chapter 4. The partial pressure of CO_2 in seawater (pCO_2), pH, carbonate ion concentration ($[CO_3^{2-}]$), saturation states of aragonite and calcite ($\Omega_{aragonite}$, $\Omega_{calcite}$), and Revelle Factor ($\partial \ln[CO_2]/\partial \ln C_T$), were calculated in MATLAB using CO2SYS (van Heuven et al., 2011) from A_T, C_T, temperature and salinity with coefficients recommended by Lueker et al. (2000). A_T and C_T were salinity normalized (indicated by nA_T and nC_T,) to the average salinity of the time series (33.7, n = 4082).

4.3 Results and discussion

4.3.1 Spatial and temporal distribution of observations

This section will discuss the distribution of observations contained in this data set. For clarity, in this section a single "observation" refers to a unique location, depth and time where a sample was collected and analyzed for either C_T, A_T or pH. Other programs have measured inorganic carbon in the SCC, such as NOAA's West Coast Ocean Acidification Cruises, but are not included in this discussion.

There are 70 locations (unique pairs of line and station numbers) within the CalCOFI grid that have inorganic carbon observations. Measurement of multiple inorganic carbon parameters count as a single observation. Figure 4.2 shows the number of observations at each location per year. Half of these locations were only measured in a single year. Figure 4.3 shows the number of observations per year from the remaining 35 locations sampled in more than a single year.

In 1984, 2013 and 2016 many observations were collected from locations that were not sampled in any other year. A map showing these unique locations and years is shown in Figure 4.4. In 1984 surface observations were made along stations 90 and 100 extending far further south than any other year (green "x", Figure 4.4). In November 2013 there was a tight grouping of observations centered around line 80 station 55, off of Point Conception (magenta "*", Figure 4.4). This tight grouping has a total of 68 observations from 7 profiles from sea surface to 515 m depth. This grouping may be of interest for future studies specific to the Point Conception region or for processes where spatial resolution is more important than having observations over time. Finally, there were 7 locations observed only in 2016, without an obvious overall pattern (Orange "+", Figure 4.4).

Aside from the notable exceptions described prior, there are four distinct time periods with respect to the number and distribution of observations made. First, between 1983–2001 a total of 531 observations were made. Observations were usually made at 10 m depth and along line 90 at stations 70, 90 and 120. Second, between 2002–2007 in which no observations were made. Third, between 2008–2017 a total of 3162 observations were made. Some notable features of this time period include the initiation of observations from subsurface profiles, a greater focus on the near shore, and a significantly higher rate of sampling (approximately 120 observations per cruise). Profiles occasionally went as deep as 3500 m but were generally restricted to 515 m and shallower. Figures 4.5 - 4.7 summarize observation depth over time. Fourth, between 2008–2021 a total of 699 observations were made. This time period is similar to the prior time period, with fewer sub surface observations and a lower rate of sampling (approximately 50 observations per cruise) due to limited funding support for bottle analysis. With dedicated funding for analysis and quality control of these samples, it may be possible to increase the sampling frequency to the previous level. As of 2022, sampling continues at a rate of approximately 50 observations per cruise.

4.3.2 Assessment of measurement quality and CO_2 system internal consistency

All measurements made prior to 2008 were made in duplicate, quality controlled, and the means were archived. Accordingly, statistics of duplicates reported here reflect sampling since 2008. The difference between duplicate C_T measurements was 1.9 ± 2.8 μmol kg^{-1} (mean ± std, n = 364) (Figure 4.8). After 2014 there is an increase in the difference between duplicate C_T measurements which is consistent with the transition to IR C_T measurements being less precise than coulometric C_T measurements. The difference between duplicate A_T measurements was 1.8

± 2.8 μmol kg^{-1} (mean ± std, n = 361) (Figure 4.9). There is not a change in the difference between duplicates A_T measurements over time. This indicates that changing the lab group which performed the open cell titration did not noticeably affect the precision of the A_T measurements. The difference between duplicate pH measurements was 0.0026 ± 0.0036 (mean ± std, n = 152) (Figure 4.10). This precision is slightly lower than that which should be achievable using spectrophotometric pH measurement (Dickson et al., 2007).

In more recent years (after 2014), the addition of pH as a measured parameter results in an over-constrained carbonate system, which allows comparison between spectrophotometric pH and pH calculated from C_T and A_T. Figure 4.11 shows this comparison. The difference between spectrophotometric pH and pH calculated from C_T and A_T was 0.008 ± 0.003 (mean ± std, n = 1435). This mean difference is within the range of what Fong and Dickson (2019) report for GO-SHIP cruises, although the standard deviation is somewhat higher in the CalCOFI data. We suspect that the main source of the higher std is the C_T measurement which is based on the lower precision IR method for CalCOFI compared to the coulometric C_T method used in GO-SHIP. A non-zero slope is observed in the difference between spectrophotometric pH and pH calculated from C_T and A_T (Figure 4.11). The trend (-0.008 ± 0.02, mean ± std) is lower than that reported across the GO-SHIP cruises (Fong & Dickson, 2019). One factor that may contribute to these differences is the use of purified indicator dye on GO-SHIP cruises and unpurified dye on CalCOFI cruises for pH measurements (Liu et al., 2011).

4.3.3 Comparison to empirical estimates of CO_2 from other hydrographic variables

Observations were compared to Empirical Seawater Property Estimation Routines "ESPER_Mixed", where mixed refers to the use of both locally interpolated regressions and

neural networks (Carter et al., 2021; Morgan, 1994; van Heuven et al., 2011). All available predictor variables were used, specifically, temperature, salinity, phosphate, nitrate, silicic acid, latitude, longitude, depth, and year. Results of the comparisons to ESPER_Mixed are presented in Figure 4.12 and Figure 4.13. The difference between C_T observations and C_T predicted using ESPER was 1.8 ± 7.6 μmol kg^{-1} (mean ± std, n = 3457). The difference between A_T observations and A_T predicted using ESPER was 0.7 ± 9.9 μmol kg^{-1} (mean ± std, n = 3377). For both C_T and A_T the mean difference is within what Carter et al. reports for the California Current, (C_T 0.5 ± 4.4 μmol kg^{-1} and A_T -0.8 ± 5.0 μmol kg^{-1}, using salinity temperature and oxygen as predictor variables) (2021). However, the difference between pH observations and pH predicted using ESPER was 0.015 ± 0.028 (mean ± std, n = 1384), was greater than what Carter et al. reports for the California Current (pH -0.006 ± 0.0012) (2021). The std of the difference between pH observations and pH predicted using ESPER is similar to the std of the difference between pH observations and pH calculated from C_T and A_T, 0.028 and 0.020 respectively (Figure 4.11, Figure 4.14). In contrast, the means of the comparisons are opposite in sign, 0.015 and -0.008 respectively. Indicating that there was a greater disagreement between pH predicted using ESPER and pH calculated from C_T and A_T than to the direct pH measurements.

The roughly tenfold greater number of observations within the CalCOFI dataset compared to the training data used for ESPER (only ~300 total measurements in the CalCOFI region) provide an excellent validation of the ESPER algorithm. While the agreement between C_T, A_T, and pH measured vs predicted by ESPER is encouraging, several systematic features appear in every figure, suggesting perhaps some room for improvement in algorithms. In summary, it is our hope that publication of this chapter (with publicly archived data) may aid the ongoing refinement of predictive tools such as ESPER.

4.3.4 Primary sampling locations

Among the 70 unique locations with observations (Figure 4.4), nine "primary" locations make up over half of the total number of observations in this dataset. Figure 4.15 shows a map of the primary locations, and Figure 4.16 shows the number of observations per year at each location, with fairly consistent observations since 2008 (Figure 4.17). The nine locations are composed of five nearshore locations (line station, 80 55, 81.8 46.9, 86.7 35, 90 30, and 93.3 30) and four offshore locations (line station, 80 80, 90 53, 90 60, and 90 90). The offshore locations are present along lines 80 and 90. The two locations along line 80, coincide with the California Current Ecosystem interdisciplinary biogeochemical moorings CCE-1 (line station, 80 80) and CCE-2 (line station, 80 55) since 2008 and 2010 respectively (Ohman et al., 2013). One of the nearshore locations (line station, 81.8 46.9) is unique due to its position within the Santa Barbara Basin, an anoxic basin.

Figure 4.18 presents the surface C_T trends at the primary locations. The nearshore locations off of Point Conception and in Santa Barbara Basin (line station, 80 55, 81.8 46.9) were the most variable. Only the two locations furthest from shore, 90 90 and 80 80, have a trend that is larger than the standard error of the slope. After 14 years of observations none of the near shore locations have a trend that is greater than the standard error of the slope. While not significant, there is a negative slope at three of these locations, opposite the ocean acidification trend. All of these challenges highlight the difficulty of discerning anthropogenic CO_2 trends from natural variability, especially in the nearshore.

Below the surface, C_T exhibits marked shoaling along line 90 between 50 and 250 m depth (Figure 4.19). As the distance from shore (and station number) decreases the C_T at a given depth increases. This eastward shoaling reflects the transport of high C_T deep water upward with

coastal upwelling caused by westward wind driven Ekman transport and the shallowing of the bottom topography (Talley et al., 2011).

4.3.5 Future work

The inorganic carbon data set presented in this Chapter will serve both scientists and stakeholders (Gallo et al., 2019). This data set contains substantial insight into carbonate chemistry of the Southern California Current, and specifically the primary sampling locations. This chapter does not aim to exhaust the information contained within, but to summarize the data set as an aid to future research. As mentioned above, one obvious use is the assimilation into empirical models to estimate inorganic carbon chemistry (Alin et al., 2012; Carter et al., 2021). To make this data set broadly available, it will be shared via the CalCOFI website (https://calcofi.org/data/ oceanographic-data/dic/), the California Current Ecosystem Long Term Ecological Research data portal (https://oceaninformatics.ucsd.edu/datazoo/catalogs/ ccelter/datasets) and the Environmental Data Initiative (https://environmentaldatainitiative.org/). Publication of this chapter in a journal such as Earth System Science Data will make the data set easily accessible to a broad audience. Further collaboration with other inorganic carbon observation programs in the California Current, such as the California Current Acidification Network (McLaughlin et al., 2015) and the NOAA West Coast Ocean Acidification Cruises could increase the value of this data set. Both in contribution to combined data sets, possibly the Coastal Ocean Data Analysis Product in North America (CODAP-NA) (Jiang et al., 2021) or the Global Interior Ocean Biogeochemical Data Product (GLODAP) (Lauvset et al., 2021) and potentially coordination of sampling efforts could be possible.

4.4 Conclusions

Time series provide important insight into climate change along with ocean biogeochemical processes. Processes such as anthropogenic ocean acidification are difficult to differentiate from background variability without multi-decadal inorganic carbon observations. The value of inorganic carbon time series is increased when collocated with other observation programs to create a more detailed description of a region of the ocean. The final step of an observation program should be to make the data easily accessible and shared broadly.

4.5 Acknowledgments

Measurements have been supported by a variety of funding sources including NSF (California Current Ecosystem Long Term Ecological Research, award OCE-16-37632), and NOAA Climate Program Office. The crew and scientists on CalCOFI cruises, and the people who made these measurements over the last 37 years are too numerous to list here but this work would not have been possible without their efforts. Guy Emanuele aided in locating historical data.

Chapter 4, in part, is currently being prepared for submission for publication of the material in Earth System Science Data. The dissertation author was the primary author of this chapter.

4.6 Figures

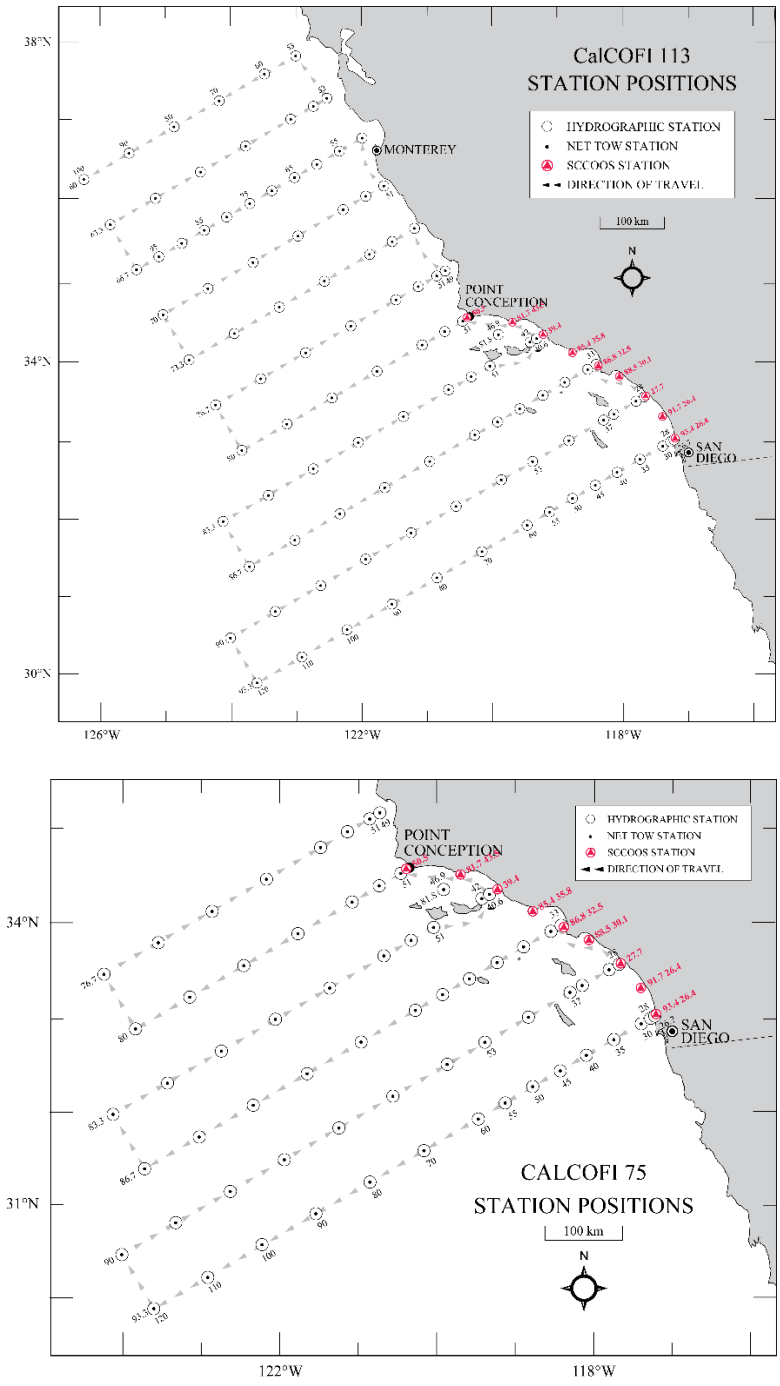

Figure 4.1. CalCOFI sampling patterns. The 75-station pattern is typical for summer and fall cruises. The 113-station sampling pattern is typical for winter and spring cruises. Maps from the CalCOFI website, https://calcofi.org/sampling-info/station-positions/.

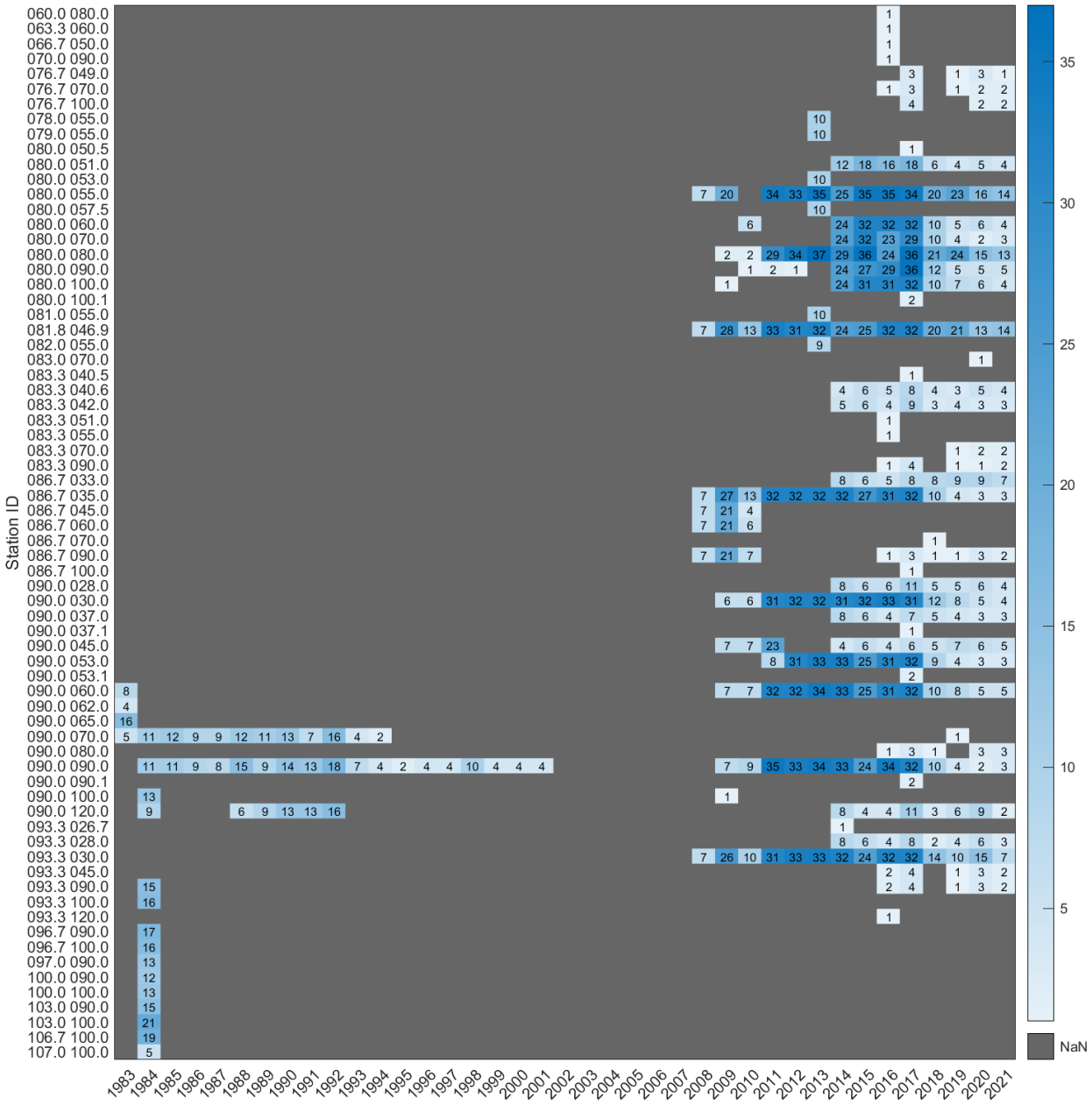

Figure 4.2. The number of inorganic carbon observations at each location per year.

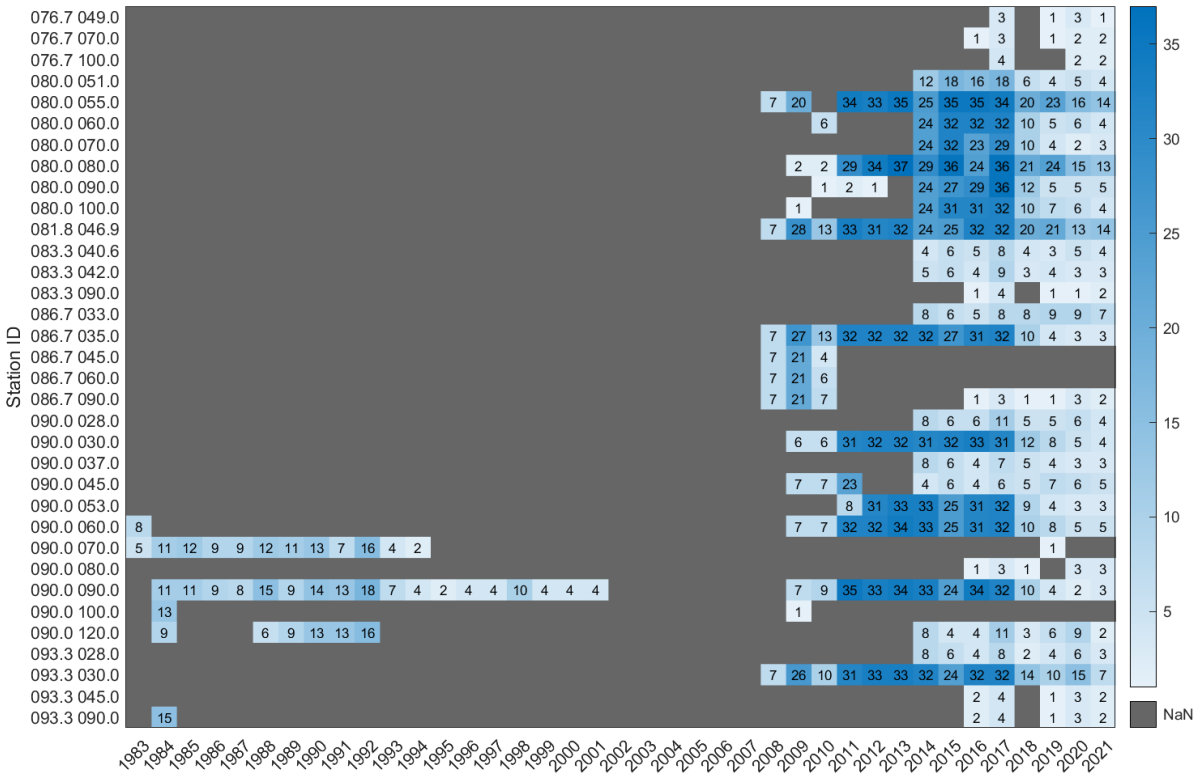

Figure 4.3. The number of inorganic carbon observations at each location per year. Limited to locations with measurements in at least two years.

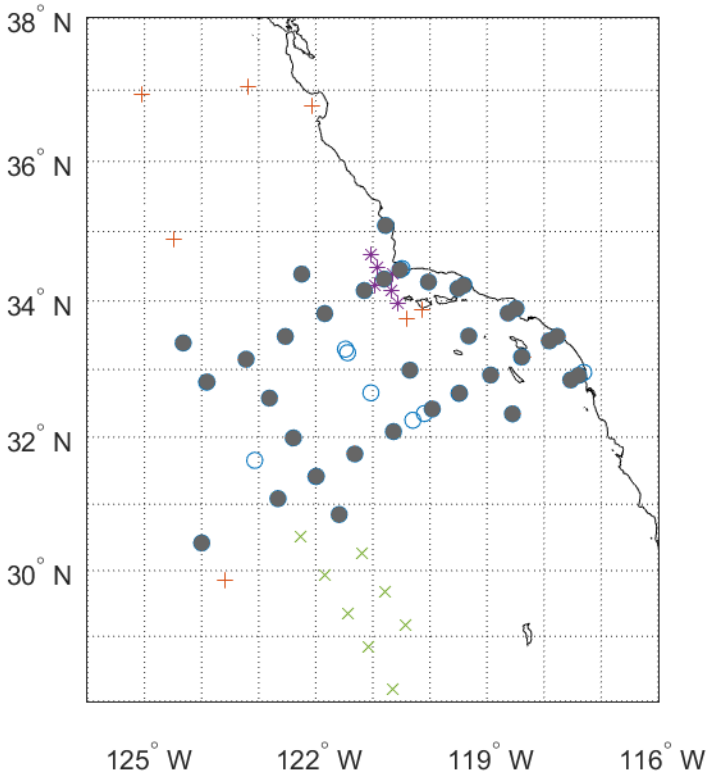

Figure 4.4. Locations with inorganic carbon observations from multiple years are shown with grey filled circles. Locations with observations from the single year of 1984, green “x”; 2013, magenta “*”; 2016, orange “+”. Locations with observations from a single year other than 1984, 2013 or 2016 are shown with unfiled blue circles.

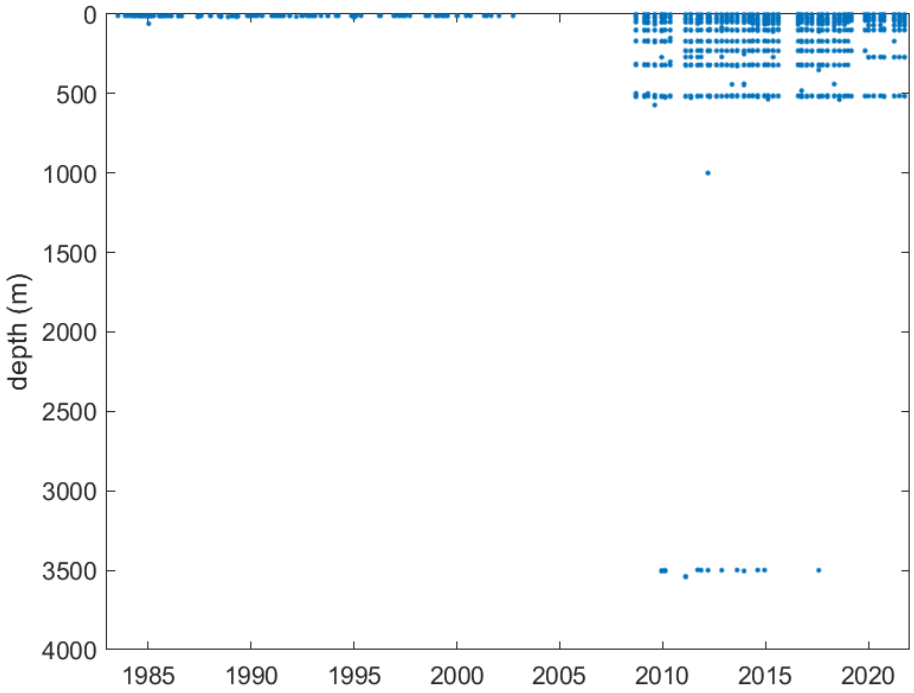

Figure 4.5. The depth of inorganic carbon observations throughout time.

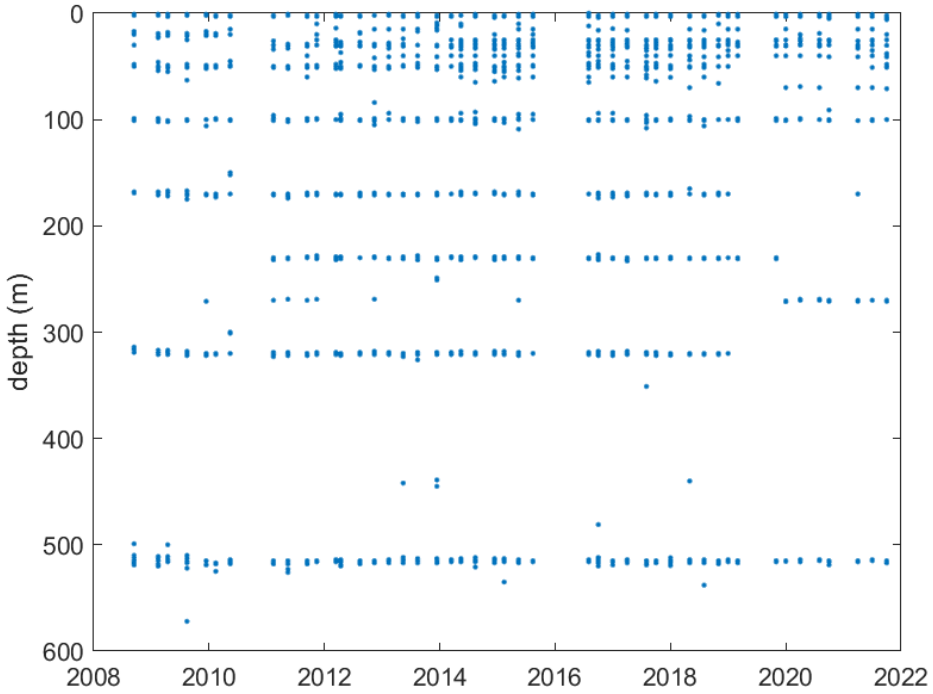

Figure 4.6. The depth of inorganic carbon observations after 2008 as the vast majority observations from 2008 are near the sea surface. Observations deeper than 600 m are also excluded (n = 17, most at ~ 3500 m).

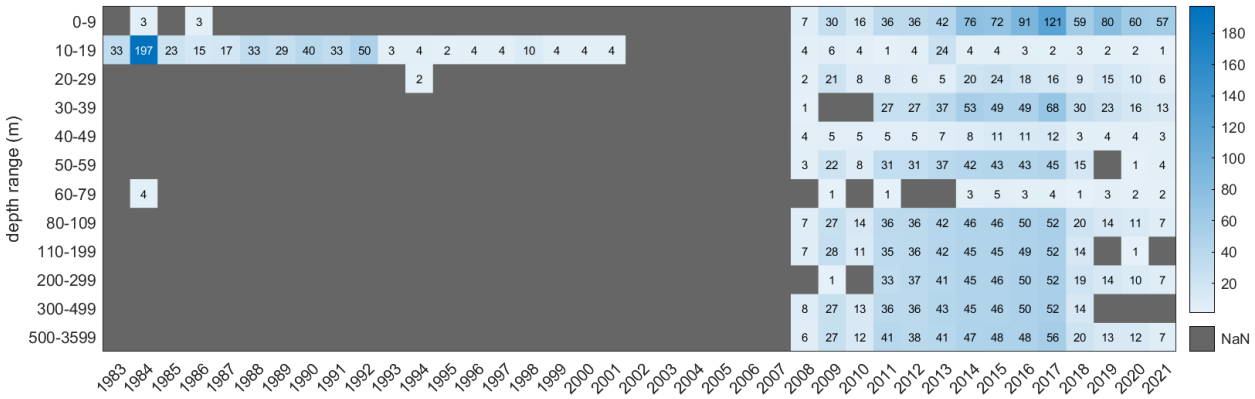

Figure 4.7. The number of inorganic carbon observations per year in each depth range.

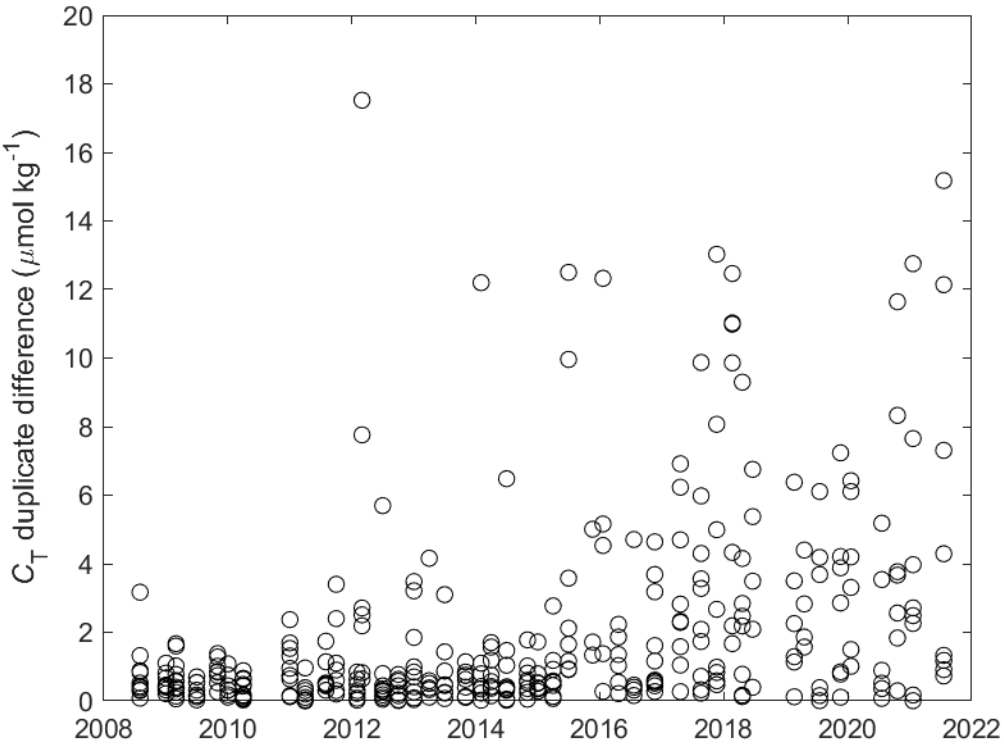

Figure 4.8. The difference between duplicate C_T measurements collected after 2008.

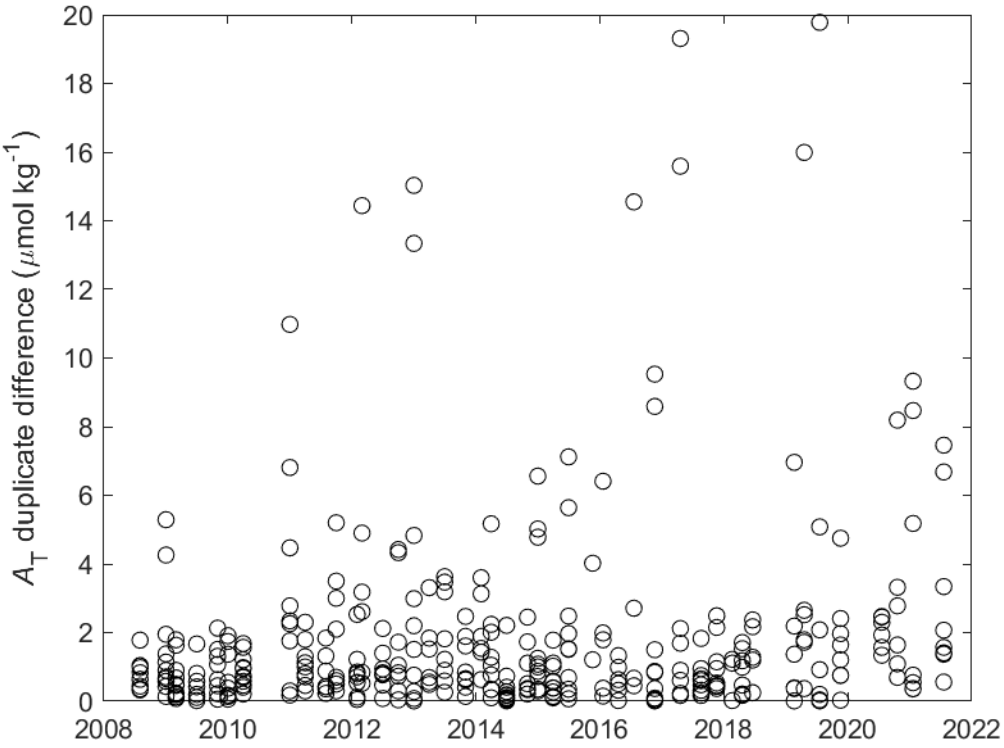

Figure 4.9. The difference between duplicate A_T measurements collected after 2008**.**

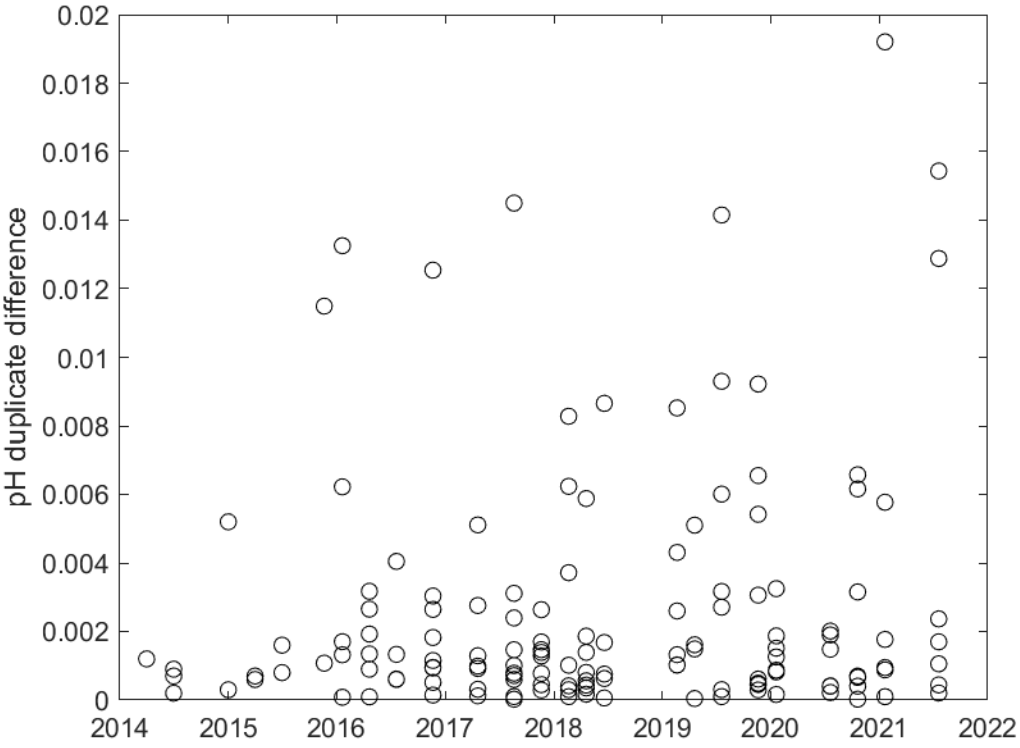

Figure 4.10. The difference between duplicate pH measurements collected after 2008.

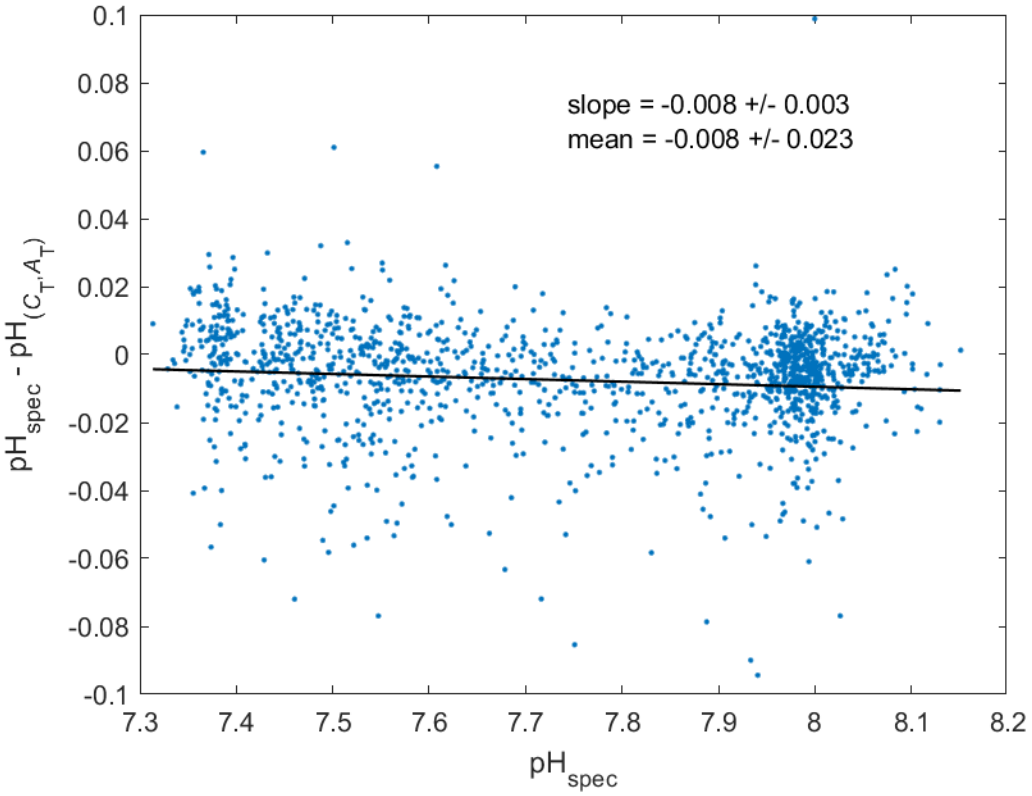

Figure 4.11. The difference between spectrophotometric pH and pH calculated from C_T and A_T was 0.008 ± 0.02 (mean ± std, n = 1435). The slope in the difference between spectrophotometric pH and pH calculated from C_T and A_T vs spectrophotometric pH in the data present here is -0.008 ± 0.003 yr^{-1} (mean ± std). All observations presented here were made after 2014 and were measured with IR C_T, open cell A_T, and spectrophotometric pH.

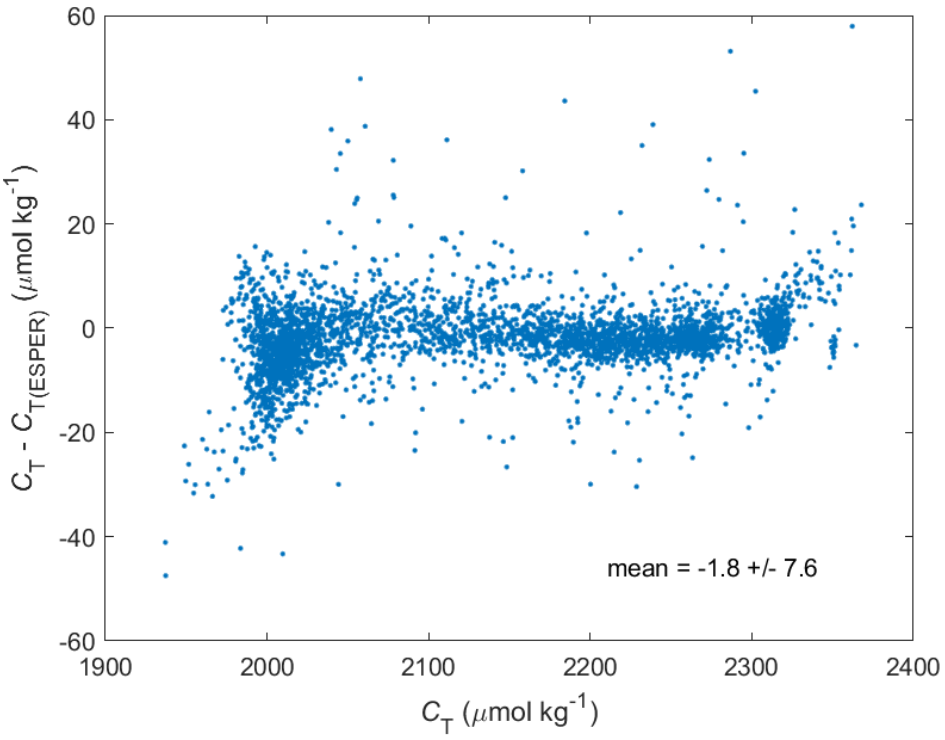

Figure 4.12. The difference between measured C_T and that predicted using ESPER_Mixed plotted against measured C_T.

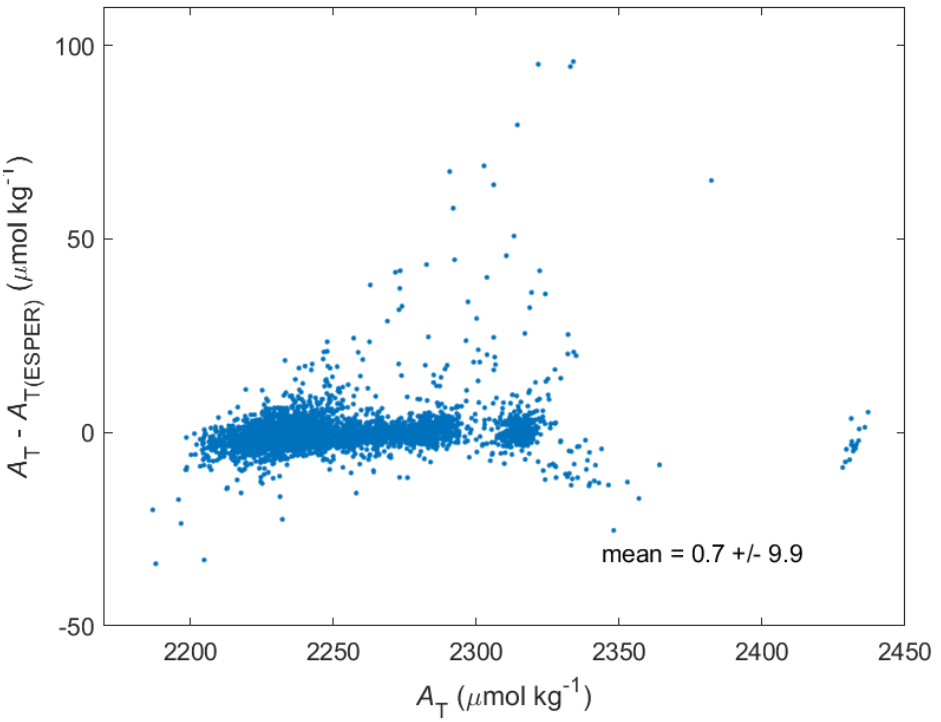

Figure 4.13. The difference between measured A_T and that predicted using ESPER_Mixed plotted against measured A_T.

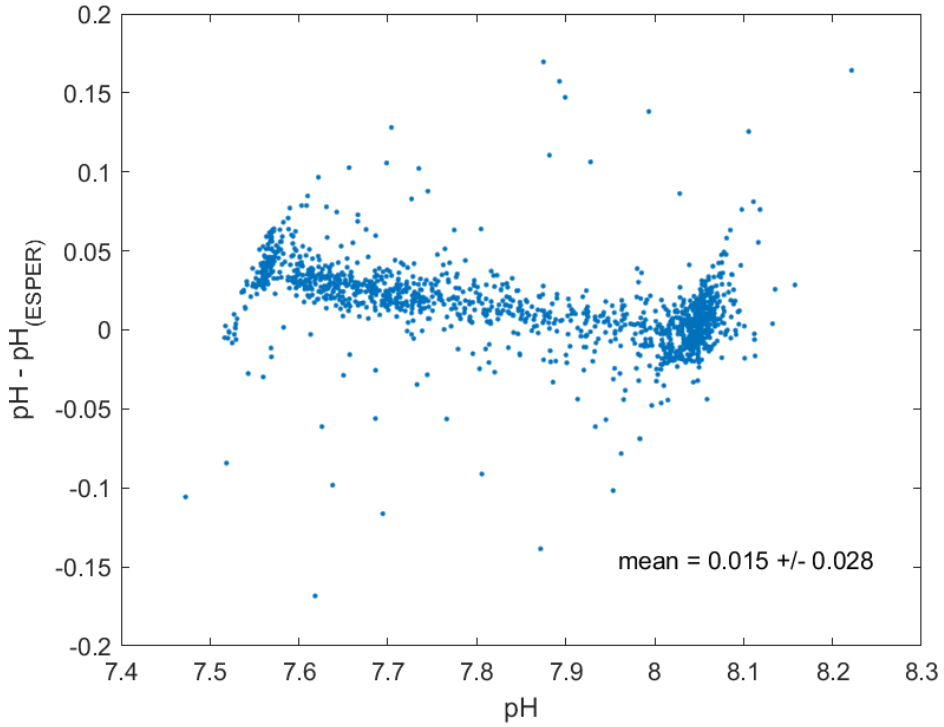

Figure 4.14. The difference between measured pH and that predicted using ESPER_Mixed plotted against measured pH. Both measured and ESPER pH are show at in situ temperature.

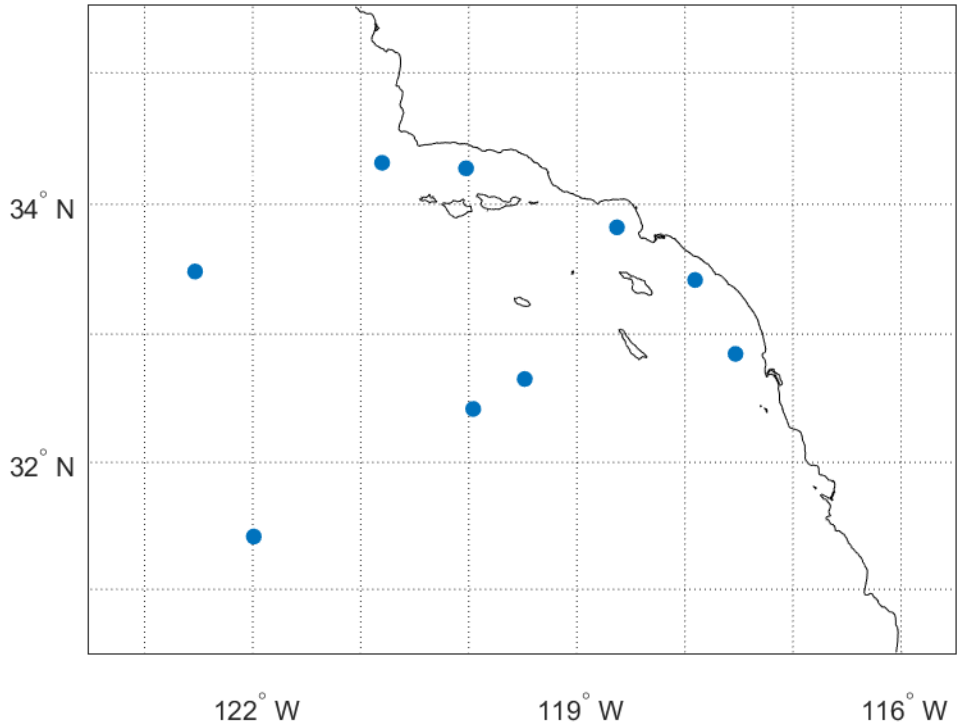

Figure 4.15. A map of the locations with more than 152 observations. Shown in Figure 4.16 and Figure 4.17.

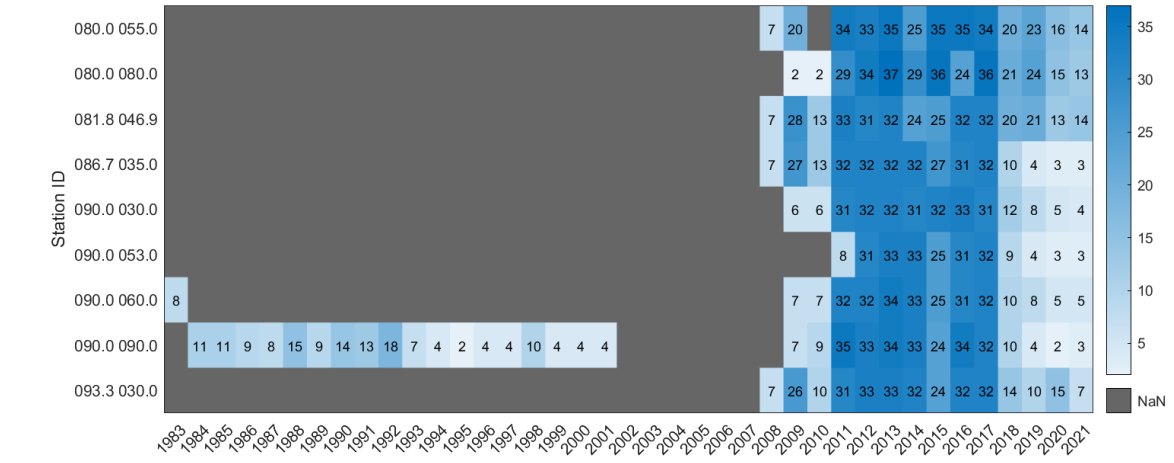

Figure 4.16. The number of inorganic carbon observations at each location per year. Limited to locations with more than 152 total observations.

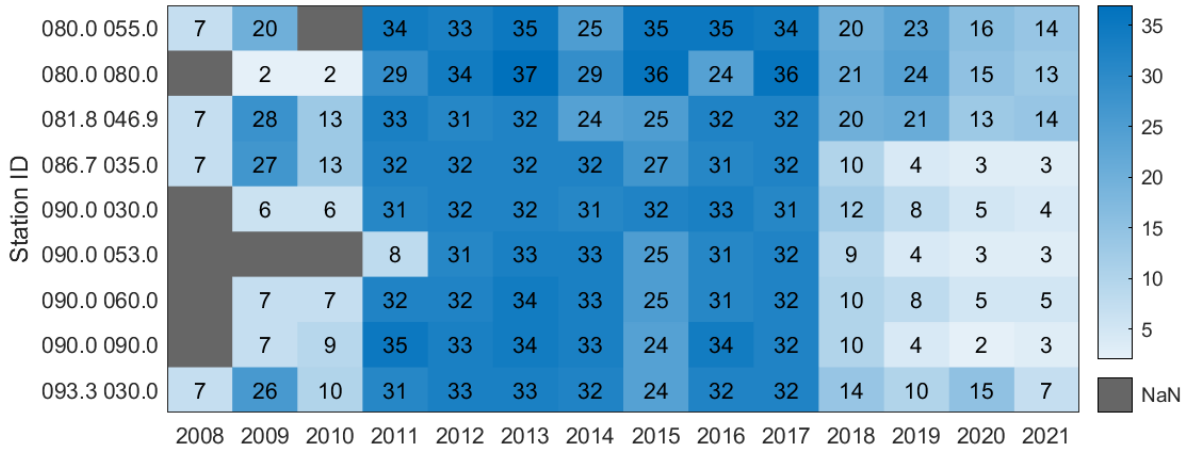

Figure 4.17. The number of inorganic carbon observations at each location per year. Limited to locations with more than 152 total observations, between 2008 and present.

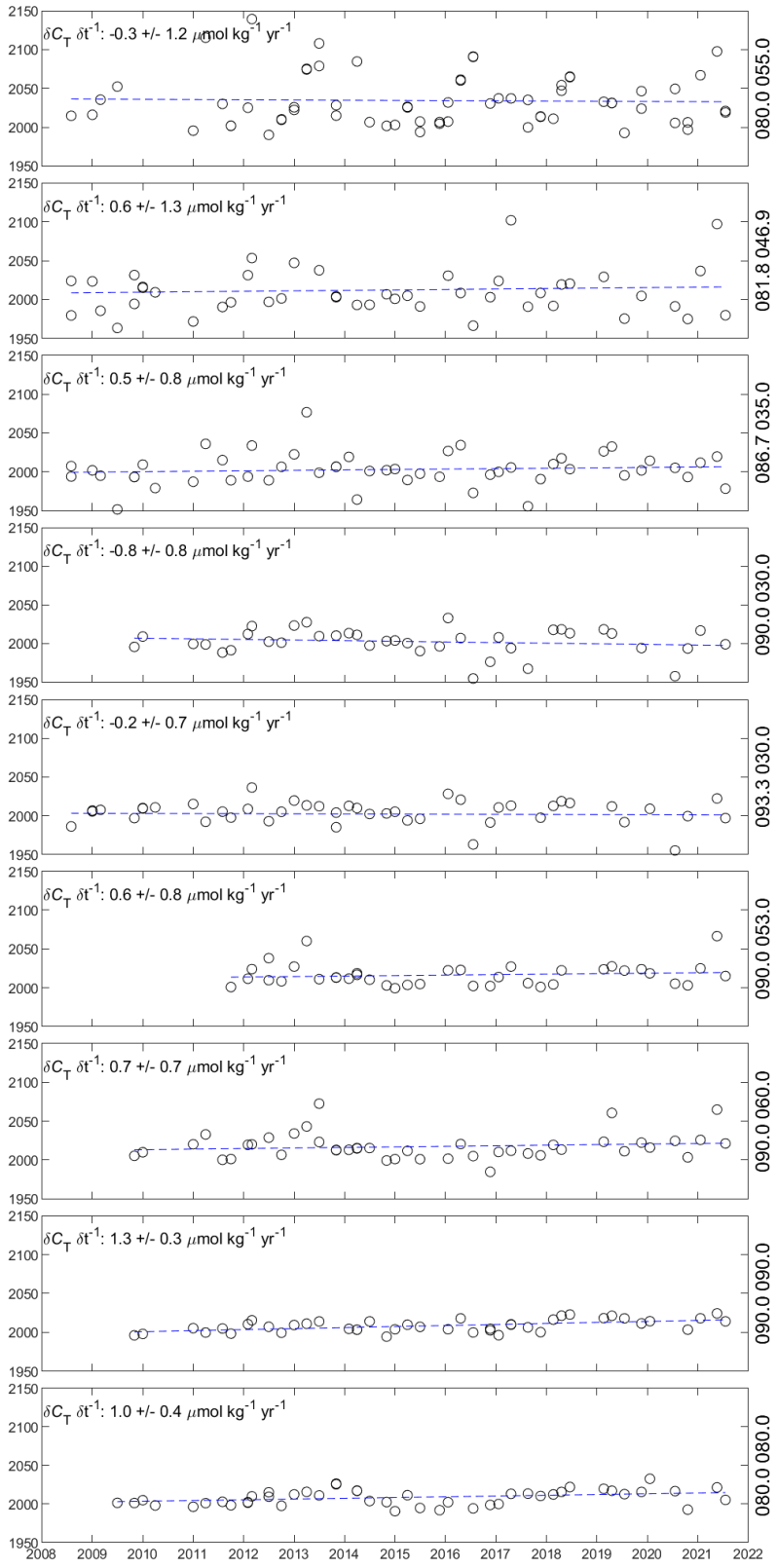

Figure 4.18. The sea surface C_T at the 9 most sampled stations. The top 5 subplots are from nearshore locations. The bottom 4 subplots are from offshore locations.

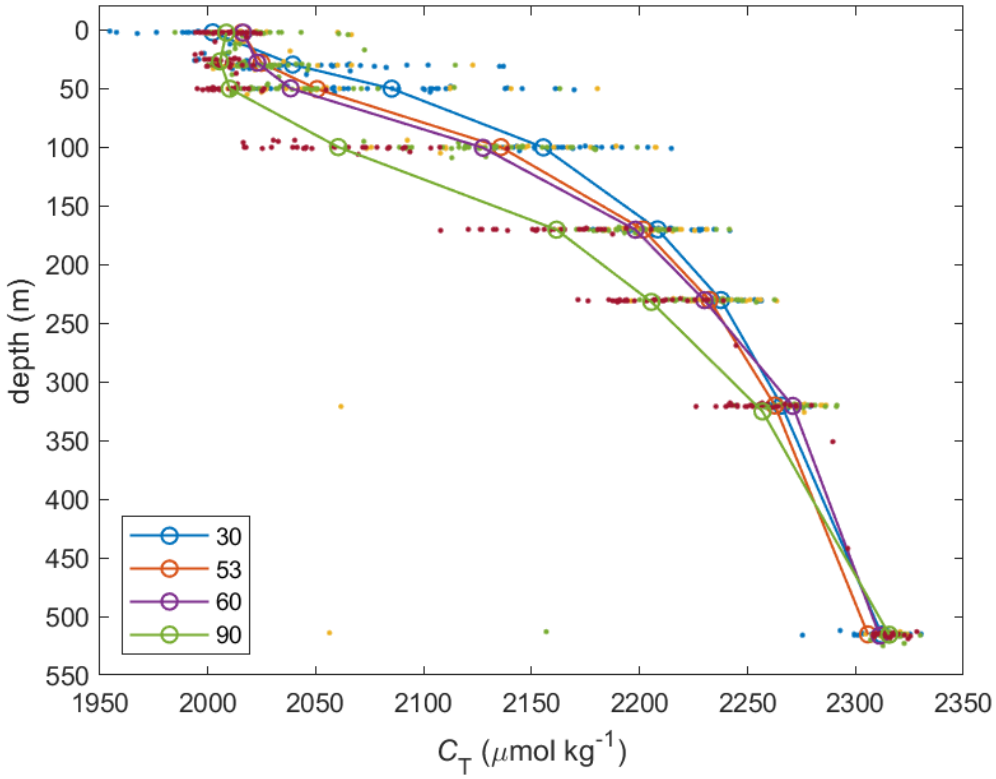

Figure 4.19. The sea surface C_T at the 9 most sampled stations. The top 5 subplots are from nearshore locations. The bottom 4 subplots are from offshore locations.

REFERENCES

Alin, S. R., Feely, R. A., Dickson, A. G., Hernández-Ayón, J. M., Juranek, L. W., Ohman, M. D., & Goericke, R. (2012). Robust empirical relationships for estimating the carbonate system in the southern California Current System and application to CalCOFI hydrographic cruise data (2005-2011). *Journal of Geophysical Research: Oceans, 117*(C5).

Bates, N., Astor, Y., Church, M., Currie, K., Dore, J., Gonaález-Dávila, M., et al. (2014). A Time-Series View of Changing Ocean Chemistry Due to Ocean Uptake of Anthropogenic CO_2 and Ocean Acidification. *Oceanography, 27*(1), 126-141.

Bates, N. R., Best, M. H. P., Neely, K., Garley, R., Dickson, A. G., & Johnson, R. J. (2012). Detecting anthropogenic carbon dioxide uptake and ocean acidification in the North Atlantic Ocean. *Biogeosciences, 9*(7), 2509-2522.

Bradshaw, A. L., Brewer, P. G., Shafer, D. K., & Williams, R. T. (1981). Measurements of total carbon dioxide and alkalinity by potentiometric titration in the GEOSECS program. *Earth and Planetary Science Letters, 55*(1), 99-115.

Carter, B., Bittig, H., Fassbender, A., Sharp, J., Takeshita, Y., Xu, Y., et al. (2021). New and updated global empirical seawater property estimation routines. *Limnology and Oceanography-Methods, 19*(12), 785-809.

Chavez, F., Pennington, J., Michisaki, R., Blum, M., Chavez, G., Friederich, J., et al. (2017). Climate Variability and Change Response of a Coastal Ocean Ecosystem. *Oceanography, 30*(4), 128-145.

Checkley, D., & Barth, J. (2009). Patterns and processes in the California Current System. *Progress in Oceanography, 83*(1-4), 49-64.

Di Lorenzo, E., & Mantua, N. (2016). Multi-year persistence of the 2014/15 North Pacific marine heatwave. *Nature Climate Change, 6*(11), 1042-+.

Dickson, A. G., Afghan, J., & Anderson, G. (2003). Reference materials for oceanic CO2 analysis: a method for the certification of total alkalinity. *Marine Chemistry, 80*(2-3), 185-197.

Dickson, A. G., Sabine, C. L., & Christian, J. R. (2007). Guide to best practices for ocean CO_2 measurements. *PICES Special Publication*.

Doney, S., Busch, D., Cooley, S., Kroeker, K., Gadgil, A., & Tomich, T. (2020). The Impacts of Ocean Acidification on Marine Ecosystems and Reliant Human Communities. *Annual Review of Environment and Resources, Vol 45, 45*, 83-112.

Ellison, S. L., & Williams, A. (2012). Quantifying uncertainty in analytical measurement.

Emerson, S. (2014). Annual net community production and the biological carbon flux in the ocean. *Global Biogeochemical Cycles, 28*(1), 14-28.

Fassbender, A., Orr, J., & Dickson, A. (2021). Technical note: Interpreting pH changes. *Biogeosciences, 18*(4), 1407-1415.

Fassbender, A. J., Sabine, C. L., & Cronin, M. F. (2016). Net community production and calcification from 7 years of NOAA Station Papa Mooring measurements. *Global Biogeochemical Cycles, 30*(2), 250-267.

Fong, M. B., & Dickson, A. G. (2019). Insights from GO-SHIP hydrography data into the thermodynamic consistency of CO2 system measurements in seawater. *Marine Chemistry, 211*, 52-63.

Friedlingstein, P., Jones, M., O'Sullivan, M., Andrew, R., Bakker, D., Hauck, J., et al. (2022). Global Carbon Budget 2021. *Earth System Science Data, 14*(4), 1917-2005.

Gallo, N. D., Drenkard, E., Thompson, A. R., Weber, E. D., Wilson-Vandenberg, D., McClatchie, S., et al. (2019). Bridging from monitoring to solutions-based thinking: lessons from CalCOFI for understanding and adapting to marine climate change impacts. *Frontiers in Marine Science, 6*, 695.

Goyet, C., & Snover, A. K. (1993). High-accuracy measurements of total dissolved inorganic carbon in the ocean - comparison of alternate detection methods. *Marine Chemistry, 44*(2-4), 235-242.

Gruber, N., Clement, D., Carter, B., Feely, R., van Heuven, S., Hoppema, M., et al. (2019). The oceanic sink for anthropogenic CO_2 from 1994 to 2007. *Science, 363*(6432), 1193-+.

Gruber, N., Keeling, C. D., & Stocker, T. F. (1998). Carbon-13 constraints on the seasonal inorganic carbon budget at the BATS site in the northwestern Sargasso Sea. *Deep Sea Research Part I: Oceanographic Research Papers, 45*(4-5), 673-717.

Hewitt, R. (1988). Historical Review of The Oceanographic Approach to Fishery Research. *California Cooperative Oceanic Fisheries Investigations Reports, 29*, 27-41.

Holte, J., Talley, L. D., Gilson, J., & Roemmich, D. (2017). An Argo mixed layer climatology and database. *Geophysical Research Letters, 44*(11), 5618-5626.

Jacox, M., Hazen, E., Zaba, K., Rudnick, D., Edwards, C., Moore, A., & Bograd, S. (2016). Impacts of the 2015-2016 El Nino on the California Current System: Early assessment and comparison to past events. *Geophysical Research Letters, 43*(13), 7072-7080.

Jiang, L.-Q., Feely, R. A., Wanninkhof, R., Greeley, D., Barbero, L., Alin, S., et al. (2021). Coastal Ocean Data Analysis Product in North America (CODAP-NA)–an internally consistent data product for discrete inorganic carbon, oxygen, and nutrients on the North American ocean margins. *Earth system science data, 13*(6), 2777-2799.

Johnson, K., Sieburth, J., Williams, P., & Brandstrom, L. (1987). Coulometric Total Carbon-dioxide Analysis For Marine Studies - Automation And Calibration. *Marine Chemistry, 21*(2), 117-133.

Keeling, C., Brix, H., & Gruber, N. (2004). Seasonal and long-term dynamics of the upper ocean carbon cycle at Station ALOHA near Hawaii. *Global Biogeochemical Cycles, 18*(4).

Keeling, C., Piper, S. C., Bacastow, R. B., Wahlen, M., Whorf, T. P., Heimann, M., & Meijer, H. A. (2005). Atmospheric CO_2 and $^{13}CO_2$ exchange with the terrestrial biosphere and oceans from 1978 to 2000: Observations and carbon cycle implications. In *A history of atmospheric CO_2 and its effects on plants, animals, and ecosystems* (pp. 83-113): Springer.

Keeling, R., & Keeling, C. (2017). *Atmospheric monthly in situ CO_2 data-Mauna Loa observatory, Hawaii*.

Kragten, J. (1994). Tutorial review. Calculating standard deviations and confidence intervals with a universally applicable spreadsheet technique. *Analyst, 119*(10), 2161-2165.

Kranz, S. A., Wang, S., Kelly, T. B., Stukel, M. R., Goericke, R., Landry, M. R., & Cassar, N. (2020). Lagrangian studies of marine production: A multimethod assessment of productivity relationships in the California Current Ecosystem upwelling region. *Journal of Geophysical Research: Oceans, 125*(6), e2019JC015984.

Landschützer, P., Laruelle, G., Roobaert, A., & Regnier, P. (2020). A uniform pCO_2 climatology combining open and coastal oceans. *Earth System Science Data, 12*(4), 2537-2553.

Lauvset, S. K., Lange, N., Tanhua, T., Bittig, H. C., Olsen, A., Kozyr, A., et al. (2021). An updated version of the global interior ocean biogeochemical data product, GLODAPv2. 2021. *Earth System Science Data, 13*(12), 5565-5589.

Lilly, L. E., Send, U., Lankhorst, M., Martz, T. R., Feely, R. A., Sutton, A. J., & Ohman, M. D. (2019). Biogeochemical Anomalies at Two Southern California Current System Moorings During the 2014–2016 Warm Anomaly-El Niño Sequence. *Journal of Geophysical Research: Oceans, 124*(10), 6886-6903.

Liu, X. W., Patsavas, M. C., & Byrne, R. H. (2011). Purification and Characterization of meta-Cresol Purple for Spectrophotometric Seawater pH Measurements. *Environmental Science & Technology, 45*(11), 4862-4868.

Lueker, T. (1998). *Carbonic acid dissociation constants determined as the ratio K_1/K_2 from the concentration of CO_2 in gas and seawater equilibrium.* (PhD), University of California, San Diego,

Lueker, T., Dickson, A., & Keeling, C. (2000). Ocean pCO_2 calculated from dissolved inorganic carbon, alkalinity, and equations for K_1 and K_2: validation based on laboratory measurements of CO_2 in gas and seawater at equilibrium. *Marine Chemistry, 70*(1-3), 105-119.

McLaughlin, K., Weisberg, S., Dickson, A., Hofmann, G., Newton, J., Aseltine-Neilson, D., et al. (2015). Core Principles of the California Current Acidification Network: Linking Chemistry, Physics, and Ecological Effects. *Oceanography, 25*(2), 160-169.

Morgan, P. P. (1994). SEAWATER: a library of MATLAB® computational routines for the properties of sea water: Version 1.2.

Munro, D. R., Quay, P. D., Juranek, L. W., & Goericke, R. (2013). Biological production rates off the Southern California coast estimated from triple O2 isotopes and O2: Ar gas ratios. *Limnology and Oceanography, 58*(4), 1312-1328.

Nagai, T., Gruber, N., Frenzel, H., Lachkar, Z., McWilliams, J. C., & Plattner, G. K. (2015). Dominant role of eddies and filaments in the offshore transport of carbon and nutrients in the C alifornia C urrent S ystem. *Journal of Geophysical Research: Oceans, 120*(8), 5318-5341.

O'Sullivan, D., & Millero, F. (1998). Continual measurement of the total inorganic carbon in surface seawater. *Marine Chemistry, 60*(1-2), 75-83. Article|Proceedings Paper.

Ohman, M. D., Rudnick, D. L., Chekalyuk, A., Davis, R. E., Feely, R. A., Kahru, M., et al. (2013). Autonomous ocean measurements in the California Current Ecosystem. *Oceanography, 26*(3), 18-25.

Rasmussen, L., Carter, M., Flick, R., Hilbern, M., Fumo, J., Cornuelle, B., et al. (2020). A Century of Southern California Coastal Ocean Temperature Measurements. *Journal of Geophysical Research-Oceans, 125*(5).

Regaudie-de-Gioux, A., Lasternas, S., Agustí, S., & Duarte, C. M. (2014). Comparing marine primary production estimates through different methods and development of conversion equations. *Frontiers in Marine Science, 1*, 19.

Riser, S. C., & Johnson, K. S. (2008). Net production of oxygen in the subtropical ocean. *Nature, 451*(7176), 323-325.

Sharp, J., Fassbender, A., Carter, B., Lavin, P., & Sutton, A. (2022). A monthly surface pCO_2 product for the California Current Large Marine Ecosystem. *Earth System Science Data, 14*(4), 2081-2108.

Takahashi, T., Sutherland, S. C., Wanninkhof, R., Sweeney, C., Feely, R. A., Chipman, D. W., et al. (2009). Climatological mean and decadal change in surface ocean pCO2, and net sea–air CO2 flux over the global oceans. *Deep Sea Research Part II: Topical Studies in Oceanography, 56*(8-10), 554-577.

Takeshita, Y., Warren, J. K., Liu, X., Spaulding, R. S., Byrne, R. H., Carter, B. R., et al. (2021). Consistency and stability of purified meta-cresol purple for spectrophotometric pH measurements in seawater. *Marine Chemistry, 236*, 104018.

Talley, L. D., Pickard, G. L., Emery, W. J., & Swift, J. H. (2011). *Descriptive physical oceanography: an introduction*: Academic press.

Todd, R. E., Rudnick, D. L., Mazloff, M. R., Davis, R. E., & Cornuelle, B. D. (2011). Poleward flows in the southern California Current System: Glider observations and numerical simulation. *Journal of Geophysical Research: Oceans, 116*(C2).

Turi, G., Lachkar, Z., Gruber, N., & Nunnich, M. (2016). Climatic modulation of recent trends in ocean acidification in the California Current System. *Environmental Research Letters, 11*(1).

van Heuven, S., Pierrot, D., & Rae, J. (2011). MATLAB Program Developed for CO_2 System Calculations. *ORNL/CDIAC-105b, Carbon Dioxide Information Analysis Center, Oak Ridge National Laboratory, U.S. Department of Energy, Oak Ridge, Tennessee*.

Vance, J., Currie, K., Zeldis, J., Dillingham, P., & Law, C. (2022). An empirical MLR for estimating surface layer DIC and a comparative assessment to other gap-filling techniques for ocean carbon time series. *Biogeosciences, 19*(1), 241-269.

VanderPlas, J. (2018). Understanding the Lomb-Scargle Periodogram. *Astrophysical Journal Supplement Series, 236*(1).

Wanninkhof, R. (2014). Relationship between wind speed and gas exchange over the ocean revisited. *Limnology and Oceanography: Methods, 12*(6), 351-362.

Wanninkhof, R., Doney, S. C., Takahashi, T., & Mcgillis, W. R. (2002). The Effect of Using Time-Averaged Winds on Regional Air-Sea CO~ 2 Fluxes. *Geophysical Monograph-American Geophysical Union, 127*, 351-356.

Weber, E. D., & Moore, T. J. (2013). Corrected conversion algorithms for the calcofi station grid and their implementation in several computer languages. *California Cooperative Oceanic Fisheries Investigations Reports, 54*, 97-106.

Weiss, R. F. (1974). Carbon dioxide in water and seawater: the solubility of a non-ideal gas. *Marine chemistry, 2*(3), 203-215.

Wolfe, W., Shipley, K., Bresnahan, P., Takeshita, Y., Wirth, T., & Martz, T. (2021). Technical note: Stability of tris pH buffer in artificial seawater stored in bags. *Ocean Science, 17*(3), 819-831.

Yang, B., Emerson, S. R., & Bushinsky, S. M. (2017). Annual net community production in the subtropical Pacific Ocean from in situ oxygen measurements on profiling floats. *Global Biogeochemical Cycles, 31*(4), 728-744.

Yang, B., Shadwick, E. H., Schultz, C., & Doney, S. C. (2021). Annual Mixed Layer Carbon Budget for the West Antarctic Peninsula Continental Shelf: Insights From Year-Round Mooring Measurements. *Journal of Geophysical Research: Oceans, 126*(4), e2020JC016920.